Alexandr Jonáš
Pavel Zemánek

Institute of Scientific Instruments of the AS CR, v.v.i., Academy of Sciences of the Czech Republic, Brno, Czech Republic

Received July 24, 2008
Revised August 25, 2008
Accepted August 25, 2008

Review

Light at work: The use of optical forces for particle manipulation, sorting, and analysis

We review the combinations of optical micro-manipulation with other techniques and their classical and emerging applications to non-contact optical separation and sorting of micro- and nanoparticle suspensions, compositional and structural analysis of specimens, and quantification of force interactions at the microscopic scale. The review aims at inspiring researchers, especially those working outside the optical micro-manipulation field, to find new and interesting applications of these methods.

Keywords:
Microfluidics / Optical chromatography and sorting / Optical force and torque / Optical tweezers and micro-manipulation / Raman microspectroscopy
DOI 10.1002/elps.200800484

1 Introduction

Light in its wider definition covers the near-infrared and ultraviolet spectral regions together with the visible range. It provides invaluable information about the macroscopic and microscopic world around us and it also enables recording, storing, and transmitting this information. In addition to illuminating and conveying information light can also move material objects. This property of light is not too well known even though two Nobel prizes in physics were recently awarded to the achievements that employed transfer of momentum from light to matter to slow down atoms (cool them) [1–3] and to form Bose–Einstein condensate – a macroscopic quantum-coherent system [4]. The first speculations about the mechanical effects of light, however, are much older: in the 17th century astronomer Johannes Kepler suggested that comets' tails were pushed away from the Sun by the pressure of light. He also proposed traveling from the Earth to the Moon by a solar sailer that was much later actually studied and even tested by NASA. The modern history of optical manipulation started almost 40 years ago by the pioneering work of Ashkin who demonstrated that a moderately focused laser beam is sufficient to influence significantly the motion of microparticles, to propel them in a liquid [5], or even to levitate them in the air [6] (see also reviews [7–9]). In 1986 he, together with his colleagues, demonstrated stable all-optical trapping using a single tightly focused laser beam – a configuration nowadays called *optical tweezers* (OT) [10]. OT currently represent the classical optical micro-manipulation tool and they have found numerous applications in the fields of biology, chemistry, and physics. In particular, the combination of OT with the precise detection of the trapped object position enabled quantitative measurements of the force interactions between the trapped object and its surrounding that was applied with a great success to the analysis of mechanical properties and working principles of individual biomolecules [11–14].

Even though the success of the classical single-beam OT has not faded, novel configurations of trapping beams together with the availability of advanced optical elements especially spatial light modulators (SLM) have brought new applications. These include multiple-particle trapping, controlled rotation of the trapped objects, optical sorting, optically driven pumps and motors, optical delivery of microparticles and nanoparticles, large-scale organization of objects on the surface or in the space (colloidal crystals), fusion of airborne droplets, optically controlled chemical microreactors, optical chromatography (OC) and combinations of optical micro-manipulation with microfluidic systems or optical spectroscopy (fluorescence and Raman), optical stretcher, and combinations of optical forces with the new possibilities of plasmonics and nanophotonics that reach into the realm of nanotechnology. In these applications, the light is used in a versatile manner to confine the micro- and nanoobjects stably in space or control their trajectory and state of motion, probe the composition and structure of the illuminated objects, and actively change their properties.

Correspondence: Dr. A. Jonáš, Institute of Scientific Instruments of the AS CR, v.v.i., Academy of Sciences of the Czech Republic, Kralovopolska 147, 61264 Brno, Czech Republic
E-mail: sasa@isibrno.cz
Fax: +42-0541514402

Abbreviations: AFM, atomic force microscope; **FACS,** fluorescence-activated cell sorting; **HOT,** holographic optical tweezers; **LPC,** laser pressure catapulting; **NA,** numerical aperture; **OC,** optical chromatography; **OT,** optical tweezers; **PFM,** photonic force microscope; **RT,** Raman tweezers; **SERS,** surface-enhanced Raman scattering; **SLM,** spatial light modulator; **SPP,** surface plasmon polariton; **SWCNT,** single-walled carbon nanotubes; **TM,** transversal magnetic

In this article we do not intend to give a comprehensive description of the field of optical micro-manipulation but we would rather like to present an overview of various optical micro-manipulation techniques, comment on their features, and describe their interesting applications. The review should help researchers, especially those working outside of the field, to be inspired by these not yet widespread methods and consider their new applications. The article is organized as follows: in Section 2 we give a brief explanation of the origin of optical forces and how they can be calculated for nanoparticles and microparticles. The following section refers to various configurations and methods for trapping or manipulation of particles using transfer of momentum or angular momentum from laser beams to material objects. We will also briefly mention other methods that use laser beams to manipulate objects but do not employ directly the optical forces. Subsequent sections will then describe various applications of the previously explained manipulation methods. Finally, we will summarize the current state in the field of optical micro-manipulation and mention new directions of its possible development.

For an interested reader, there are a number of books available that touch this subject in some way. Greulich focused mainly on the biological applications of OT and optical scalpel [15]. The book edited by Sheetz *et al.* is dedicated to the design considerations of optical traps, precise measurement of optical forces, and applications in biology [16]. Ashkin has published an overview book about the history and development of optical trapping including atom cooling and trapping, which is not treated in this paper [9]. Recently Berns and Greulich edited a comprehensive volume of the Methods in Cell Biology focused on the laser manipulation of cells and tissues [17], Andrews edited a book dealing with the applications of tailored light distributions for optical micro-manipulation [18], and Noy edited a monograph on the molecular force measurements [14]. A concise resource letter covering a number of important research papers up to 2002 was published by Lang and Block [19]. In each section, we will further mention review papers dealing with their particular subjects.

2 The origin and strength of optical forces

Optical forces result from the exchange of momentum between the incident photons and the irradiated object. Light scattering and absorption from/by an object change the direction and magnitude of the propagating light wave and, thus, the flux of momentum associated with the photons constituting the wave. According to Newton's second law, the rate of change of the photon momentum is associated with the force acting on the photons; consequently the same force – but of opposite direction – is applied to the irradiated object by virtue of Newton's third law. The force due to the single photon scattering has noticeable effect only on very small objects with sufficiently small momentum such as cold atoms. In order to influence the behavior of bigger objects with sizes up to tens of micrometers, coordinated action of many photons is required, which can be achieved only with a very high-intensity light source such as a focused laser beam.

When a particle whose optical density (refractive index) is higher than that of the surrounding medium is illuminated by a moderately focused laser beam with a Gaussian transversal intensity profile, two principal trends of the particle behavior can be recognized. First, the particle is dragged by the light in the direction of the incident beam propagation due to the scattering force coming from the radiation pressure of the light. At the same time, the particle is attracted toward the location of the highest optical intensity (see Fig. 1A). In contrast, if the particle's refractive index is lower relative to the surrounding medium, the particle is repelled from the regions of high optical intensity; the radiation pressure still pushes it in the beam propagation direction. In general, the optical force is linearly proportional to the laser power P incident on the object and it can be expressed as

$$F_{\mathrm{opt}} = \frac{n_1 P}{c} Q \tag{1}$$

where n_1 is the refractive index of the surrounding medium, c is the speed of light in vacuum, and Q is the trapping efficiency factor that depends on the size, shape, material, and position of the particle with respect to the spatial profile of the beam. In the case of purely reflected light (for example, from a perfect mirror) Q is equal to 2. In some cases the maximal optical force can reach hundreds of pN but in majority of experiments it is in the range of tens of fN up to tens of pN.

Typical applications of OT involve dielectric particles (*e.g.* polystyrene or silica) with sizes in the so-called Mie regime (from 200 nm to ~7 μm) or living cells. However, spatial manipulation of nanoobjects (including metallic ones) with sizes in the range of tens of nanometers has also been reported (see Section 4.7). In the case of optical trapping of absorbing metallic microobjects, there is an upper limit on the particle size that can be trapped stably in 3-D using exclusively optical forces; this is due to a more complex scattering pattern and associated effects such as heating and electron motion in the skin depth of the metal. Thus, manipulation of larger absorbing objects is limited to confinement against the surface in a single-beam trap [20–22] or a scanning beam trap [23].

2.1 Optical forces acting on nanoparticles

In the description of the optical trapping forces, we will consider first the interaction of light with nanoparticles whose radius a satisfies $a \leq \lambda/20$, where λ is the wavelength of the trapping light in the medium. Even though this is experimentally not as widespread case as the optical trapping of Mie particles, the understanding and description of this configuration is much more intuitive and easier as analytical equations for the optical forces can be obtained. Furthermore, some general trends of optical force behavior

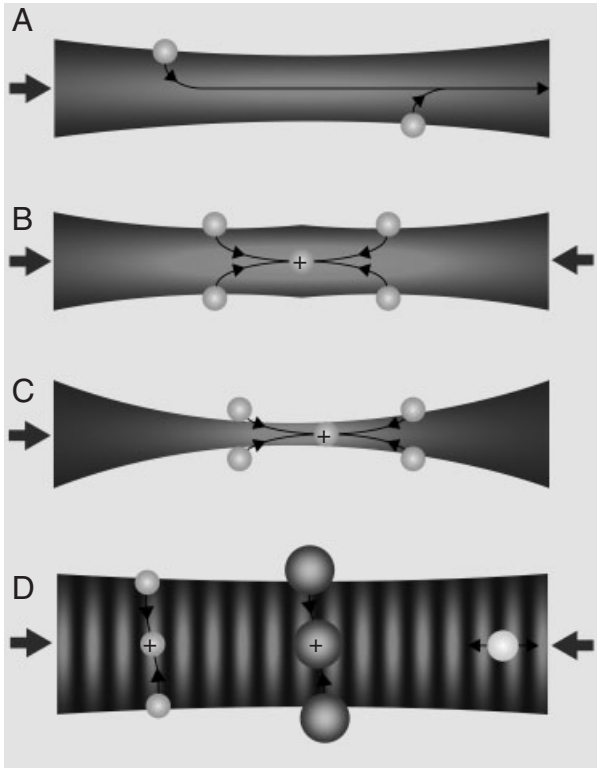

Figure 1. Optical trapping and manipulation of particles with refractive index higher than the refractive index of the surrounding medium. (A) A single moderately focused Gaussian beam attracts the particles to its axis *via* the transverse gradient force and propels them along its propagation direction *via* the dominating axial scattering force. In air the particles are accelerated, whereas in liquid, where the motion is overdamped, the particles move with terminal velocity done by the balance between the Stokes friction force and the optical force: $v = F_{\mathrm{opt}}/\gamma$, where γ is the viscous drag. (B) Two moderately focused counter-propagating (non-interfering) beams with slightly displaced foci compensate their scattering forces. Consequently, the particles are confined on the optical axis between the two beam focal planes (marked by +). A dual-beam trap or optical bottle is formed. (C) A single tightly focused beam forms the base of the single beam gradient force trap. Particles are confined behind the focus on the optical axis by the axial and radial gradient forces. (D) Standing wave created by the interference of two counter-propagating coherent beams. According to their sizes, the particles are confined either in the high-intensity (left) or low-intensity (center) regions of the interference fringes. Certain particle sizes (right) are only confined radially on the optical axis but do not feel the axial intensity modulations.

can also be at least qualitatively extrapolated to the larger particle sizes. Therefore, we will devote the optical trapping of nanoparticles more space in comparison with the following section dealing with optical forces acting on bigger microparticles (Mie particles).

A dielectric nanoparticle illuminated by a light wave behaves like an induced point dipole that oscillates with the frequency of the incident electric field. Such an oscillating dipole is then subject to the forces stemming from the interaction with the electromagnetic field in its vicinity. Since the field oscillates very fast the motion of the particle cannot follow these changes; therefore, only a time-averaged value of the electromagnetic force is important for evaluating the changes in the motional state of the particle. This force consists of two terms: the first one corresponds to the force acting on the charges of the dipole placed in a spatially inhomogeneous electric field and the second one corresponds to the Lorentz force acting on the moving dipole charges:

$$\langle F_m \rangle = \frac{1}{T}\int_{-T/2}^{T/2} \sum_{j=x,y,z} \bar{p}_j \frac{\partial \bar{E}_m}{\partial r_j}\mathrm{d}t + \frac{1}{T}\int_{-T/2}^{T/2} \sum_{j,k=x,y,z} \epsilon_{mjk}\frac{\partial \bar{p}_j}{\partial t}\bar{B}_k \mathrm{d}t \tag{2}$$

where T is the period of the time-harmonic field, $\bar{p}_k$, $\bar{E}_k$, $\bar{B}_k$ are the real-valued kth components of the time-harmonic dipole $\bar{\mathbf{p}}(\mathbf{r},t) = \Re\{\mathbf{p}(\mathbf{r})\exp(-\mathrm{i}\omega t)\}$, and electric and magnetic fields $\bar{\mathbf{E}}(\mathbf{r},t) = \Re\{\mathbf{E}(\mathbf{r})\exp(-\mathrm{i}\omega t)\}$ and $\bar{\mathbf{B}}(\mathbf{r},t) = \Re\{\mathbf{B}(\mathbf{r})\exp(-\mathrm{i}\omega t)\}$, respectively, r_j are the spatial co-ordinates, and ϵ_{mjk} denotes the Levi-Civita tensor. Indices m, j, k run through the x, y, and z components of the vectors. The use of the Maxwell equations for the complex amplitudes of the vectors then gives [24]

$$\langle F_m \rangle \equiv F_m = \frac{1}{2}\Re\left\{\sum_{j=x,y,z} p_j \frac{\partial E_j^*}{\partial r_m}\right\} \tag{3}$$

where we dropped the symbols for the time averaging; $\Re\{\}$ and $\{\}^*$ denote the real part and complex-conjugated value of the quantity in the brackets, respectively, p_j is the jth component of the induced dipole that satisfies $p_j = \alpha E_j$, and α is the polarizability of the particle. In general, polarizability has real α' and imaginary α'' parts. The imaginary part α'' is associated with the particle absorption (for example, in metals) or with the interaction of the induced dipole with itself through the scattered light [25]. The polarizability can be expressed as

$$\alpha = \alpha' + \mathrm{i}\alpha'' = \frac{\alpha_0}{1 - \frac{2}{3}\frac{\mathrm{i}k^3\alpha_0}{4\pi\epsilon_0\epsilon_1}} \simeq \alpha_0 + \mathrm{i}\frac{|\alpha_0|^2 k^3}{6\pi\epsilon_0\epsilon_1} \tag{4}$$

where ϵ_0 is the permittivity of vacuum, $\epsilon_1 \equiv n_1^2$ is the relative permittivity of the medium surrounding the particle, $k = 2\pi n_1/\lambda_0$, $|\alpha_0|$ denotes the absolute value of α_0, and α_0 can be obtained from the Lorentz–Lorenz relation as follows:

$$\alpha_0 = 3\epsilon_0 V \frac{\epsilon_2 - \epsilon_1}{\epsilon_2 + 2\epsilon_1} \tag{5}$$

where $\epsilon_2 \equiv n_2^2$ is the relative permittivity of the particle and n_2 its refractive index. For an absorbing particle ϵ_2 and consequently α_0 are complex. Therefore,

$$\alpha' \simeq \Re(\alpha_0),\ \alpha'' \simeq \Im(\alpha_0) + \frac{|\alpha_0|^2 k^3}{6\pi\epsilon_0\epsilon_1} \tag{6}$$

If the complex electric field component of the light wave E_m is expressed using real amplitude E'_m and real phase ϕ':

$E_m \equiv E'_m \exp(\mathrm{i}\phi')$, Eq. (3) can be further rewritten as

$$F_m = \frac{1}{2}\sum_{j=x,y,z}\left[\alpha'\frac{1}{2}\frac{\partial({E'_j}^2)}{\partial r_m} + \alpha''{E'_j}^2\frac{\partial\phi'}{\partial r_m}\right] \tag{7}$$

Therefore, the optical force acting on a nanoparticle can be understood as a sum of the so-called *gradient* or *dipole force* (the first term in Eq. 7) and the *scattering force* (the second term in Eq. 7). The gradient force is caused by the gradient of the optical intensity $I \sim \sum_{j=x,y,z} E'^2_j$

$$F_m^{\mathrm{grad}} = \frac{1}{4}\alpha'\sum_{j=x,y,z}\frac{\partial({E'_j}^2)}{\partial r_m} \tag{8}$$

and it is proportional to the real (dispersive) part of the particle polarizability. The scattering force is proportional to the optical intensity (radiation pressure), the imaginary (dissipative) part of the particle polarizability, and also the gradient of the wave phase, and it is given as follows:

$$F_m^{\mathrm{scat}} = \frac{1}{2}\alpha''\sum_{j=x,y,z}{E'_j}^2\frac{\partial\phi'}{\partial_{r_m}} \tag{9}$$

The scattering force itself is not capable of confining the object in space just by optical means even if more complicated spatial light intensity distributions are considered [26]. To compensate scattering force and to confine the object, other counter-acting forces such as gravity, hydrodynamic force, *etc.* must be employed. On the other hand, the spatial particle confinement solely by optical means is possible if spatial gradients of the optical intensity are present. The place where the particle is confined is called *optical trap*.

In order to illustrate the properties of both types of forces let us express the optical force acting on the same particle in an incident plane wave, a standing wave created by interference of two counter-propagating plane waves, and a moderately focused Gaussian beam ($w_0 \geq 10\lambda$) with the beam waist radius w_0 and Rayleigh length $z_R = \pi w_0^2/\lambda$:

Plane wave	Standing wave
$E_x(z) = E_0\exp(\mathrm{i}kz)$	$E_x(z) = 2E_0\cos(kz)$
$F_z^{\mathrm{gr}}(z) = 0$	$F_z^{\mathrm{gr}}(z) = \alpha' kE_0^2\sin(2kz)$
$F_z^{\mathrm{scat}}(z) = \frac{1}{2}\alpha'' kE_0^2$	$F_z^{\mathrm{scat}}(z) = 0$

Gaussian beam ($w_0 \geq 10\lambda$, $z \ll z_R$)

$$E_x(r,z) = E_0\frac{z_R}{z_R+\mathrm{i}z}\exp\left[\mathrm{i}kz + \mathrm{i}k\frac{r^2}{2z-\mathrm{i}z_R}\right] \tag{10}$$

$$F_r^{\mathrm{gr}}(r,z) \simeq \alpha' kE_0^2\frac{-rz_R^3}{2(z^2+z_R^2)^2}\exp\left(-\frac{kr^2z_R}{z^2+z_R^2}\right)$$

$$F_z^{\mathrm{gr}}(0,z) = -\frac{1}{2}\alpha' E_0^2\frac{z}{z_R^2}$$

$$F_z^{\mathrm{scat}}(0,z) \simeq \frac{1}{2}\alpha'' kE_0^2$$

where r is the radial co-ordinate $r^2 = x^2 + y^2$ and E_0^2 can be related to the incident Gaussian beam power P: $E_0^2 = 4P/(\pi w_0^2 n_2 \epsilon_0 c)$.

The example of the standing wave shows that if $\alpha' > 0$ ($n_2 > n_1$ in Eq. (5), *i.e.* the refractive index of a non-absorbing particle is larger compared with the surrounding medium), the nanoparticle is confined in the intensity maximum of the interference fringe (antinode). Here, the axial gradient force acting on the particle is zero and a small displacement of the particle from its equilibrium position leads to a restoring force that pulls the particle back. In this configuration, the total axial scattering force is zero as the scattering forces resulting from the two counter-propagating waves cancel each other. In contrast, under a plane wave illumination the axial intensity gradient is zero and the particle is propelled by the scattering force in the light propagation direction without a stable confinement. In the case of absorbing particles ($\Im(\alpha_0) \neq 0$) the scattering force also contains – in addition to the radiation reaction force [27] – a contribution due to the light absorption. In air or vacuum the motion of the illuminated particles is accelerated. In a liquid, where the motion is overdamped, the particles almost instantaneously reach a terminal velocity v done by the balance between the optical force and the Stokes friction force: $v = F_{\mathrm{opt}}/\gamma$, where γ is the viscous drag coefficient.

In the case of a single moderately focused Gaussian beam both radial and axial forces are present. In the radial direction, the dominant gradient force F_r^{gr} pushes an optically denser nanoparticle ($n_2 > n_1$) toward the radial equilibrium located on the beam's optical axis. Therefore, the axial gradient and scattering optical forces are expressed in Eq. (10) only for the on-axis nanoparticle locations. Here, the axial gradient force can be sufficient to overcome the scattering force and the axial equilibrium can be reached [28]. Thus, the so-called *single-beam optical trap* is created that forms the basis of OT [10] Using the approximation of a moderately focused Gaussian beam (see above) such a single-beam optical trap is formed on the optical axis at the distance z_{eq} behind the beam waist:

$$z_{\mathrm{eq}} = \frac{\alpha''}{\alpha'}kz_R^2 \tag{11}$$

If Eq. (5) is evaluated for a nanoparticle with $a \leq \lambda/20$, it can be shown [28, 29] that the gradient force is dominant even for relatively moderate intensity gradients and therefore $z_{\mathrm{eq}} \simeq 0$. For sufficiently small displacements of the trapped particle from the equilibrium position ($z - z_{\mathrm{eq}} \ll z_r; r \ll w_0$), the net radial and axial optical forces are linearly proportional to the displacement; this feature has found numerous applications in the external force measurements (see Section 4.1). The constant of proportionality between the particle displacement in the respective direction and the optical force acting on it is called *trap stiffness*. It also serves as a criterion for evaluating the optical trap performance with higher stiffness being indicative of a better trap.

If the refractive index of a non-absorbing nanoparticle is smaller relative to the surrounding medium ($n_2 < n_1$), the nanoparticle is pushed by the gradient forces to the places of lower intensity. In the case of a Gaussian beam it is pushed away from the beam axis and, therefore, it cannot be spatially confined. Several techniques of how to confine such particles are described in Section 3.4.

Let us stress here the different dependences of the gradient and scattering forces acting on nanoparticles on the non-absorbing particle size. While the gradient force increases linearly with the particle volume ($\alpha' \sim V$), the scattering force rises as V^2 (since $\alpha'' \sim V^2$). Therefore, in a moderately focused beam the scattering force becomes dominant with increasing particle radius. Eventually, the particles can no longer be axially trapped; instead they are propelled along the beam propagation direction (see Fig. 1A). In the case of a highly absorbing particle, the dominant force contribution destabilizing the spatial confinement is due to the light absorption. Similar to the gradient force, it is also proportional to the particle volume ($\alpha'' \sim \Im(\alpha_0) \sim V$). Thus, even for tiny particle sizes the absorption force competes with the gradient force and causes difficulties with the particle confinement in a single beam.

Even though the terminology of gradient and scattering forces and presented conclusions are valid only in the domain of nanoparticles, they can be applied with caution also to slightly bigger particles in order to obtain at least an estimation of the expected particle behavior. One has to be aware, however, that outside of the nanoparticle domain the forces change less rapidly with the increasing particle size and, eventually, the phenomenon of structural resonances appears, which causes non-monotonous changes in the force magnitude with growing particle size. For the sake of simplicity, we will use the terminology of the gradient and scattering forces even for bigger particles to distinguish whether the particle behavior is ruled by the intensity gradients or radiation pressure effects.

2.2 Optical forces acting on microobjects

It is much more complicated to express the force interaction of a spatially inhomogeneous optical field with an object of larger size (comparable to the trapping light wavelength) and/or irregular shape. A general approach for the optical force calculations in this case lies in evaluating the integral of the Maxwell stress tensor over an arbitrary closed surface enclosing the studied object. Under the steady-state conditions only the time-averaged values of the electromagnetic forces can be observed; therefore, the final optical force acting on the object reads as [30]

$$\langle F_i \rangle = \left\langle \oint_S \sum_j T_{ij}^M n_j \, \mathrm{d}S \right\rangle \tag{12}$$

where T_{ij} are the components of the Maxwell stress tensor and n_j are the components of the unit normal vector pointing outwards of the integration surface S. The stress tensor components have the following form:

$$T_{ij}^M = \epsilon \bar{E}_i \bar{E}_j + \mu \bar{H}_i \bar{H}_j - \frac{1}{2}(\epsilon \bar{E}^2 + \mu \bar{H}^2)\delta_{ij} \tag{13}$$

where ϵ and μ are the permittivity and the permeability of the medium around the object, respectively, and the vectors $\bar{\mathbf{E}}$, $\bar{\mathbf{B}}$ describe the final electric and magnetic fields outside the object given by the superposition of the incident and scattered fields.

The scattered field can be expressed analytically only for a limited number of symmetries of the object. The most frequently treated shape is a sphere where the Mie scattering theory is used [31–36]. A group of spheres can be treated using the multiple Mie scattering theory [37, 38]. Except spherical objects, spheroidal or cylindrical ones are also often considered theoretically [39–41]. Optical forces acting on particles with more complex shapes must be calculated using numerical approaches – for example, coupled dipole method [42, 43], finite element method [44], or finite-difference time-domain method [45–48]. A Matlab toolbox is available for the calculation of optical forces acting on spherical and spheroidal objects in Gaussian and other beams [49]. If the object is much larger than the trapping light wavelength, the ray-optics model can be used [33, 50–52]. For the understanding of the rest of the paper, however, the exact knowledge of the optical forces is not so important as the final behavior of the objects can be estimated qualitatively without tedious calculations.

Figure 1 illustrates frequently used configurations of the trapping laser beams and particle behavior in them. In the following sections, we will describe in more detail the key features and benefits of these configurations.

3 Experimental realizations of optical trapping and manipulation

The early experiments in the field of optical trapping and manipulation are connected closely to the work of Ashkin and his team. He was the first one who realized that even a moderately focused laser beam can be used to propel microobjects and atoms. He demonstrated guiding of particles [5], their levitation against the gravity in vacuum [53] and air [6], observation of Mie structural resonances in a levitated particle [54], particle confinement in 3-D by a dual-beam trap [5], single-beam trapping [10], and trapping using feed-back system [53]. These scientific achievements that paved the way for his numerous followers are summarized in several of his overview publications [7–8]. Except these publications there exist several very good introductory or overview articles that deal with selected topics of optical micro-manipulation and its applications [19, 55–63]. Therefore, we will not go into too much detail in this section and we will rather focus on the principles of each method and describe configurations that are used to manipulate or trap the particles.

3.1 Dual-beam optical trap

The first trap that used exclusively the forces of light to confine particles in 3-D was based on two counter-propagating non-interfering moderately focused laser beams with their foci placed in front of each other [5] (see Fig. 1B). Such a configuration ensures compensation of the counteracting axial scattering and gradient forces in between the beam foci while the radial gradient forces of both beams keep the object localized on the beams axes. Because of its simplicity and robustness with respect to the quality of the beams, this configuration, which is nowadays called *dual-beam trap*, was much later adopted for dual-beam and multiple-beam fiber trapping schemes [64, 65], optical stretcher [66–68], integrated opto-fluidic trapping systems [69], Raman microspectroscopy of trapped objects [70], and 3-D trapping using moderately focused beams [71–73]. Another great advantage of the dual beam trap is the low intensity of the trapping beams sufficient for a stable 3-D confinement, which suppress the risk of photodamage (''optocution'') of living specimens.

3.2 Single-beam trap: OT

The best-known tool for optical micro-manipulation is the single-beam gradient optical trap – OT [10]. OT have found numerous applications in various branches of physics, colloidal chemistry, and cell and molecular biology, especially in the measurements of weak external forces that will be discussed in more detail in Section 4.1. OT use a single tightly focused laser beam, which ensures 3-D spatial confinement of microobjects and nanoobjects having refractive index higher than the surrounding medium *via* gradient optical forces (see Fig. 1C). If biological specimens are to be manipulated, usually near-infrared wavelengths are used (Nd:YAG or fiber lasers at a wavelength of $\sim$1064 nm) in order to minimize the impact on the trapped specimen [74]. Positioning of the trapping beam focus with respect to the surrounding medium or surface enables 3-D non-contact manipulation with the trapped object. An obvious advantage of OT is that the beam approaches the sample only from one side and therefore it can be easily integrated with conventional optical microscopes. On the other hand, in the single-beam arrangement the axial gradient force must compensate the axial scattering force, which is difficult for highly scattering or absorbing particles (having too high refractive index) [49, 75]. Therefore, majority of experiments have been done with high numerical aperture (NA) oil-immersion microscope objectives with NA $\simeq 1.2 - 1.3$ and magnification 60–100 $\times$. As common high-quality objectives have low transmittance in the near-infrared spectral region, low-cost achromat objectives are frequently utilized, which give very good ratio of trap strength to objective price. A disadvantage of oil-immersion objectives is the significant decrease in trap performance (measured by the reduction in the trap stiffness) when the trapped object is manipulated far from the coverslip–water interface. The reason is the increase in spherical aberrations due to the refractive index mismatch at the interface [35, 76–78] which can be only partially compensated by the selection of the proper refractive index of the immersion oil [79]. Therefore, water-immersion objectives are employed if long-range stable manipulation along the beam propagation direction is demanded [34, 80]. A detailed protocol of how to set up and align the OT system can be found in [61]. There also exist several companies on the market selling commercial systems with various degrees of complexity (http://www.cellrobotics.com; http://www.arryx.com; http://www.elliotscientific.com; http://www.palm-microlaser.com; http://www.netdyalog.com/news/jpk/06/020.asp?117611-183367-940908-137504; http://www.meopta.com).

3.3 Multiple-particle trapping

The OT in their classical form use a single focused laser beam; therefore, only one object at a time can be trapped in a controlled manner. This of course imposes a limitation on all applications that need simultaneous manipulation with many particles, preferably in an independent and controlled manner. Some examples addressed in more detail in the following sections include spatial or surface arrangement of many microparticles (colloids) or living cells [71, 81–84], high-throughput optical manipulation [85–87], manipulation with and rotation of non-spherical and elongated objects [73, 88], or multipoint microrheology and velocimetry based on optically trapped probes [89, 90].

Gradually several methods have been developed to address this issue. One of them suggested by Sasaki *et al.* uses a single laser beam, which is scanned rapidly between several positions – desired optical trapping locations – in a single focal plane [91]. An object can be confined at one of these positions while the trapping beam briefly stops there during the scanning cycle. When the beam illuminates a different position, the object is again released and free to diffuse out of the trap location. However, the particles must not escape out of the range of the trapping beam to be re-trapped and therefore the scanning cycle must be sufficiently fast [92, 93]. Such *time-sharing optical trapping* works well if the beam repetition rate is within tens of Hz to kHz. Usually, the following beam deflection systems are used: galvano-optical mirrors [91], piezo-mirrors [94], acousto-optical deflectors [95], electro-optical modulators [96], and moving lenses with miniature coil-magnet assembly [97]. Owing to their inertia the moving mirrors or lenses provide repetition rates slower by several orders of magnitude in comparison with the acousto- or electro-optical modulators. This method originally enables one to scan the trap only in a single focal plane [91, 95] but it was also extended into two different axial planes by Vossen *et al.* [71].

Another way of generating multiple trapping beams is splitting a single laser beam into more beams by polarizing beam splitters [98] or diffractive elements [99]. The highest

degree of freedom can be currently reached using SLM that enable to configure dynamically the number of trapping beams and their wavefront profiles for different trapping tasks. Trapping systems based on SLM are commonly termed *holographic OT* (HOT) [56, 100, 101] and they enable to generate variable number of optical traps placed in various lateral and axial positions. Recently Jesacher *et al.* employed double passage of the beam through SLM to shape both the amplitude and the phase of the trapping beam. Using this approach they tailored phase gradient along the high-intensity light pattern, which caused the scattering force (see Eq. 9) to push the object along this ''light pathway'' [102]. A special chapter devoted to HOT can be found in [18] and a comprehensive list of references is compiled in [103]. Glückstad *et al.* used an imaging method based on generalized phase contrast to manipulate with many particles in a single plane [104] and later on they used two counter-propagating beams to get full and fast dynamic 3-D control over the particle positions [72]. Under certain circumstances the multiple trapped particles can also be used as handles (micro-fingers) to manipulate with another larger particle that is not directly illuminated by the trapping light [105, 106]. Codes for generating holograms for driving the SLM are available in LabView (http://www.physics.gla.ac.uk/Optics/projects/tweezers/slmcontrol/BlueTweezersMulti.llb) or Java [107] platforms.

Other solutions for multiple-particle trapping are not as flexible as the above-mentioned techniques, the trap positioning is limited, but they are much simpler and easier to integrate into compact lab-on-a-chip systems. Ogura *et al.* used an array of surface-emitting laser diodes to generate several optical traps [108], Tam *et al.* used a digital micromirror device combined with the imaging fiber-bundle [109], and Sun *et al.* used microlens array and Talbot effect to generate a 3-D array of optical traps [110, 111]. Merenda *et al.* used quite a novel solution based on a matrix of micromirrors illuminated by a single collimated laser beam [112] (see Fig. 2). They integrated the mirrors into a microfluidic system and they used the same mirrors to collect the fluorescence signal from the trapped particles. No demands on using high NA optics for trapping and no restrictions on the field of view make the system interesting for opto-fluidic integrations even though the obtained density of the traps was only 20 traps/mm^2.

Interference of several coherent laser beams can also generate multiple optical traps; depending on the particle size and refractive index, these traps are located either in the high-intensity part or in the low-intensity part of the interference fringes (see Fig. 1D). Interference of two tilted co-propagating laser beams creates the so-called *interferometric tweezers* that provide several optical traps; however, the objects are trapped only laterally and they have to be pushed against a surface in order to compensate the axial scattering force and to achieve a 3-D confinement [113–116]. The use of a third counter-propagating but non-interfering beam can also compensate the scattering force of the two co-propagating beams and provide full 3-D spatial confinement of multiple objects [117]. Interference of several co-propagating co-axial beams with different axial wave vector components creates periodic intensity variations along the propagation direction, which was also utilized for axial object confinement [118, 119]. Multiple-particle trapping along the beam propagation axis was demonstrated using two counter-propagating coherent beams forming the so-called *standing wave trap* [75, 120, 121]. Even though the inter-trap distances are fixed, the positions of the traps can be precisely moved in space by phase change in one of the interfering beams. Therefore, the whole interference structure with up to thousands of confined particles [122] can be precisely and simultaneously translated and forms the so-called *optical conveyor belt* [85–87]. Interference of several beams arranged in a single plane [29, 123, 124] or in space [118, 125] has also been considered.

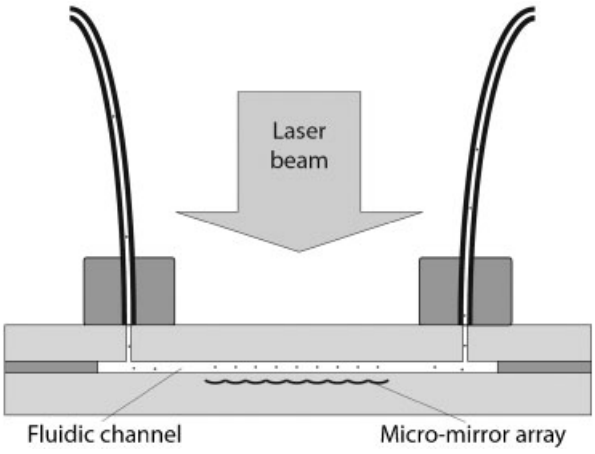

Figure 2. Schematic illustration of a microfluidic device for multiple-particle trapping using a matrix of micro-mirrors. The solution of particles flows between two microscope slides: the bottom microscope slide embedding the micromirror array and the top microscope slide with holes for fluidic access. Simply directing a collimated laser beam on the fluidic device creates the traps in the fluidic channel. Reprinted with permission from [112]. Copyright (2007), Optical Society of America.

Many emerging applications of optical forces, such as the study of Brownian motion of colloidal particles in external potentials or optical sorting, do not need actual particle confinement. In these applications arrays of optical traps or tailored spatial intensity distributions (so-called optical potential landscapes) are used to influence the dynamics of motion of particles passing though the light pattern (see Section 4.6).

3.4 Trapping of low-refractive-index particles

If the refractive index of the particle is smaller than that of the surrounding medium, the particle (*e.g.* a micro-bubble or a hollow colloidal particle with air-filled cavity) is pushed out of the high-intensity region by the gradient force and, therefore, it cannot be trapped in the focus of classical OT.

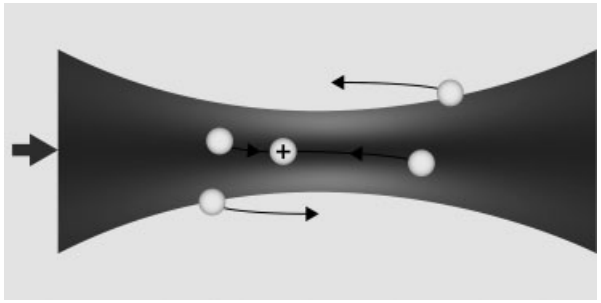

Figure 3. 3-D spatial trapping of particles with refractive index lower than the refractive index of the surrounding medium. A hollow beam (optical vortex) having intensity minimum on the optical axis must be used.

An optical vortex has intensity minimum on the beam axis and enables 3-D trapping of such particles above the focus. Here the balance is established between the axial scattering force pushing the objects toward focus and the gradient force acting in opposite direction (see Fig. 3 and Eq. 10) [126–128]. Surprisingly, however, spatial confinement of micro-bubbles was reported in a single focused beam of a 100 fs pulsed laser (250 kHz repetition rate with an average power of 250 mW) which was self-focused in water [129]. Another possibility is to create so-called *optical bottle*, a region where the optical intensity minimum is surrounded by high-intensity region [119, 130–135], and to localize spatially the low-refractive-index particles there. The problem, however, is how to get the particle into this region. Two-dimensional trapping of low-index particles is possible in the low-intensity part of the interference fringe [115] or annular light profile [136–138]. Scanning OT [139] or two rotating traps [140] create a low-intensity optical region in the center of the scanning pattern where the low index particles can be trapped in 3-D too.

3.5 Near-field optical manipulation

The term *near-field* describes electromagnetic field that does not propagate in space and exists only in a close vicinity (on the order of the light wavelength) of interfaces, sub-wavelength apertures, or sub-wavelength-sized structures. The intensity of such a field (also called evanescent field) decays exponentially with increasing distance from the interface and, therefore, the interaction between the light and medium is limited to a distance of about one wavelength away from the surface. Since this field is not radiating, its spatial variations are not constrained by the diffraction limit and sub-wavelength-sized regions of high intensity can be obtained [27, 141]. Using surfaces with structured optical properties and proper mode of their illumination, extended areas with sub-wavelength intensity modulations can be easily obtained. These properties have recently found numerous applications in the fluorescent microscopy (so-called total internal reflection fluorescence microscopy) [142] and they also enabled to beat the diffraction limit of the classical optical microscopy giving birth to a new generation of optical microscopes – so-called near-field scanning optical microscopes [143–145].

The classical method of the evanescent field generation uses total internal reflection at a dielectric interface between a glass prism and a lower refractive index medium (*e.g.* water). In the so-called Kretschmann configuration the sample mounted in a liquid is put above the prism and the evanescent wave penetrates into it and influences the particles dispersed there (see Fig. 4). This set-up does not need focusing optics (it is sometimes called lens-free) and it provides more flexibility in the design and much larger illuminated area over which the particles can be manipulated or organized [146–151]. Disadvantage is usually a more complex and less stable set-up. Since the evanescent wave has the highest optical intensity near the surface, the high-index particles are pulled by the gradient force to the vicinity of the surface. However, due to the scattering force caused by the evanescent wave propagation along the surface, the particles are guided in the evanescent wave propagation direction [152] (see Fig. 4). Particle or living cell guiding can also be obtained by the evanescent wave penetrating from fibers [153, 154] or optical waveguides [155–161] (see Fig. 5).

Particle velocity up to 130 μm/s can be obtained with an injected laser power equal to 25 mW [161]. Guiding of metallic nanoparticles or microparticles above the waveguide was also reported [162, 163]. In the case of metallic microparticles it was demonstrated that the particles are attracted to the waveguide if transversal magnetic (TM) polarization of the evanescent wave was used [161]. Especially the waveguides offer an excellent possibility to integrate microfluidic and optical systems into real opto-fluidic circuits suitable for lab-on-a-chip applications [164].

A counter-propagating geometry of two evanescent waves was used to localize particles above the waveguide [165, 166], create 2-D self-arranged colloidal crystals [81, 167] or structures consisting of thousands of microobjects above the interface [82–84], deliver the microparticles

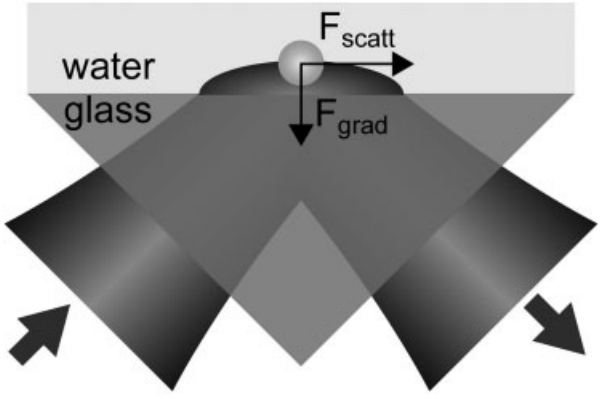

Figure 4. Kretschmann configuration for the generation of the near-field (evanescent wave) along the interface between the prism top surface and aqueous environment above it.

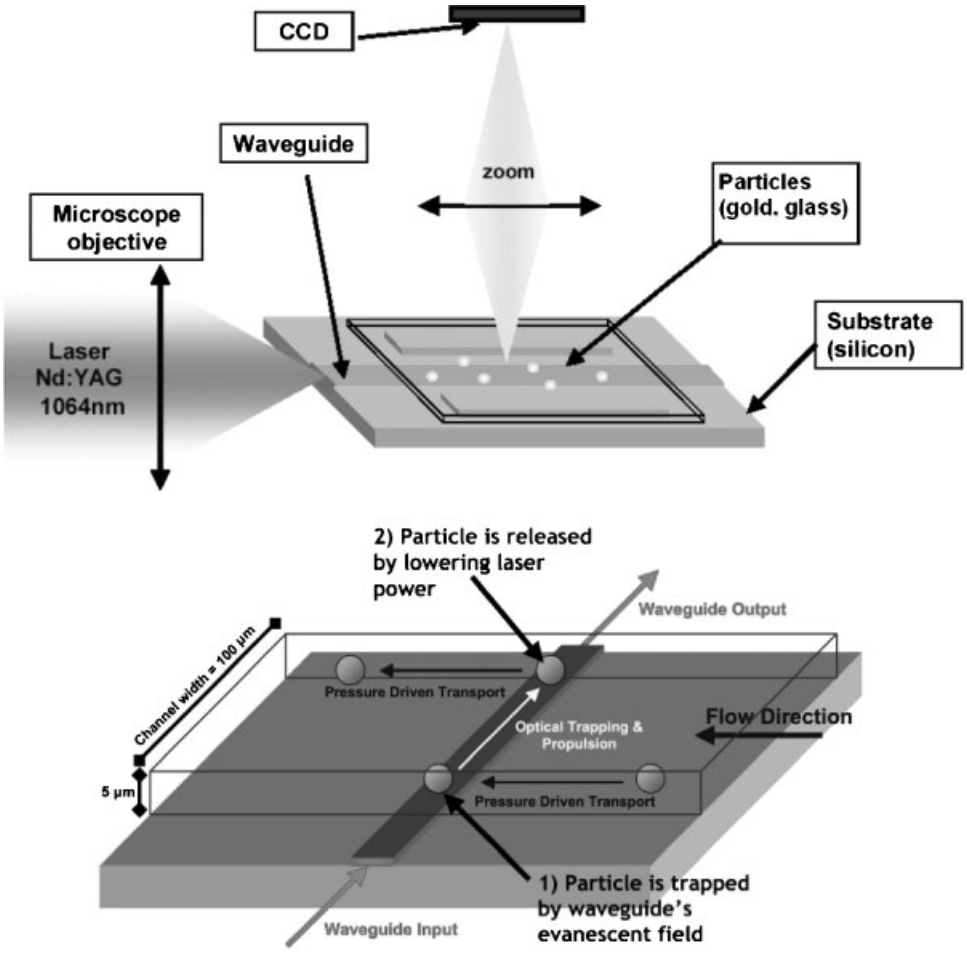

Figure 5. Examples of experimental arrangements enabling particle confinement and delivery in microfluidic systems using the evanescent field above an optical waveguide. Reprinted with permission from [161] (top) and [160] (bottom). Copyright (2007), Optical Society of America.

bi-directionally [87] or sort sub-micrometer size objects according to their sizes [166].

The Kretschmann geometry is extremely efficient for coupling the incident light into so-called whispering-gallery modes of the manipulated spherical objects that can enhance the optical force by several orders of magnitude [168]. The evanescent field and consequently the acting optical force can be further enhanced by an order of magnitude by using a dielectric waveguide on the top of the prism. Such a waveguide provides coupling of the incident field into its cavity where the field intensity increases and penetrates out as an amplified evanescent wave [83, 84, 169, 170]. Theoretical studies have shown that the particles can also be spatially confined in the evanescent field that is highly localized around the nano-aperture or nanometer-sized tip [171–173].

Special microscope objectives with NA exceeding 1.4 (so-called TIRF objectives) have been designed to generate evanescent field illumination for excitation of fluorophors in living cells. They have been also used to generate efficient optical traps with significantly reduced trapping volume for trapping [174] or optical stretching of microobjects (red blood cells) by a highly inhomogeneous field [175] (optical stretcher is described in Section 4.3). A review of the topic of near-field manipulation can be found in a special chapter of [18] or in [62].

3.6 Plasmon-based optical manipulation

This very recent type of optical micro-manipulation employs the enhancement of the electric field intensity near a metal surface or a metallic nanoparticle due to excitation of collective electron oscillations – surface plasmon polaritons (SPP) – in the metal surface layer. Under the SPP excitation conditions even less laser power is needed to manipulate with the objects enabling also large-area manipulation. Typical set-up for generating SPP again uses Kretschmann geometry with the top surface of the prism covered by a metal (usually gold or silver) layer. Electric field enhancement near this layer is capable of increasing the surface-guiding optical forces by 2 orders of magnitude [176] or to localize simultaneously thousands of particles [177]. Force due to the SPP excitation in a system of metal layers can be by one or 2 orders of magnitude stronger comparing to a dielectric interface [178, 179].

The so-called localized surface plasmons can be excited in isolated metallic nanoparticles; this again leads to the enhancement of electric field close to the particles and, consequently, higher optical forces acting on such particles [180–184]. Spatial confinement of particles was obtained above such a structured metal surface [185–189] due to the strong intensity gradients at the edges of metallic objects. Instead of a solid metal layer a random distribution of metallic nanoparticles illuminated perpendicularly to the surface can also be used [190]. For more details we refer to recent reviews on this topic [190–192].

3.7 Optically induced rotation of microobjects

Up to now we have dealt with the transfer of linear momentum from a light beam to material objects, which enables their stable spatial confinement or acceleration. In this section we will address the possibilities of transferring the angular momentum from the light to the trapped objects, which can cause them to rotate around a certain axis. To this end, the following principal mechanisms have been employed: the angular momentum is carried by the light itself and transferred to the object, angular-momentum-free beam is scattered by an object with a helical shape, or asymmetric objects are rotated by multiple OT or varying direction of the trapping beam polarization. A more detailed description of this topic can be found in special chapters of [18, 193, 194].

The most straightforward way is to use multiple-beam OT and grip a single asymmetric object at its different parts. These trapped parts follow the spatial motion of the individual trapping beams and, consequently, the object is rotated and also trapped in 3-D [73, 88]. Other methods based on this principle use rotation of an asymmetric trapping beam or interference pattern [194–198]. It was demonstrated that the torques produced this way are quite significant [199].

When a circularly polarized beam passes through a birefringent material that changes the light polarization from right-handed to left-handed (or *vice versa*), the polarization changes result in torque that rotates the object (similar to the classical Bethe's experiment) [200, 201]. This can be understood on the level of individual circularly polarized photons carrying so-called spin-angular momentum of size $\hbar$ which is transferred to the object when the photon passes through it. The maximum angular momentum change is $2\hbar$ for an object causing phase retardation $\lambda/2$ (lambda-half waveplate). Upon illumination with circularly polarized light, birefringent objects (calcite, quartz, or vaterite particles) rotate with a constant angular velocity. For a particle immersed in a viscous liquid (overdamped system), this terminal angular velocity is reached almost instantaneously and its value is determined by the balance between the optical torque and the viscous drag torque of the surrounding liquid [202–205] (see Section 4.4).

Particles elongated along one axis possess a higher polarizability along this axis and therefore they are called shape-birefringent. Such particles can again spin in a circularly polarized beam. However, they have to be prepared with a special shape in order to prevent them from orienting with their long axis along the beam propagation direction; this can be achieved *via* photopolymerization [206] or microlithography [207]. If such objects are placed into a linearly polarized beam they orient with their longer axis along the direction of the light polarization [206–208]. Rotation of this polarization by a rotating lambda-half plate then ensures particle rotation. This mechanism was employed in the orientation of cells with chloroplasts [209] or in the quantitative measurement of torsional stiffness of biomolecules [203, 210] and it represents an alternative to magnetic tweezers [211–214] in these applications [215–218].

Photopolymerization at the microscale has been also used to create objects with a helical shape. Upon illumination with a single beam they are trapped in this beam and scatter light in such a way that the net angular momentum of photons is changed. Therefore, the object starts to rotate around its axis similar to a windmill [219–223]. Light-driven micro-gears have also been demonstrated [224]. A rotating ZnO and Al_2O_3 nanorods [225] or colloids with surface covered partially with a metal layer [226] have also been reported.

Recently beams with a helical spatial phase distribution (so-called optical vortices) have been studied [193, 227–231]. These beams posses the so-called orbital angular momentum of size $m\hbar$, where m (integer) is related to the helicity and is termed the topological charge of the helix. Such beams can be generated by diffractive optical elements [232, 233] or SLM [56]. Since both techniques also enable generating multiple trapping beams, they form the basis for implementation of advanced microfluidic system components (*e.g.* optically driven pumps – see Section 5.3). Absorbing particles sufficiently big so that they cover the central low-intensity region of the beam and their center is localized on the beam axis can rotate under the influence of both spin and orbital beam angular momenta [234–237] – forming a so-called *optical spanner*. Smaller particles are confined in the high-intensity circular fringes and move around them due to the orbital angular momentum exchange [238–240].

3.8 Comparison with non-optical micro-manipulation methods

There exist several micro-manipulation methods based on various principles that predate optical trapping. The so-called dielectrophoresis is based on the concept that is very similar to the gradient optical force in a strongly inhomogeneous light field except the alternating electric field is of much lower frequency (typically by 7–10 orders of magnitude). Therefore, the frequency dependence of the particle

permittivity can be utilized over a wider range of frequencies and positive or negative dielectrophoretic migration can be obtained with particle moving toward the high- or low-intensity regions of the field, respectively [241]. Usually microelectrodes are necessary to create localized spatially inhomogeneous field and, therefore, the objects can be trapped but not manipulated in 3-D [242]. However, a more elaborate system of electrodes can provide objects delivery or rotation by switching the field intensities on individual electrodes [243]. There exist a series of examples of how these techniques have been used for trapping and manipulation of micron-sized and nano-sized objects, field-flow fractionation, *etc*. [241–244]. The presence of AC power induces heating in the system and the necessity for using electrodes limits the flexibility of the dielectrophoretic techniques for micro-manipulation. This obstacle was overcome in an elegant manner by Chiou *et al*. who used dielectrophoresis in combination with photoelectrodes dynamically controlled and reshaped by the structured illumination patterns (so-called *optoelectronic tweezers*) [245]. Much lower laser power was needed for particle confinement compared with OT and very complex object manipulation including delivery and sorting on a single surface was demonstrated.

Magnetic tweezers enable confinement, manipulation, and controlled rotation of super-paramagnetic micro-particles in an inhomogeneous magnetic field [14, 211–214]. Owing to their magnetic moment $\boldsymbol{\mu}$ induced in an external magnetic field $\boldsymbol{B}$, super-paramagnetic particles experience a force proportional to the magnetic field gradient $F_i = \sum_{j=x,y,z} \mu_j \frac{\partial B}{\partial v_j}$, analogically to the optical gradient force. Moreover, since the magnetic dipole moment of the particle assumes a preferred orientation in the magnetic field, magnetic tweezers can also apply well-defined torque to the particles by controlled rotation of the magnetic field [211, 216]. Magnetic tweezers micro-manipulation differs from the optical trapping in that a magnetic field maximum cannot be created in free space and cannot be manipulated other than by shaping the magnetic elements. This makes the creation of a stable 3-D magnetic force trap challenging, typically requiring the presence of a feedback loop or an external force balancing the magnetic force. On the other hand, it results in the ability to create a uniform force over a large area, enabling many systems to be probed at once and permitting fast parallelized data collection. Magnetic tweezers have found numerous applications in the mechanical single-molecule experiments [14, 216] and microrheological measurements on both artificial and living systems [246, 247] (see also Section 4.4).

Hydrodynamic focusing [248, 249] is based on the laminar properties of the fluid flow at the microscale; thus, when a particle is injected into such a flow it follows a stable streamline. In a carefully designed system of merging microfluidic channels with well-controlled fluid velocities, counter-acting hydrodynamic forces enable to squeeze the stream or modify the streamline trajectory and consequently also the particle movement.

Another mechanism of particle motion in a fluid is caused by thermal gradients existing in the fluid. This effect has many names, *e.g*. thermodiffusion, Ludwig-Soret effect, thermophoresis and typically causes particle motion from hot to cold regions. The thermal gradients can be generated, for example, by absorption of light in a metal layer or metallic particles causing inhomogeneous heating of the surrounding liquid. They lead to fluid thermal convection and the above-mentioned thermophoresis – in this context also called radiometric forces or photothermophoresis [250–252]. Usually both convection and thermophoresis are stronger than the optical forces [22]; however, if all these effects are comparable, unexpected particles motion or self-organization can be observed [177, 252, 253]. A completely different mechanism propels droplets or bubbles on the surface of a liquid with thermal gradients created by laser absorption. It is a consequence of the difference of contact angles (surface tension) on the opposite sides of the object, which can move it up to hundreds of micrometers along the surface (so-called Marangoni effect or thermocapillary force) [254–259].

More detailed comparison of various micro-manipulation techniques, their ranges of applicable forces, spatial and temporal resolutions, and additional features can be found in reviews [14, 216, 217, 260].

3.9 Optical microablation and microdissection: laser scalpel

Optical trapping and micro-manipulation techniques are mainly based on the use of continuous-wave (cw) lasers whose light beams are shaped in such a way to create stable traps for spatial confinement of micro- and nanoobjects or extended potential landscapes for selective control of the trajectory of such objects. In all these applications, the wavelength of the used light is chosen in order to minimize the absorption of the light in the target objects and, consequently, their possible damage. In contrast, *optical microablation and microdissection* (frequently also called *laser scalpel*) rely on the precisely localized destruction of the material by the deposition of energy contained in the light beam. Therefore, microscopic alteration or ablation of the target specimen (*e.g*. cells or sub-cellular structures, tissues, semiconductor, metallic, or polymeric surfaces, colloidal particles, *etc*.) is achieved. Unlike in the case of optical micro-manipulation, the absorption of light is a necessary prerequisite for the laser scalpel operation. Another difference between the two techniques is the use of pulsed laser beams for the ablative interventions, which allow the deposition of the light energy within the specimen on a very fast time scale (typically nanoseconds or shorter), thus triggering a number of physical processes (often non-linear, *e.g*. multiphoton absorption, plasma formation induced by optical breakdown of the specimen) that lead to the localized destruction of the specimen [261].

The idea of using a highly focused light beam for targeted destruction or ablation of the specimen is almost 100 years old. In 1912, Tschachotin built an ultraviolet

micro-irradiation device for the purpose of destroying selected regions of single cells and embryos [262]. The real advent of the optical scalpel, however, is tightly connected to the invention of the laser in 1959. As early as in 1962 Bessis *et al*. built the first laser scalpel using the ruby laser for ablation of sub-cellular organelles [263]. Since then, the laser scalpel has been used in a number of successful applications especially in the field of cell and developmental biology (see [15, 17] and references therein for a comprehensive review). A typical experimental approach relies on removing a selected structural element or organelle within the cell (*e.g.* mitotic chromosomes [264–266], centrosomes [267], individual mitochondria [268, 269], or microtubules [270, 271]) and studying the effect of this removal on the fate of the cell.

Laser microablation and micromachining techniques have been used extensively in analytical and synthetic chemistry and material science for quantitative optical and mass spectroscopic analysis of the composition of solid substrates [272], controlled synthesis of organic and inorganic nanoparticles [273, 274], and manufacturing of microfluidic systems [275]. Laser-based microablation is also a very promising technique for manufacturing the optical, mechanical, and electronic components of integrated photonic and microelectro-mechanical systems [276–278] that are vital components of lab-on-a-chip analytical devices capable of analyzing rapidly the chemical composition of sub-picoliter sample volumes [279–282].

3.10 Laser-pressure catapulting

Laser pressure catapulting (LPC) in combination with laser scalpel enables sterile isolation of selected cells or subcellular structures from the sample tissue for further structural and compositional analysis. The experimental procedure consists of two steps: first, a selected region within the sample (that is often placed on a special UV-absorbing polymer foil for increasing the efficiency of the ablation) is micro-ablated using a UV-wavelength laser scalpel. Subsequently, the ablated part of the specimen is transferred into an appropriate collection vial by using an intense focused or defocused pulse of the ablation laser beam. This light-mediated transfer does not require any mechanical contact with the transported sample; however, it is not based on the optical forces associated with the laser pulse. It is mediated by the pressure shock waves that follow the plasma generation in the irradiated specimen and/or photothermal ablation of the sample [283].

LPC technique was first introduced by Schütze and Lahr who applied it to the analysis of mRNA of a single cell isolated from archival colon adenocarcinoma [284]. Since its introduction LPC has been successfully applied to isolate and catapult cells from various types of tissues ranging from histological specimens to plant tissues and even delicate stem cells (see [17] and references therein for a review). Recently, 1 mm long living nematode *Caenorhabditis elegans* was successfully transported with LPC technique without impairing its viability (http://www.palm-microlaser.com).

4 Experimental devices and techniques using optical forces

Various realizations of optical micro-manipulation mentioned in the previous section have found exciting applications in which the optical forces are combined with other methods in order to create unique tools to study the processes at the micro- and nanoscale.

4.1 Measurement of weak interaction forces: optical pico-tensiometer

Combination of OT with sensitive detection of the trapped particle's position represented a major breakthrough in the application of the optical trapping techniques as it allowed the precise quantification of external forces acting on the trapped particle. In these experiments, the trapped particle serves as a probe that is displaced from its equilibrium position in the trap as a result of the measured external forces generated, for example, by interaction with a solid surface [285, 286], fluid flow [89], or pulling action of a molecule attached to the particle [11, 287, 288]. The force measurements are then based on the assumption of a linear relationship between the displacement of the trapped particle and the applied external force (see Fig. 6). Prior to the measurement, it is necessary to calibrate the force–displacement conversion constant (optical trap stiffness) that depends on the laser power, size and optical properties of the trapped probe, and optical properties of the immersion medium [57, 74]. With the use of the OT, it is possible to

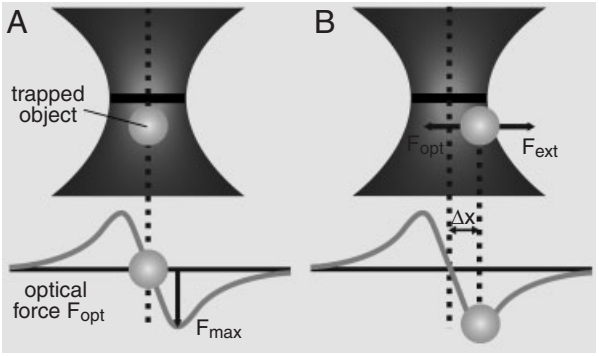

Figure 6. Principle of the external force measurement using OT. (A) When no external force is applied, trapped particle is resting at its equilibrium position in the trap with no net optical force F_{opt} acting on it. (B) External force F_{ext} causes displacement $\triangle x$ of the trapped particle from its equilibrium position; consequently, optical force F_{opt} starts acting on the particle that is equal in size and opposite in direction to F_{ext}. For small displacements from the equilibrium, relationship $F_{opt} = -\kappa\Delta x$ holds where κ is the optical trap stiffness. Maximal external force that can be measured is F_{max}.

measure weak external forces in the sub-pN range, which is not accessible using other force probes ((*e.g.* atomic force microscope (AFM) or micropipettes [14]).

Various techniques have been applied to detect the position of optically trapped particles with nanometer- or even subnanometer-range precision (see also a recent review by Greenleaf *et al.* [216]): direct imaging of the particle using video microscopy [289–291] or position-sensitive quadrant photodiode [95], back-focal plane interferometry with the light scattered from the trapped particle [34, 80, 288, 289–295], detection of changes of the polarization state of the trapping beam [287, 296, 297], or measurement of the intensity of the two-photon fluorescence excited in the trapped particle by the trapping beam [298, 299]. Using fast electronic feedback loops for controlling the trap position and/or stiffness in connection with on-line particle position detection, versatility of a force-measuring optical trapping system can be increased by introducing *position clamp* or *force clamp* operation modes [16, 57, 95]. In the position clamp mode the feedback stabilizes the trapped particle at a given position within the sample by changing the trapping force and the feedback error signal corresponds to the external force variations. Such a configuration is suitable for measuring the force-extension curves of individual polymer chains [300] or stall forces of molecular motors [301]. In the force clamp mode, on the other hand, the feedback system keeps the optical force acting on the trapped probe constant while the external force displaces the particle within the sample. This arrangement has been used to study the working cycle of molecular motors under a constant load [302, 303]. Recently, an all-optical force-clamping method was introduced that operates without an electronic feedback, thus increasing significantly the bandwidth of the force and displacement measurements [304]. Fast Matlab-based routines for precise calibration of position and force measurements with OT have been developed and are freely available [305–307].

Force-measuring OT in their various modifications have found numerous successful applications in characterizing the structure of and force interactions between molecular components of living cells – molecular motors carrying out intracellular transport (myosin-actin and kinesin/dynein-microtubule systems), DNA and RNA polymerases, biopolymers (DNA, RNA, actin, microtubules), and ligand-receptor systems (*e.g.* antibody-antigen) (see [11–14, 216–218] for a comprehensive review). These experiments helped significantly in understanding the fundamental functioning of biological cells with important implications for medicine. Recently a commercial system has been presented by JPK Instruments (http://www.netdyalog.com/news/jpk/ 06/020.asp?117611-183367-940908-137504) that should enable a wide range of users to perform single-molecule mechanical measurements without a need of developing their own experimental set-up.

Force measurements with OT are a subject worth its own review article (or rather a book) and detailed description goes beyond the scope of the present review. A comprehensive list of publications covering the theory, design considerations, and practical applications of OT up to 2002 can be found in [19] and further details are available in excellent overviews about optical trapping techniques, their recent trends, and applications [14–16, 55, 57, 58, 60–62].

4.2 Thermal noise imaging

An optically trapped micro- or nanoparticle can serve as a local probe for imaging the topography and mechanical properties of its immediate neighborhood. This can be achieved *via* scanning the particle through the sample while recording simultaneously its position in all three dimensions with the use of the above-mentioned position detection techniques. The probe displacements from its equilibrium position in the trap then correspond to its interactions with the structural features of the sample. In an analogy with the AFM that provides atomic-resolution maps of the surface topography, this scanning-probe imaging device has been termed *photonic force microscope* (PFM) [80, 299]. In contrast to AFM that generates the images by scanning a sharp tip attached to a flexible cantilever over the surface, PFM uses optical forces to hold the probe and, therefore, does not require direct mechanical contact with the sample. Consequently, it is possible to obtain images of internal specimen structures, provided the specimen is transparent for the used trapping light. Moreover, in contrast to AFM that can image only surface topography, PFM is capable of full 3-D imaging.

Since PFM relies on optical forces to hold the local probe, it is inherently soft: the stiffness of its cantilever (formed by focused light beam) is much smaller than that of an AFM. This brings about high sensitivity that is necessary for imaging delicate biological samples (*e.g.* living cells [299]). On the other hand, the soft spring constant of PFM leads to an increased disturbing influence of the probe's Brownian motion on the imaging resolution in the direct scanning imaging mode (AFM-like). An elegant solution to this problem lies in exploiting the thermal position fluctuations as a natural position scanner rather than suppressing them. In the so-called *thermal noise imaging* mode, the position of the randomly moving trapped probe is recorded with high resolution and bandwidth using back-focal plane interferometry [292, 293]. Subsequently, statistical analysis of the probe's position (calculation of a 3-D probe position histogram) is carried out [308]. A 3-D histogram of probe positions shows how often the probe visited a certain volume element during data acquisition. As the probe cannot explore volume elements occupied by solid objects, the resulting 3-D position histogram contains excluded volumes corresponding to these objects. This approach was used successfully for imaging the internal structure of a filamentous agar gel [294]. In general, thermal noise imaging is also suitable for mapping the profile of interaction potentials between the probe and external objects

[285, 286] and characterization of the local visco-elastic properties of the sample [309] (see also Section 4.4).

4.3 Optical stretcher

In most of their applications, the optical forces are used for stable confinement of micro- and nanoobjects (optical trapping) or for controlling the trajectory of such objects (optical sorting and delivery – see Sections 4.5 and 4.6). In these cases, confining and/or propulsive optical forces are the result of the total momentum transferred to the objects center of mass from a light beam. The momentum transfer, however, actually occurs at the object surface where the material properties of the environment (in particular, the dielectric constant) change abruptly. Such surface momentum transfer then leads to the surface stresses that can cause the deformation of the illuminated object, provided it is sufficiently soft. The main source of the surface forces is not the reflection of light from the surface; rather, they stem from the balance of changes in the light momentum in the medium inside the object that has a different dielectric constant. In case the dielectric constant of the object is higher than that of the surrounding medium (most practical cases), these forces always point outwards from the illuminated object and, thus, they lead to object stretching rather than its compression [66]. Their magnitude is then significantly larger than the total force acting on the object's center of mass (see Fig. 7).

The above phenomenon was exploited by Guck *et al.* to create so-called *optical stretcher* – a device that uses the forces of light for controlled deformation of cells or other soft dielectrics suspended in aqueous environment [67]. They adopted the dual-beam optical trap configuration [5, 64] (see also Fig. 1B), in their case consisting of two precisely aligned optical fibers facing each other that emitted slightly divergent infrared laser beams (see Fig. 8). Because of the Gaussian transversal profile of both beams, high refractive index objects (*e.g.* cells suspended in water) are pulled toward the beams axis and, subsequently, move along this axis to the location where the scattering forces of both beams just balance each other. At this position, the objects are stably confined and their stretching in the light field of the two beams can be studied. As the beams are not tightly focused, the risk of damaging the manipulated objects by the high radiation intensity is largely eliminated even for rather high total used power (800 mW in each beam). The first optical stretcher experiments showed its sensitivity that allowed distinguishing between individual cytoskeletal cell phenotypes (red blood cells, BALB 3T3 fibroblasts) on the basis of their elastic response to the applied forces (see also [310] for further examples). This remarkable feature was later exploited for diagnostic purposes when it was found that the cell deformability and its dynamic behavior can serve as inherent cell markers for testing malignant transformation and metastatic competence [68].

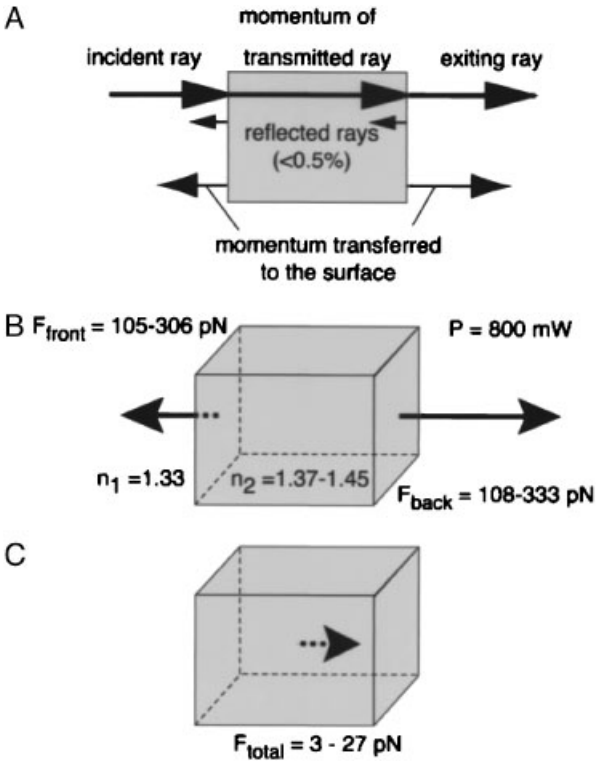

Figure 7. Momentum transfer and resulting forces on a dielectric cubical box illuminated with a single-beam incident from the left. (A) Momentum transferred to the surface by incident/exiting rays. (B) Surface forces acting on the front and back faces of the object for the total incident power of 800 mW and object's refractive index range 1.37–1.45. (C) Total propulsive force acting the object's center of mass. Reprinted with permission from [67]. Copyright (2001), Biophysical Society.

As the optical stretcher can be easily integrated into a microfluidic system [311], it is readily combinable with other lab-on-a-chip optical techniques, *e.g.* various modes of the optical spectroscopy, active optical sorting based on the results of the cell mechanical response [312], *etc.*

4.4 Microrheology

Microrheology studies storage and dissipation of mechanical energy in materials as a function of length scale, operating typically in the micrometer and sub-micrometer range. Microrheologic measurements are based on either the statistical analysis of spontaneous thermal motion of local probes contained within the studied sample (passive mode) or manipulation of these probes using an external force transducer, *e.g.* optical trap, and studying probe's response (active mode). Distinct advantages of microrheology over traditional bulk rheometry are the possibility of accessing high-frequency response range unattainable with conventional high-inertia apparatuses and studying the material properties at various scales, thus characterizing hierarchical structures of complex fluids [246, 313].

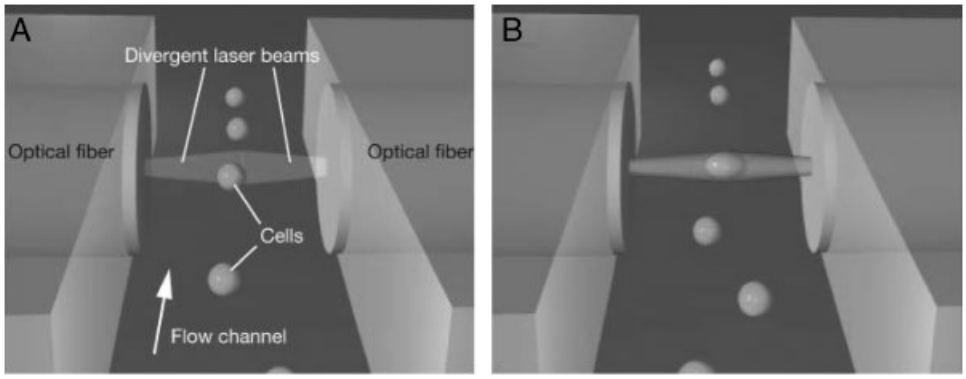

Figure 8. Optically induced surface forces lead to trapping and stretching of cells. Cells flowing through a microfluidic channel can be serially trapped (A) and deformed (B) with two counter-propagating divergent laser beams. Reprinted with permission from [68]. Copyright (2005), Biophysical Society.

Measurement of local fluid viscosity at the micrometer scale represents the simplest microrheologic study. Pralle *et al.* used PFM to obtain medium viscosity in the vicinity of a micron-sized trapped probe from the analysis of its stochastic motion [309]. Similar approach using a different calibration method for the probe position sensor was adopted by Pesce *et al.* [78, 314]. Lugowski *et al.* dragged an optically trapped probe with a constant velocity through the fluid and monitored its deviation from the equilibrium position in the trap that is inversely proportional to the fluid viscosity [315]. The group of Rubinsztein-Dunlop used the rotation of spherical birefringent vaterite particle trapped in a circularly polarized beam to measure the local fluid viscosity even inside a prototype cellular structure [95, 204, 316]. In their measurements, the viscosity v was determined from the measured steady-state rotation rate Ω of the trapped particle as $v = \Delta\sigma P/(8\pi a^3\Omega\omega)$, where $\Delta\sigma$ is the change in the beam circular polarization, P is the total beam power, a is the particle radius, and ω is the angular frequency of the optical field.

In general, complex fluids (such as dilute polymer solutions) display both viscous and elastic properties that depend on the frequency of the applied shear strain. Viscoelasticity of the medium is typically characterized by the value of complex shear modulus whose real part corresponds to the energy storage (elasticity) and imaginary part to the energy loss (viscosity). There exist a number of experimental methods for extracting the value of complex shear modulus [246]. Using passive recording of motion of an optically trapped particle in connection with the fluctuation-dissipation theorem and the generalized Stokes –Einstein relation, Addas *et al.* determined visco-elastic properties of dilute suspension of fd viruses – semiflexible bacteriophages [317]. Starrs and Bartlett used the analysis of one- and two-particle correlation between two optically trapped particles to characterize the local and bulk rheology of a semi-dilute viscoelastic solution of non-adsorbing polystyrene in decalin [318]. The utility of microrheology to probe nanoscale structure and response in colloid-polymer suspensions was demonstrated by Chen *et al.* who employed one- and two-point microrheology to study the depletion layer surrounding the probe particle [319]. In order to eliminate crosstalk between the trapping beams in two-bead microrheology, Atakhorrami *et al.* employed two independent lasers of different wavelengths [320].

A rich field of its own is the microrheology of living cells. The cell cytoskeleton is a highly dynamical system of biopolymers and auxiliary crosslinking proteins with rich kinetics of the crosslinkers and the polymerization–depolymerization cycles of the filaments themselves. Moreover, some of the crosslinkers are motor proteins, which are capable of generating forces and directional motion between the filaments by consuming chemical energy, adding further to the complexity of the cytoskeleton dynamics [247]. Optical trapping techniques have been used to study the intracellular transport [321, 322], mechanisms of force transduction in cells [323], cytoskeleton depolymerization [324], and cell motility [17] (see also review papers [247, 325] for further references).

Research area closely related to microrheology is the analysis of the fluid velocity field at the microscale level. Usually, this is accomplished by tracking tracer particles or fluorescently labeled molecules with an optical microscope and a CCD camera (particle image velocimetry [326]). Optical trapping of tracer particles enables more complex studies especially in cases where the parameters of the fluid flow are varied or the experimental systems are so complex that it is difficult to inject sufficient amount of tracers into the system for repeated measurements. Knöner *et al.* used dual OT to keep a large rotating vaterite particle that generated a vortex flow field in one trap and a small tracer particle in the second trap [89]. After its release from the trap the tracer particle followed the streamlines and its trajectory was recorded by videomicroscopy and subsequently analyzed. The same method was fully explored by Di Leonardo *et al.* using the potential of HOT [90]. They trapped a series of particles in various positions across the microfluidic channel and released them for a short time so that they followed the fluid motion. Analyses of CCD record of all particles' positions in parallel revealed their velocities and, consequently, the fluid velocity distribution could be reconstructed (see Fig. 9). The particles were then re-trapped and the whole procedure was repeated several times at the same or different probe positions. This technique was

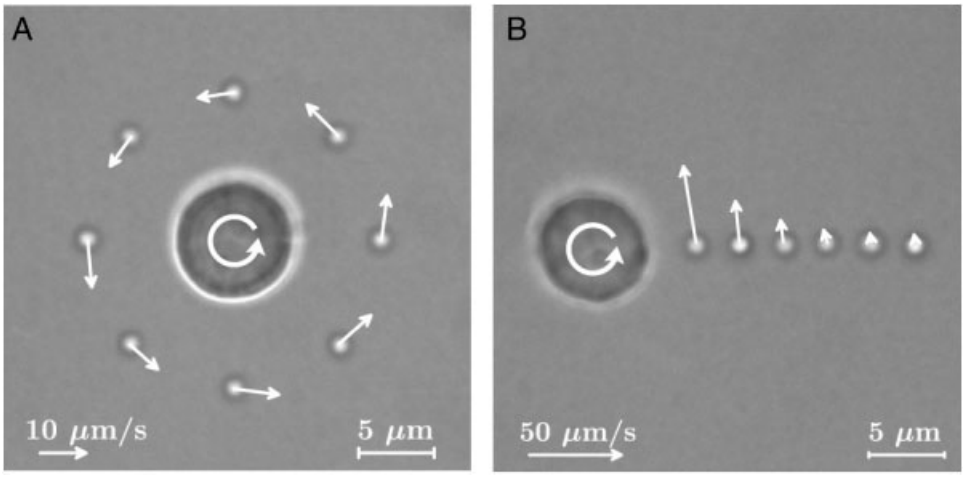

Figure 9. (A) Measured flow field (arrows) around a 4 μm radius vaterite particle spinning at $\Omega = 2.4$ Hz. (B) Measured flow field (arrows) at six different radial distances from a 3.7 μm radius vaterite particle spinning at 5.2 Hz. Arrows in the bottom left corners indicate velocity units. Reprinted with permission from [90]. Copyright (2006) by the American Physical Society.

demonstrated in the study of fluid flow around a rotating particle or at the exit of microfluidic channel.

4.5 Optical chromatography

OC is formally similar to the classical affinity-based chromatographic separation in the sense it uses differences in the strength of interaction between a light wave (representing effectively the ''stationary phase'') and microobjects of various sizes and/or materials (analytes) suspended in a flowing fluid (mobile phase) for their effective separation. The underlying physical principles of OC, however, are quite different from the classical chromatography and they are closer to the field flow fractionation methods [327]. In a typical OC experimental arrangement, colloidal suspension is flowing in the direction opposite to the propagation of a moderately focused laser beam (see Fig. 10). The total force acting on a particle in the flow is given by

$$F_{\mathrm{optchrom}} = F_{\mathrm{opt}} - \gamma v_{\mathrm{fl}} \qquad (14)$$

where v_{fl} is the velocity of the fluid (suspension) and γ the hydrodynamic drag coefficient of the particle. As both optical force F_{opt} and hydrodynamic drag force $F_{\mathrm{h}} = -\gamma v_{\mathrm{fl}}$ depend on the particle size but with different scaling, particle separation according to their size can be achieved. Figure 11 compares OC with other non-optical separation techniques according to the diameter of the sorted particles and illustrates the potential of OC for separation of large particles that are outside of the scope of conventional techniques.

OC was first introduced by Imasaka *et al.* [328] who pointed out its unique features and advantages for separation and concentration of suspended colloidal particles or large macromolecules. In particular, OC allows fast adjustment of the particle separation criteria by changing the beam focusing and/or power (analogy to the change of the separation column in the classical chromatography), accurate prediction of the positions of separated particles along the separation column (provided their physical properties such as the size and refractive index are known), very high

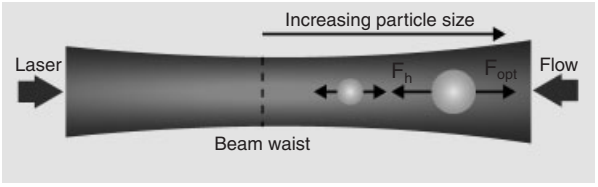

Figure 10. Principle of OC. Suspended particles of various sizes subject to illumination by a moderately focused laser beam and flow of the carrier fluid organize themselves along the beam axis according to their sizes in ascending order (in the beam propagation direction). F_{opt} – optical force; F_{h} – hydrodynamic drag force.

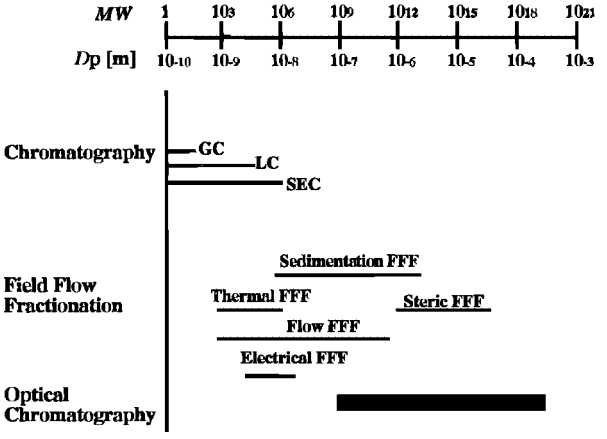

Figure 11. Comparison of working range of molecular weights/particle sizes for OC and other chromatographic methods (GC, LC, SEC) and field flow fractionation (FFF) methods. MW – molecular weight and D_{p} – particle diameter. Reprinted with permission from [329]. Copyright (1997), American Chemical Society.

efficiency of detection of the separated particles, and simultaneous concentration and separation of very dilute samples. Moreover, the size of the separation column can be reduced to micrometers and OC can be combined with optical trapping by introducing a second perpendicular laser beam, thus enabling controlled *in situ* chemical reactions to be performed in successive stages.

Theoretical analyses of OC have been performed by Kaneta *et al* who assumed spherical particles much larger than the laser wavelength and, therefore, used ray-optics model to express the optical force acting on the particles [329, 330]. They also assumed that the optical forces result from a moderately focused Gaussian beam Eq. (10) of the spatial intensity profile $I(z,r)$ [331]:

$$I(z,r) = I_0 \frac{w_0^2}{w(z)^2} \exp\left(-\frac{2r^2}{w(z)^2}\right) \tag{15}$$

$$w(z)^2 = w_0^2\left[1 + \left(\frac{z}{z_R}\right)^2\right]$$

where w_0 is the beam waist of the Gaussian beam representing the ''radius'' of the beam focus and z_R is the Rayleigh length $z_R = \pi w_0^2/\lambda$. It is important that the laser intensity $I(z,r)$ also varies in the axial direction reaching its maximum at the beam waist ($z = 0$); consequently, the equilibrium conditions for various particles can exist at various locations along this direction. Under the above assumptions they found that the retention distance z_{ret} can be expressed as

$$z_{\mathrm{ret}} = z_R\sqrt{\frac{n_1 P Q_s a}{3\pi\eta c v_{\mathrm{fl}} w_0^2} - 1} \tag{16}$$

where Q_s depends on the refractive indices of the particle and the medium. Equation (16) describes how the retention distance can be tuned if the parameters of the beam, particle, and suspension medium are changed [329]. In particular, the laser power can be easily adjusted during the experiment giving an extra degree of freedom for controlling the positions of the analyzed particle sizes. Kaneta *et al.* also described the minimal and maximal particle diameters d_{min} and d_{max} that can be detected with a given laser power:

$$d_{\mathrm{min}} = 2a_{\mathrm{min}} = \frac{3\pi\eta v_{\mathrm{fl}} c w_0^2}{n_1 P Q_s}$$

$$d_{\mathrm{max}} = 2a_{\mathrm{max}} = \frac{2n_1 P Q_s(0)}{3\pi\eta v_{\mathrm{fl}} c} \tag{17}$$

The minimal particle size d_{min} corresponds to the situation when $z_{\mathrm{ret}} = 0$. For smaller particles, the maximal achievable optical force is not sufficient to overcome the hydrodynamic drag and the particles are eluted from the analyzed sample, being dragged by the fluid flow away from the analysis region. The maximal particle size d_{max} then corresponds to the situation when the particle is much greater than the laser beam radius and the optical force does not depend on the particle size anymore. The dynamic range of separable particle sizes, expressed as $d_{\mathrm{max}}/d_{\mathrm{min}}$, typically extends over 3 orders of magnitude and can be still increased by using higher laser power P, slower fluid flow velocity v_{fl}, and smaller beam waist w_0 [329]. Theoretical estimates have predicted that particles with diameters differing by as little as 0.4% can be resolved.

Experimentally, OC has been used for separation of colloidal microparticles of various sizes – typically in the range from 1 to 6 μm [328, 329] – or red blood cells (erythrocytes) [329]. The same separation principle was also applied to protein immunoassays. In the presence of antigen, antibody-coated beads formed clusters with larger effective radius and, thus, they could be easily separated from individual unbound beads [332, 333]. The measured detection sensitivity for the antigen concentration was in the range of nanomoles or nanograms *per* milliliter. Even the real-time monitoring of immunological reactions was demonstrated as the clustering of the beads was accompanied by their motion to new equilibrium positions. Reversed process of antibody-antigen complex dissociation was also observed. It was speculated that this way single protein molecules can be detected.

OC has also been used for the particle size determination. After separating polystyrene particles with OC, the laser power was gradually reduced, permitting sequential elution of small to large particles from the working solution. Subsequently, the particle size was calculated from the laser power at which the particle was eluted with a medium flow. Since the laser power measurement is easier and more precise than determination of the beam waist position in retention distance-based measurements, the precision of the particle size determination was improved by a factor of 3.3 [330].

Hart and Terray demonstrated that also particles of the same size but of different compositions (manifested by different refractive indices of polystyrene, PMMA, and silica beads) can be distinguished by OC [334] (see Fig. 12). In this case, the particle separation results solely from the difference of optical forces acting on particles made of different materials. The same authors further enhanced OC by combining it with microfluidic systems. Using soft lithography they fabricated a microchannel with varying width resulting in corresponding differences of the fluid flow velocity along the channel [335]. By tuning carefully the position of the beam focus relative to the regions of different fluid flow velocities, they were able to increase the retention distance of particles of the same size but different material compositions (polystyrene, PMMA). On the other hand, suitable tailoring of the fluid flow velocity profile can also be useful for reducing the separation distance between analytes with large differences in size and/or refractive index that cannot otherwise be analyzed simultaneously or analyzing particles that can wander out of the observable beam region. Using this idea Terray *et al.* separated *Bacillus anthracis* spores (size of ~1–2 μm) and Mulberry pollen grains (14 μm) particles thus demonstrating the potential of OC

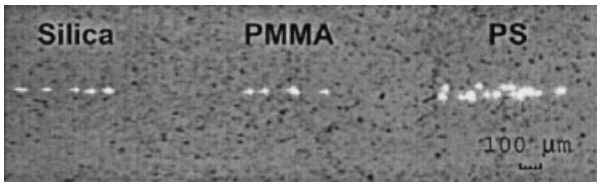

Figure 12. Optical separation of uniformly sized 2.2 μm polystyrene, PMMA, and silica beads (visualized by laser light scattering in the picture). Experimental conditions: laser power 0.77 W and fluid linear velocity 32 μm/s. Reprinted with permission from [334]. Copyright (2003), American Institute of Physics.

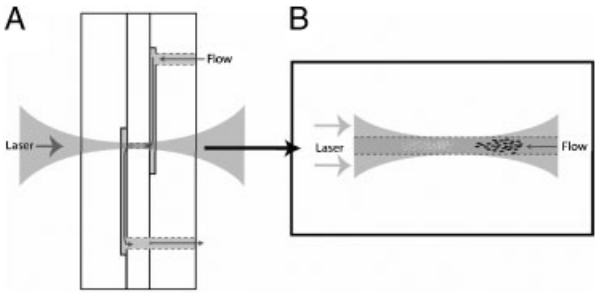

Figure 13. Glass micro-flowcell for OC laser filter. (A) Construction of the microfluidic device showing the pathway for fluid (shown in gray) into and out of the separation channel, and the laser beam focused through the channel. (B) Illustration of a separation in which sample particles are constrained to the focal point of the beam by the size of the separation channel that is filled by the laser beam. Reprinted with permission from [336]. Copyright (2007), Optical Society of America.

combined with microfluidics in forensic and security-related applications [335]. The use of such a system, however, is limited to rather dilute samples because large numbers of particles modify the spatial beam intensity distribution and cause instability in the retention distance or even inability to trap the particles.

The above-described OC configurations enable to separate only a fraction of injected particles (typically up to 10–50 particles out of thousands) because the beam waist is usually much narrower than the width of the fluid transport channel. Therefore, the OC set-up and detection procedure have been modified in order to interrogate automatically all the injected particles in a continuous carrier fluid stream [336]. In this modified configuration a narrow separation channel, where the laser beam propagates, is placed perpendicular to the main inlet and outlet channels (see Fig. 13). The width of the separation channel (50 μm) is such that the laser beam completely fills its cross section; thus, all the particles in the fluid flow experience optical forces. In order to improve imaging of the particles after separation for the purpose of the automated particle concentration analysis, a second channel with twice as large width (100 μm) and, therefore, slower particle velocity is introduced in the device downstream of the separation channel. After analyzing the particle concentration, the fluid carries the particles out of the device where they can be collected for additional processing. Since all the particles in the flow are influenced by the laser beam when they pass through the separation channel, the above configuration can be used to concentrate efficiently dilute samples, which has been demonstrated on polystyrene microspheres and *B. anthracis* spores [336]. This possibility enabled to shift the OC from an analytical to a preparative experimental technique.

Yet another type of OC – the so-called cross-type OC – is based on a moderately focused laser beam propagating perpendicularly to the fluid flow [337]. In this method particles of different sizes and/or materials are pushed across the channel by the radiation pressure into different streamlines within the flowing fluid. Once the particles leave the illuminated region, they remain confined in their respective streamlines, effectively separated in the transversal direction. The advantage of the cross-type OC over the above-discussed axial-type OC lies in the continuous separation of the incoming particle stream and, thus, easier particle delivery and much larger throughput. This technique is similar to the fluid flow fractionation methods that induce particle size-sensitive forces across the carrier fluid flow – for example, by cross flow or thermal gradients – and then make use of the parabolic profile of the fluid velocity in the channel for the particle separation along the flow direction [338–340].

4.6 Optical sorting

Optical sorting represents a relatively new class of optical micro-manipulation techniques that attracts still-increasing interest. It is closely related to OC, the main difference between the two techniques being in the employment of complex *optical potential landscapes* formed by specially tailored light intensity distributions in the optical sorting applications. In principle, two different approaches to optically induced particle sorting can be distinguished. The first one called *active sorting* includes an active decision-making step for determining the fate of a particular particle. It is based on a well-defined input (for example, fluorescence or spectroscopic signal from the particle, typical image pattern, *etc.*) that triggers the action, which uses optical forces to move analyzed objects into different positions and separate them. *Passive sorting* is a much younger method; it is based on the difference in sensitivity of the forces in an optical potential landscape to the sorted particle properties (size, shape, material). In this case no active decision-making step is needed; particles of different properties follow different trajectories when driven through such a landscape [125, 341].

Majority of optical force-based sorting techniques use fluid flow to deliver the analytes to the sorting region and employ the associated viscous drag force acting on the objects as a counter-part to the sorting optical force. In contrast to the flow-field fractionation methods [327] the parabolic velocity profile of the fluid is usually not employed in the sorting. Comprehensive up-to-date reviews of optical sorting techniques have been published recently [342, 343].

In the following sections, we will give an overview of the principles of these techniques together with some recent applications.

4.6.1 Active sorting with optical forces

This type of active sorting is based on mechanisms similar to the macroscopic fluorescence-activated cell sorting (FACS) [344] applied in the microfluidic regime [345]. The identification of analytes is similar to FACS: fluorescence, spectroscopic data, scattering, or image recognition are employed. The system of deflection of selected particles that uses optical forces, however, is quite different from FACS. This system typically consists of a sample input channel, an optional hydrodynamic focusing of the analyte, a region of the sample analyses, an optical switch, and a microfluidic junction separating samples to different output channels (waste and collection being the simplest example). Figure 14 shows a scheme of such an arrangement. In contrast to the conventional high-throughput FACS, these micro-systems can handle only small numbers of objects (typically 100–100 000) with high yield and are therefore beneficial for handling unique objects that are difficult to obtain in large quantities. Typical sample volumes are in the range of units to tens of μL, yield reaches up to 90% of the input with sorting rates about tens to hundreds of objects *per* second. Another advantages of microfluidic systems are their low price permitting a disposable use and the possibility of carrying the analytical system to the samples (especially for biohazardous materials) and integrate it with other lab-on-a-chip systems or sorting switches.

There are several possibilities for setting up an optical switch. Buican *et al.* [346] used radiation pressure of a moderately focused laser beam propagating perpendicular to the direction of analyte motion deflecting selected particles into different channels. This planar geometry provides the advantage of easy combination with optical waveguides or semiconductor lasers integrated within the microfluidic system [347, 69].

Applegate *et al.* generated a linear trap with size $1 \times 100\,\mu m$ by moderate focusing of a laser diode bar beam and tilted the long axis of this trap with respect to the fluid flow [348–350] (see Fig. 15). Particles suspended in the flow were guided in the high light intensity region and moved transversally across the flow [351]. The angle of tilt of the trap's long axis and the time period for which the laser beam is switched on determine how much the particle is deviated laterally from its original trajectory. Because of strictly laminar flow in the microchannels and slow diffusion, the particle remains in a constant lateral position after interaction with the trap, following the same streamline. Thus, if the main channel splits into several outlets, particles following different streamlines are sent to different outlets and separated. The advantage of this set-up is its simplicity and low price but the sorting speed is just five objects *per* second in the fluid flow with a velocity of $500\,\mu m/s$.

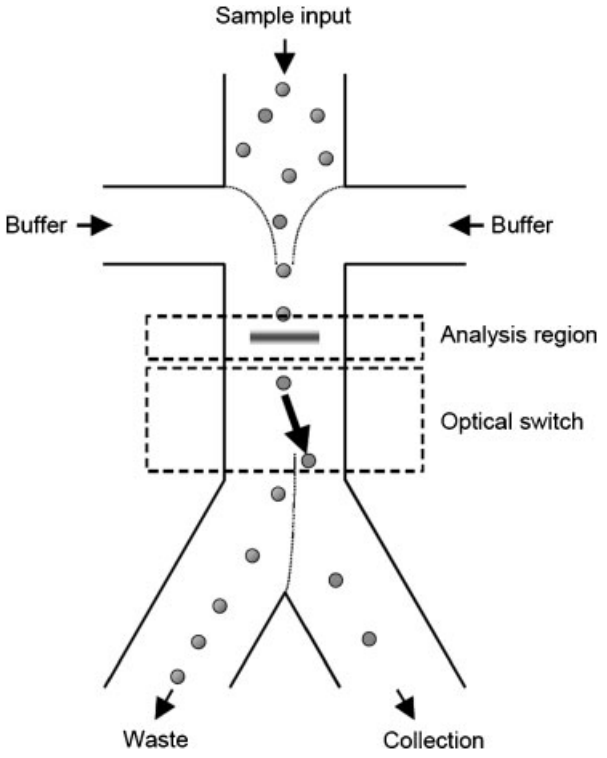

Figure 14. Layout of microfluidic sorting system with an optical switch. According to the switch activation state, the analyzed object either goes to the waste channel (switch off) or it is deviated to the collection channel (switch on). Because only lateral optical trapping is needed, the laser beam is just moderately focused by microscope objective with low NA. Also the interaction of the object with the deflection beam is minimized only to the period of object deflection. Therefore, the living cells are less stressed and sorting does not shorten their viability. Reprinted by permission from Macmillan Publishers: Nature Biotechnology [345], copyright (2005).

Chapin *et al.* and Rodrigo *et al.* used the same 2-D geometry and employed HOT in a closed-loop and interactive real-time feature recognition sorting system [352, 353]. No fluid flow was used to drive the particles that were optically trapped and manipulated actively along optimal trajectories determined in parallel.

4.6.2 Passive sorting with optical forces

The pioneering work on the passive optical sorting was done in 2002 [341, 125]. Therefore, this type of optical sorting is still at its infancy, especially regarding its applications outside of the field of physics. Passive optical sorting uses more complex laser beam intensity patterns – optical potential landscapes – with specifically designed spatial variations of optical intensity. Optical forces in such intensity patterns then depend on the particles shape, size, and refractive index, which forms the basis for the efficient particle sorting (see Fig. 1D). Detailed theoretical and experimental studies on the sensitivity of the optical force to the particle size and refractive index for 1-D periodic

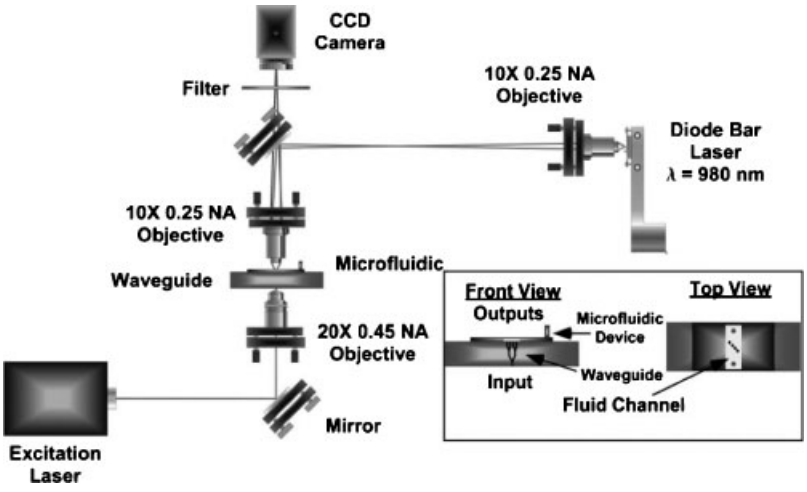

Figure 15. Schematic of integrated microfluidic sorting system based on optical waveguide integration using diode laser bar trapping. The trapping laser is aligned over the waveguide outputs. Reprinted with permission from [349]. Copyright (2006), Royal Society of Chemistry.

interference structures have already been published [75, 85, 87, 166, 354–356]. The particle behavior in 2-D optical potential energy landscapes in the presence of flow or thermal noise has also been intensively studied [125, 341, 357–363]. Therefore, in this section we will stay at the qualitative level referring interested readers to the above publications.

The oldest sorting configuration used *fluid flow and static optical pattern*. In this configuration, fluid flow ensures the delivery of analytes and its velocity also represents a free tunable parameter of the system for optimizing the sorting efficiency [125]. The optical patterns have been created by several different methods in the form of periodic or aperiodic shapes. Holographic tweezers were used by Korda *et al.* to create a 2-D array of optical traps [341]. They discovered that particle trajectories depend on the angle between the trap array lattice and the fluid velocity vector. MacDonald *et al.* used interference of several co-propagating beams with tuned intensities and phase shifts to create a periodic 3-D optical lattice of intensity maxima and minima [125]. They demonstrated sorting of microparticles of different sizes and also microparticles of the same size but different materials (refractive indices – see Fig. 16).

Sun *et al.* used a microlens array to obtain in a simple way a pattern of static optical traps [110]. Milne *et al.* used an acousto-optical deflection system for generating more complex tunable light intensity patterns [364]. Their sorting system contained an optical funnel that first focused the particles flowing in a microfluidic channel toward one side of this channel. Subsequently, the particles were sorted by driving them through several regions illuminated with different optical intensities separated by dark regions. This illumination pattern released particles of different properties at various lateral positions across the flow and so it separated them (see Fig. 17). A configuration similar to the cross-type OC used radiation pressure generated by an evanescent wave propagating along the surface of the microfluidic system perpendicular to the fluid flow [365]. Again, particles of different properties were deflected to

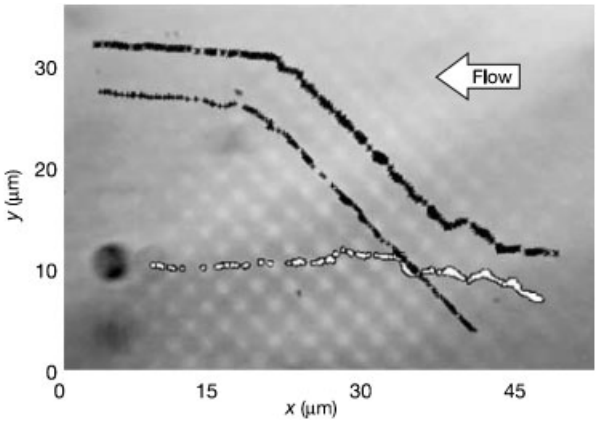

Figure 16. Optical fractionation by size. Black crosses represent the frame-by-frame positions (tracked at standard video rates with about 8 nm precision) of two 2-μm diameter protein microcapsules (drug delivery agents) as they flow from right to left across the optical lattice. The flow speed is 20 μm/s with a total incident laser power of 530 mW. Again, significant angular deflection is achieved, while a co-flowing 4-μm-diameter capsule of the same sort flows nearly straight through the lattice (white dots). The collection of 2-μm capsules allows a controlled study of drug delivery at the cellular level. Reprinted by permission from Macmillan Publishers: Nature [125], copyright (2003).

different streamlines and subsequently dragged to different output channels thus being sorted. Genoptics adopted a configuration of a beam propagating perpendicular to the sample plane with the laser beam having a prolate lateral shape. Fluid flow was substituted by the movement of a closed sample chamber perpendicular to the beam longer axis. Gradient force tends to keep the particles in the beam and moves them with respect to the sample chamber surface against the viscous drag force and surface interactions. Depending on the particle properties either they can be released from the beam or they stay confined in the beam and are delivered to the edge of the sample chamber [366, 367]. They named this method optophoresis and demonstrated its potential in distinguishing one population of cells

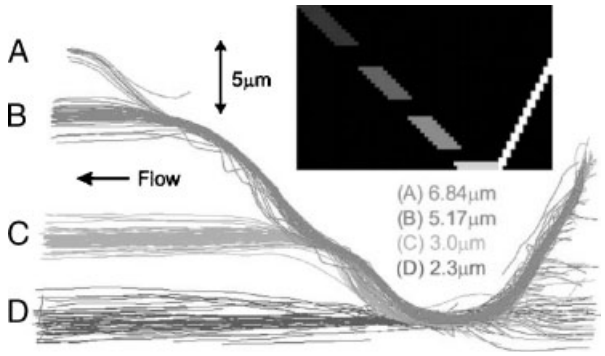

Figure 17. Plotted trajectories of (A) 11 6.84 μm, (B) 47 5.17 μm, (C) 78 3.0 μm, and (D) 38 2.3 μm silica spheres flowing through an optical landscape with light intensity distribution illustrated in the figure inset (gray scale levels correspond to the illumination light intensity, the brightest line on the right of the illumination pattern represents an optical funnel). Reprinted with permission from [364]. Copyright (2007), Optical Society of America.

from the other, thus proving its suitability for pharmaceutical and clinical applications.

Static fluid and dynamic optical pattern provides an interesting way of how to sort objects in closed, static samples. The movement of the optical pattern substitutes the fluid flow so that the counter-acting interaction between the Stokes drag force and optical force can be established. In this configuration the sorted particles accumulate at the edges of the illuminated region. Ricárdez-Vargas *et al.* generated vibrating interference fringes by interference of two co-propagating slightly tilted laser beams; the fringe motion was induced by motion of a piezo-mirror [356]. Saw-tooth motion of the interference pattern induced surface delivery of the particles confined in the fringes; the particles were carried along with the fringes during the slow part of the fringe motion and stayed in place during the fast backward motion of the fringe (inchworm-like delivery mode). Particles of different sizes can be addressed in the second step by changing the direction of the saw-tooth slope and spatial period of the fringes (see Fig. 18).

Even sub-micrometer-sized particles were sorted using a traveling standing wave created by interference of two counter-propagating evanescent waves [166]. This approach was based on the dependency of the standing wave forces on the particle size [75, 354]. The coherent counter-propagating evanescent waves of unequal intensity created a tilted washboard optical potential with the direction of the tilt opposite to the direction of the interference fringe motion (see Fig. 19). Consequently, particles of sizes sensitive to the standing wave potential landscape were delivered in the direction of the traveling standing wave, whereas particles of insensitive sizes were pushed by the radiation pressure in the opposite direction (the direction of the potential landscape tilt). The smallest difference between the sorted polystyrene particle sizes was 60 nm (sorting of 350 and 410 nm particles). This method was further enhanced combining two traveling standing waves in opposite directions and of different wavelengths emitted out of facets of two photonic crystal fibers [368].

Optical sorting using *static fluid and static optical pattern* employs either thermal position fluctuations or combination of radiation pressure with different particles sensitivity to the optical interference pattern for inducing the particle motion. Paterson *et al.* [369] exploited lateral intensity profile of a Bessel beam forming a tilted periodic (washboard) optical potential landscape [370]. Thermal noise activated hops of particles in the lateral plane from the outer fringes toward the inner fringes due to the tilt of the potential toward the beam center. Since particles of different sizes or materials felt different heights of the potential barrier between the fringes, this resulted in different average drift velocities toward the beam center. Once the particle reached the center, it was separated in the direction perpendicular to the lateral plane by the radiation pressure. This set-up was used to sort, for example, white and red blood cells [369]. The same principle has been adopted by Hayashi *et al.* using assymetric double well potentials [371].

Another method employs the imbalance of optical forces acting on particles of different sizes and/or refractive indices placed within an interference field of three beams [372]. Two of the beams co-propagate and create interference fringes on the top surface of the sample-filled cuvette where they overlap (see Fig. 20). The behavior of suspended particles in the direction perpendicular to the fringes is similar to the well-studied configuration of a particle placed within a standing wave [75, 85, 166]. The particles settle with their centers in the fringe maximum or minimum according to their sizes, but there also exist intermediate particle sizes that feel no force coming from the intensity modulation across the interference fringes. Along the fringes, the particles are pushed by the radiation pressure exerted by both beams. This force significantly varies with the particle size and refractive index and it also strongly depends on the transversal equilibrium location of the particle, *i.e.* if the particle settles in the fringe intensity maximum or minimum. Therefore, particles of different properties move with different velocities along the fringes. In order to achieve particle sorting, a third beam is added that is counter-propagating with respect to the above two beams and the polarization of which is perpendicular to them to minimize any interference effects with them. The intensity of the third beam is tuned so that its radiation pressure reverses the motion of the slower particles. This results in the static optical sorting of two types of microparticles to opposite directions by the radiation pressure, without any fluid flow or fringe movement (compare behaviors of particles I–IV in the inset of Fig. 20). Sorting of microparticles of different sizes and separation of yeast cells from yeast spores was demonstrated and the experimentally tested throughput of this method was about 0.5–5 particles *per* second.

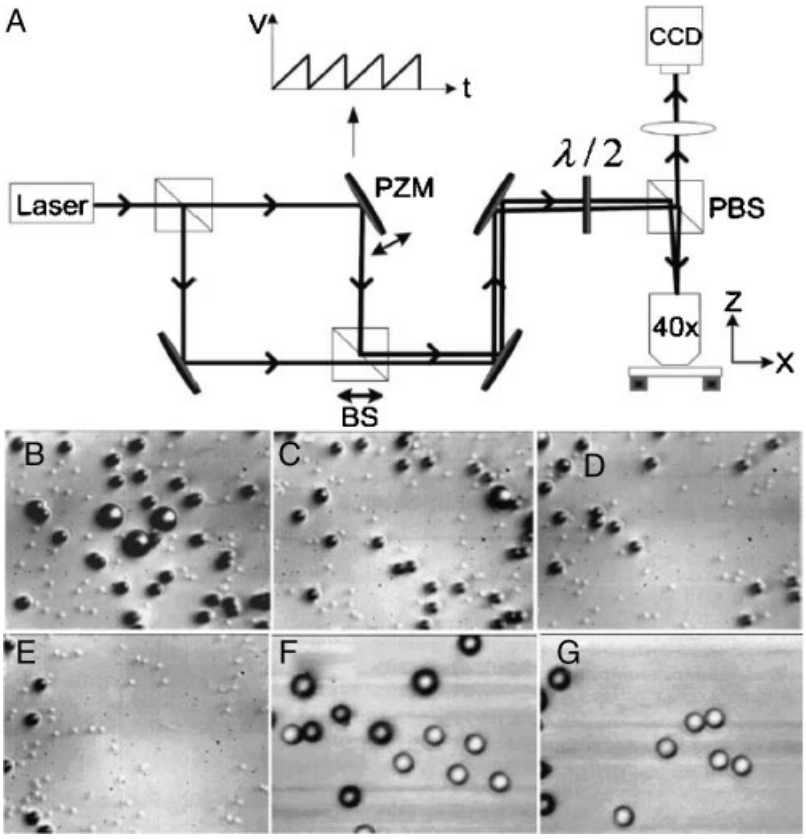

Figure 18. (A) Experimental set-up for optical sorting in a moving pattern of interference fringes. Frames (B–E) show sorting of three types of particles: 1 μm diameter silica particles and 2 and 5 μm latex particles. (B) All particles are mixed together; (C) the 5 μm particles are removed to the right; (D and E) 2 μm particles are removed in the opposite direction. Frames (F–G) show sorting of 5 μm diameter spheres of latex and silica latex looks darker than silica. Reprinted with permission from [356]. Copyright (2006), American Institute of Physics.

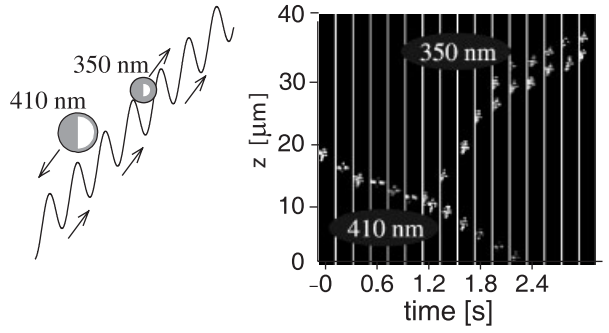

Figure 19. Principle (left) and examples (right) of sorting of submicrometer-sized colloids differing in size by only 60 nm (diameters 350 and 410 nm, respectively). Smaller beads sensitive to the standing wave trapping potential are delivered by the moving pattern like on a conveyor belt in the positive direction of the *z*-axis, whereas the larger beads insensitive to the periodic modulation of the potential move in the negative *z*-axis direction due to the tilt of the periodic potential.

Fluid flow combined with dynamic optical pattern further extends the range of the tunable system parameters for obtaining a better sorting performance. However, its potential is yet not fully explored and investigated. The majority of methods working with the static fluid or static optical pattern can be extended to this category. Moreover, much more complex 2-D patterned motion including so-called ratcheting can be applied to the sorted particle suspensions [362, 373–375].

4.7 Manipulation of nanoobjects

Manipulation of nanoobjects has been attracting increasing attention as the size of confined objects approaches the molecular scale. Thus, it opens new possibilities for single-molecule chemistry and biochemistry experiments. Even if the nanoobjects (molecules) cannot be truly confined, the presence of the gradient optical field can still lead to a significant slowing of their thermal motion dynamics, thus creating favorable conditions for controlling multi-molecular chemical reactions and assembly of super-molecular complexes.

Strictly speaking the size of a nanoobject should be smaller than 100 nm in at least one dimension. In this section we will treat this limitation in a more relaxed way focusing on the manipulation with objects much smaller than the trapping light wavelength. As demonstrated in the theoretical treatment of the nanoparticle trapping (see Eq. 10), even a moderately focused beam produces gradient forces stronger than the scattering ones and therefore enables spatial confinement of nanoobjects. Even though the scattering force is not conservative and therefore its potential cannot be defined, it is still possible to introduce the minimal characteristic work that is needed for a trapped particle to leave the optical trap. This work is called the depth of the optical trap and it characterizes the trapping stability. Nanoparticles confined and manipulated in a liquid are subject to the thermal motion, which becomes the dominant effect disturbing the stability of the

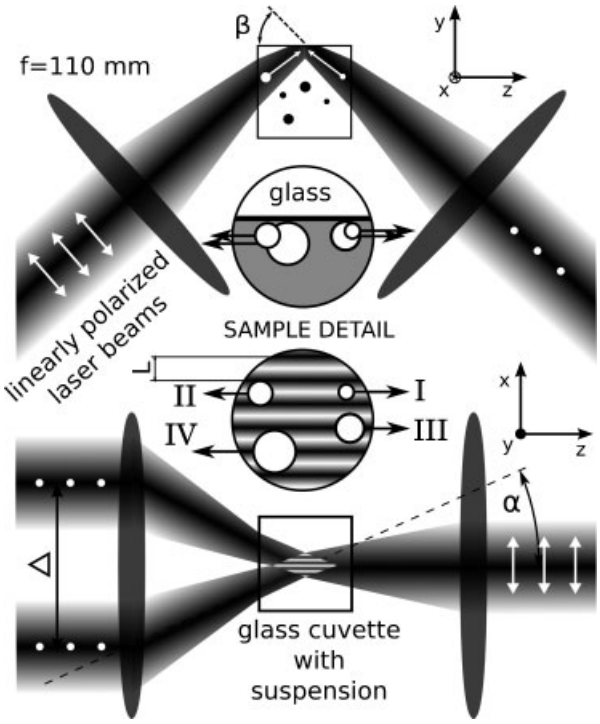

Figure 20. Experimental configuration for the optical sorting in three-beam interference field. The beams overlap on the top surface of the sample filled cuvette and form sorting region of size $40 \times 60\,\mu m^2$ elongated along *z*-axis. The distance between the interference fringes *L* is adjusted by changing the distance Δ between the two beams coming from the left. The Roman letters in the inset indicate four different types of objects behavior.

confinement. Long-term spatial confinement of nanoparticles thus requires optical trap with the potential depth much larger than the thermal energy k_BT, where k_B is the Boltzmann constant and T absolute temperature of the surrounding medium. The depth of the optical trap for a nanoparticle scales linearly with the particle volume and the total beam power and it also depends on the relative refractive index of the particle [28]. Therefore, if the particle volume is very small, proportionally higher laser power is needed to overcome the thermal energy and confine it [75]. Alternatively, increase in the refractive index of the particle (for example, by using metallic nanoparticles with large real part of the complex permittivity) can lead to a deeper trap for the same particle size and total beam power even though one has to be aware of the increasing effect of the scattering force that destabilizes the trapping [120].

Svoboda and Block demonstrated 3-D single-beam trapping of polystyrene and gold nanoparticles of diameters 38 and 36 nm, respectively [376]. They also showed for the first time that the absorbing metallic nanoobjects can be trapped more strongly and stably in comparison with non-absorbing objects of similar size. This is caused by higher $\Re\{\alpha_0\}$ of metallic nanoparticles that leads to the stronger gradient forces. Masuhara's group performed many pioneering experiments on optical trapping of nanoparticles. They studied optically induced assembly of several kinds of polymers [377–379] and nanoparticles [380–383] in the trap, pushing the size of the trapped nanoparticles down to 10–20 nm.

Stable optical trapping of gold nanoparticles of sizes ranging from 18 to 254 nm using single-beam OT has been demonstrated by Hansen *et al.* [384]. Forty nanometer diameter gold nanoparticles trapped and manipulated with OT also served as probes in the scanning near-field optical microscopy [385]. Silver nanoparticles of average diameter ~90 nm and a variety of shapes were trapped in 2-D with typical power at the sample in the range of 50–200 mW by a laser operated at 820 nm. This wavelength is longer (red-detuned) than the resonance wavelength of the localized surface plasmons; red-detuning of the trapping beam facilitates the confinement of the particles in the beam intensity maximum. It was observed that these particles could not be trapped with a shorter wavelength of 514 nm, which is below the wavelength of the plasmon resonance (blue-detuned) [386]. Silver nanoparticle of diameter 40 nm was manipulated on the surface by OT (at a wavelength of 830 nm with 50 mW of output power) to form a dimer with a similar immobilized particle. The enhancement of the electric filed in the nanometer-sized gap between the two particles was used to enhance the Raman signal of thiophenol *via* SERS phenomenon (see Section 4.8) [387]. Smaller silver particles (20–25 nm in diameter) dispersed in Rhodamine 6G and NaCl solution formed a cluster in the focus of the OT facilitating observation of surface-enhanced hyper-Raman scattering spectrum of Rhodamine for concentration between 10^{-7} and 10^{-11} M [388]. Stable 3-D optical trapping and manipulation of silver nanoparticles with diameters 20–275 nm has been recently demonstrated by Bosanac *et al.* [389].

Au nanorods 40–80 nm in length and 10–15 nm in diameter were confined utilizing the enhancement of the gradient force at the trapping wavelength longer than the resonance wavelength of the longitudinal localized plasmon mode [390]. These nanorods oriented along the linear polarization of the light. For wavelengths below the resonant wavelength, the nanorods were repelled from the high-intensity region. The same phenomenon was also demonstrated in optical trapping of Au nanoparticle of diameters 100 and 250 nm in the dark central region of an optical vortex with the trapping laser wavelength lower than the plasmon resonance wavelength [391]. Force enhancement by localized plasmon excitation was also used to trap Au bipyramids (100 nm long and 30 nm in diameter) and Au/Ag core/shell nanorods (60 nm long with 13 nm diameter core and shell thickness of 2 nm) [392]. Further applications of tightly focused laser beams in the fabrication of nanostructures are described in a recent review [393]. It is highly probable that the optical trapping exploring the excitation of the localized surface plasmons in elongated or core-shell structured particles will find numerous applications in sorting of nanoobjects and as optically manipulated probes for excitation of the SERS in less than atto-liter volumes (see also Section 4.8).

Except single-beam OT standing wave has been also considered for the nanoparticle manipulation because of the

scattering force elimination in the counter-propagating beam geometry and steeper intensity gradients along the beams propagation direction. Therefore, the power demands for the stable confinement of nanoparticles can be by ~1 order of magnitude lower and the beams can be less focused [120, 121]. Another tool for the nanoparticle manipulation is the evanescent field. Gold nanoparticles of diameters 20–80 nm were propelled in the evanescent wave above the waveguide with a speed of 4–8 μm/s with modal power 500 mW and TM polarization (at a wavelength of 1047 nm) [162, 163]. Much bigger gold nanospheres of diameter 250 nm were guided with a velocity up to 500 μm/s with modal power 150 mW at a wavelength of 1066 nm [158]. A small dielectric spherical particle attached to the end of a single mode optical fiber forms the so-called fiber-optic OT that are able, as demonstrated by Numata *et al.* [394], to confine in 2-D gold nanoparticles of sizes 40, 100 and 200 nm against the surface. Semiconductor nanowires (GaN, SnO_2, ZnO, Si) with diameters as small as 20 nm and aspect ratios of more than 100 have been trapped, transferred, and assembled into arbitrary structures in fluid using infrared OT [395]. CdTe quantum dots of nanometer size solved in D_20 were optically trapped and fixed to the hydrophilic glass substrate using high repetition-rate picosecond Nd:YLF laser [396].

Bundles of single-walled carbon nanotubes (SWCNT) (length 100–200 nm and diameter 1.3 nm) were manipulated by HOT [397]. Multi-wall carbon nanotubes were manipulated with the help of silver nanoparticles attached to them and serving as trapping handles [398]. This method is similar to the manipulation with biological macromolecules mentioned in Section 4.1 and it was also applied to trap individual microtubules and microtubule bundles and measure their elastic properties and dynamics of their polymerization [399]. Optical trapping and thermal effects were combined to obtain multi-dimensional optical trapping and rotation of carbon nanotube bundles [253, 400]. Optical forces (probably in combination with thermophoresis) helped to deposit SWCNT on optical fiber end facets [401, 402]. Their direct deposition on the glass surface by OT has also been reported [403]. Marago *et al.* used time-sharing trap to study SWCNT behavior under various properties of the immersion fluid (aqueous and organic solvents, presence of surfactants) [404]. Asymmetric inorganic nanorods served as nanorotors when illuminated by a single focused beam [225].

4.8 Raman spectroscopy of optically trapped objects: Raman tweezers

Raman spectroscopy is an extremely powerful analytical technique that allows selective, external label-free analysis of the molecular composition of studied samples based on the identification of characteristic peaks in the spectrum of inelastic scattering of the incident radiation from vibrating molecular bonds. When carried out in the so-called fingerprint spectral region, Raman spectroscopy is capable of distinguishing between molecules with very small structural differences (*i.e.* the presence of a single unsaturated bond in a lipid molecule). Raman microspectroscopy – the combination of spectroscopy with optical microscopy in either far-field or near-field imaging modes – then allows analyzing the composition of sub-micron-sized specimens or obtaining composition maps of larger samples with micron- or even sub-micron resolution [405, 145]. In addition to providing spatially resolved compositional information, Raman microspectroscopy can be performed in the time-lapse mode, thus permitting to follow the temporal development of the processes that take place in the studied sample [406].

In order to conduct Raman microspectroscopic measurements one must be able to control the position of the analyzed specimen with respect to the Raman probe beam. Sample position control can be easily achieved when the sample is fixed or when it can be attached to a solid support that is subsequently scanned through the probe beam focus. There are, however, a number of important specimens with sizes in the micron and sub-micron range (*e.g.* colloidal particles, microdroplets, vesicles, or living cells) that exist normally in suspensions or aerosols and whose function or structure require the presence of the fluid environment. Such specimens are subject to the Brownian motion and streaming of the surrounding fluid and, consequently, they can travel a significant distance within the time required for acquiring the spectrum. Attempts to apply standard immobilization procedures (*e.g.* chemical bonding or adsorption to a substrate, micropipette suction) to these specimens often lead to an undesired alternation of their properties. Moreover, the presence of a support substrate can cause a significant spectral background obscuring the observed Raman scattering spectra of the target specimen.

Optical trapping represents an elegant approach for addressing the above-mentioned experimental challenges. Since both OT and Raman microspectroscopy rely on the use of a strongly focused laser beam, it is straightforward to combine both techniques using a single beam for both trapping and spectroscopy. Figure 21 shows the simplest experimental set-up that enables achieving this task. Incident laser beam is focused to a diffraction-limited spot with a high NA objective lens in order to create the optical trap and, simultaneously, excite Raman scattering in the trapped microobject. The same objective lens also serves to collect the light backscattered from the trapped object that is subsequently directed to a spectrograph, after passing through a notch filter, which cuts off the Rayleigh scattered light. In a more advanced version, trapping and Raman laser beams are independent in order to provide higher flexibility for optimizing the parameters of both beams (power, beam focus size, wavelength) for their respective tasks. Decoupling the trapping and Raman laser beams also allows modulating the position of the trapped object relative to the Raman beam focus and, subsequently, introducing

a phase-sensitive detection of the Raman spectra that permits a significant reduction in the spectral background [407].

The combination of Raman microspectroscopy with optical trapping – usually termed Raman tweezers (RT) – was proposed almost 25 years ago [408] and, since its introduction, it has found numerous applications especially in the fields of analytical and physical chemistry and cell and molecular biology (see the review by Petrov [409]). Typical target specimens for RT are aerosols, suspended microdroplets or colloidal particles, and living cells that can be studied *in situ* under relevant environmental conditions. Moreover, the possibility of analyzing individual target microobjects enables to detect directly the variations of their properties and composition that would be otherwise lost in an ensemble-averaged measurement.

Using RT, dynamics of chemical reactions within an individual optically trapped microparticle has been studied. Figure 22 reprinted from [410] shows the time series of Raman spectra acquired from a trapped styrene droplet within which the styrene emulsion polymerization takes place. The progress of the polymerization process can be monitored from the decrease in the amplitude of spectral peak at 3005 cm^{-1} corresponding to monomeric styrene. Similar experiments were performed by Esen *et al.* who used UV light from a mercury arc lamp to initiate the polymerization in the trapped acrylate aerosol droplet [411]. The dynamics of cooling and evaporation of a single levitated sulfuric acid/H_2O droplet exposed to surrounding gaseous atmosphere of varying humidity was studied by Mund and Zellner [412]. Such droplets are of considerable interest to atmospheric chemistry; they are formed in the Earth's stratosphere by the oxidation of SO_2 followed by nucleation with H_2O vapor. Another atmosphere-related study was conducted by King *et al.* [413] who investigated the kinetics and product composition of oxidation of biogenic and water-soluble compounds in aqueous and organic aerosol droplets by ozone. The composition of aerosol particles was chosen to mimic the conditions in the Earth's atmosphere. An infrared RT system was applied by Ajito *et al.* to study liquid–liquid extraction of *p*-nonylphenol from aqueous bulk solution into a single trapped toluene droplet of sub-picoliter volume [414]. Both Raman spectra and the size of the trapped droplet were used to monitor the uptake of *p*-nonylphenol into the toluene droplet and calculate the distribution coefficient of *p*-nonylphenol between both environments. Houlne *et al.* used a silica microparticle trapped in solution far away from the sample chamber boundaries as a solid-phase support for model peptide synthesis reaction and monitored its kinetics without the disturbing influence of the reaction container surfaces on the free diffusion of the reagents into the reaction center [415].

One of the fastest developing and most successful applications of the RT is the study of individual living cells and artificial cell model systems. Biological cells consist of

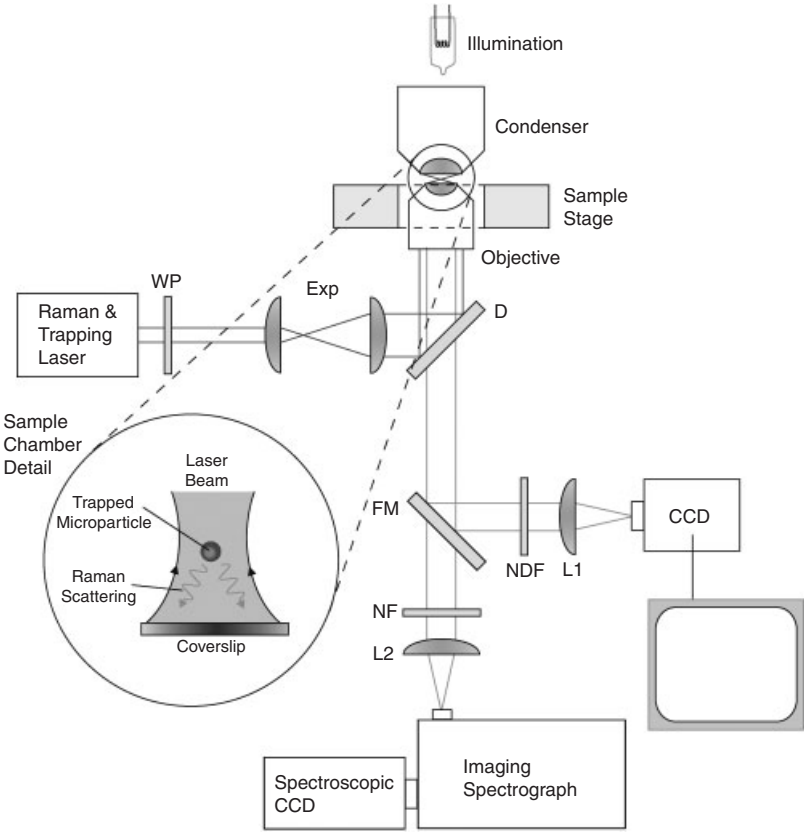

Figure 21. Basic experimental set-up for Raman microspectroscopy of optically trapped microparticles. A single laser beam is used for both optical trapping and excitation of the Raman scattering spectra. WP – $\lambda/2$ wave plate; Exp – beam expander; D – dichroic mirror; FM – flip mirror; NDF – neutral density filter; L1, L2 – lenses; NF – notch filter.

complex mixtures of various molecular types (proteins, nucleic acids, lipids, and polysaccharides) whose spatial and temporal concentration distributions are intimately connected to the cell physiological state. RT enable non-contact confinement of the freely floating suspended cells and subsequent identification of individual cell constituents without the need for their exogenous labeling. This is vital as both cell immobilization on a support surface and labeling with exogenous markers (*e.g.* fluorescent dyes) can alter significantly the physiological state of the cell. The first use of the RT for the analysis of biological systems was reported in 2002 by Ajito and Torimitsu [416]. They recorded Raman spectra of optically trapped synaptosomes (nerve-ending vesicular particles 500–700 nm in diameter isolated from rat brain neurons) suspended in phosphate buffer. Depending on the synaptosome concentration in the solution, multiple or individual particles were trapped and analyzed (see Fig. 23A). In all cases, the recorded Raman spectra contained characteristic peaks corresponding to lipids (CH_2 deformation mode at 1445 cm^{-1}) and proteins (amide I mode at 1657 cm^{-1}) (see Fig. 23B) confirming the presence of these two molecular species in the synaptosomes. Also in 2002, Xie *et al.* used the RT to obtain the Raman scattering spectra of single red blood cells and yeast cells, both living and dead after several minute's exposure to boiling water [417]. A significant difference between the Raman spectra of living and dead yeast cells was observed (see Fig. 24). The same authors then investigated the dynamics of the heat denaturation of proteins in bacterial and yeast cells using phenylalanine band at 1004 cm^{-1} as a reference and compared the results from live cell measurements with experiments done on model protein and amino acid solutions [418]. The comparison of both measurements suggested that the observed differences in Raman spectra can be attributed to the changes in the local phenylalanine environment resulting from thermal denaturation of the proteins. More subtle changes in the cell molecular composition can be triggered by exposing the cell to a small perturbation of the local environment parameters (*e.g.* change in pH, salt concentration, presence of toxins or nutrients, *etc.*). Studying the cell response to such ambient stress on a single cell level is very important for elucidating the mechanisms that allow the cell to recover from the stress and eventually develop tolerance toward the stress factors. A study of the yeast cell response to the heat and hyperosmotic stress conditions was conducted by Singh *et al.* [419]. Upon exposure to hyperosmotic environment (10% glucose solution), the trapped cell reacted (with a certain time lag) by producing glycerol in order to balance the osmotic pressure difference and also larger amount of ethanol as expected in the fermentation mode. A similar stress-response study was done on red blood cells exposed to alcohol solution [420]. Normal and thalassemic red blood cells were characterized using RT for the resonant Raman spectroscopy of hemoglobin in combination with the cell deformability measurements [421]. RT have found

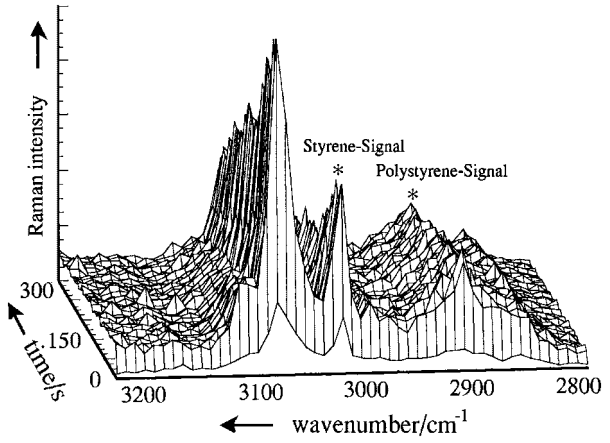

Figure 22. Raman spectra of the C–H-stretching region as a function of time of an optically trapped emulsion droplet during the styrene polymerization process. With kind permission from Springer Science+Business Media [410].

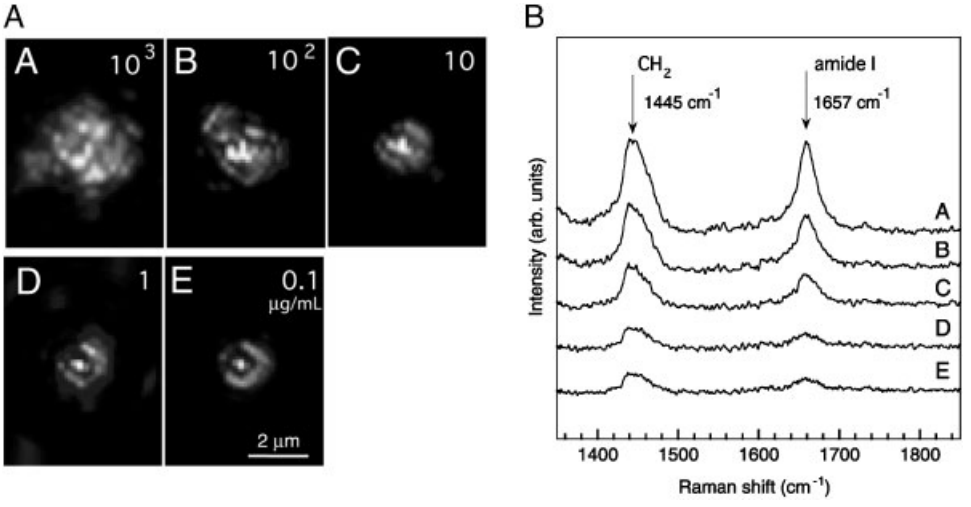

Figure 23. (A) Aggregated and individual optically trapped synaptosomes observed in the backreflected light of the trapping laser. The synaptosome concentrations are (A) 10^3 µg/mL, (B) 10^2 µg/mL, (C) 10 µg/mL, (D) 1 µg/mL, and (E) 0.1 µg/mL, respectively. (B) Raman spectra of aggregated and individual synaptosomes corresponding to the images in part (A). Reprinted with permission from [416]. Copyright (2002), Royal Society of Chemistry.

a number of applications in the field of detection and identification of suspended bacterial cells: Raman spectra were used to separate bacteria from similarly sized non-living objects [422], discriminate between six different bacterial species [423], and detect the onset of kinetic germination of bacterial spores [424]. Artificial phospholipid membrane vesicles are another frequent target of RT investigation. These particles serve as an essential model for the transport inside and across biological cell membranes [425] and they also play an important role in the medical and pharmaceutical research as containers for the targeted drug delivery [426]. Individual unilamellar vesicles (~600 nm in diameter) prepared from various phospholipid molecules were investigated by Cherney *et al.* [427]. They were able to distinguish clearly between different phospholipids used for vesicle preparation and they also observed differences in the vesicle membrane permeability that were directly correlated with the liquid-crystal transition temperature of the particular used lipid molecule. Further investigation of the temperature-induced phase transitions in the vesicle membranes was conducted by Fox *et al.* [428, 429] who observed subtle spectral changes indicative of sub- and pretransitions and main transitions in phospholipid vesicle membranes. The obtained results were in good agreement with the differential scanning calorimetry measurements. The same authors observed the changes in the vesicle membrane disorder upon interaction with non-steroidal antiinflammatory drugs (ibuprofen, salicylate) [430]; they monitored the drug-induced changes in the membrane permeability and partitioning of different drugs into the vesicle membrane.

Current trends in the field of RT are geared toward the applications of the technique in the routine chemical, biological, and medical analysis. To this end, RT have been combined with microfluidic systems that allow fast, controlled exchange of the microliter volumes of working fluids in the sample chamber, injection and collection of the analyzed specimen through multiple inlet/outlet ports, and incorporation of various optical sorting techniques [431, 432] (see Section 4.6). Such a combination of RT with a microfluidic system was employed by Ramser *et al.* to study the oxygenation cycle in single optically trapped red blood cells [433, 434]. The transition between the oxygenated and de-oxygenated hemoglobin states was triggered by flushing the working channel with the solution of sodium dithionite in HEPES buffer *via* electro-osmotic flow. For microfluidic RT applications, a trapping scheme was proposed, which uses dual-beam optical trap based on two optical fibers [70]. An even more compact system was designed by Cran-McGreehin *et al.* who integrated microfluidic channels directly onto semiconductor laser material creating a compact integrated optical trap that requires no alignment and is fully portable [69].

In a classical single-beam optical trap, it is impossible to control fully the orientation of the trapped object; thus, RT based on such a trapping scheme is not suitable for obtaining Raman maps of the trapped objects that report on the molecular distribution within the object. However, using HOT with multiple trapping beams generated by computer-controlled phase masks, Creely *et al.* were able to obtain spatially resolved images of proteins and lipids inside floating Jurkat cells (see Fig. 25) [435, 436]. To a certain

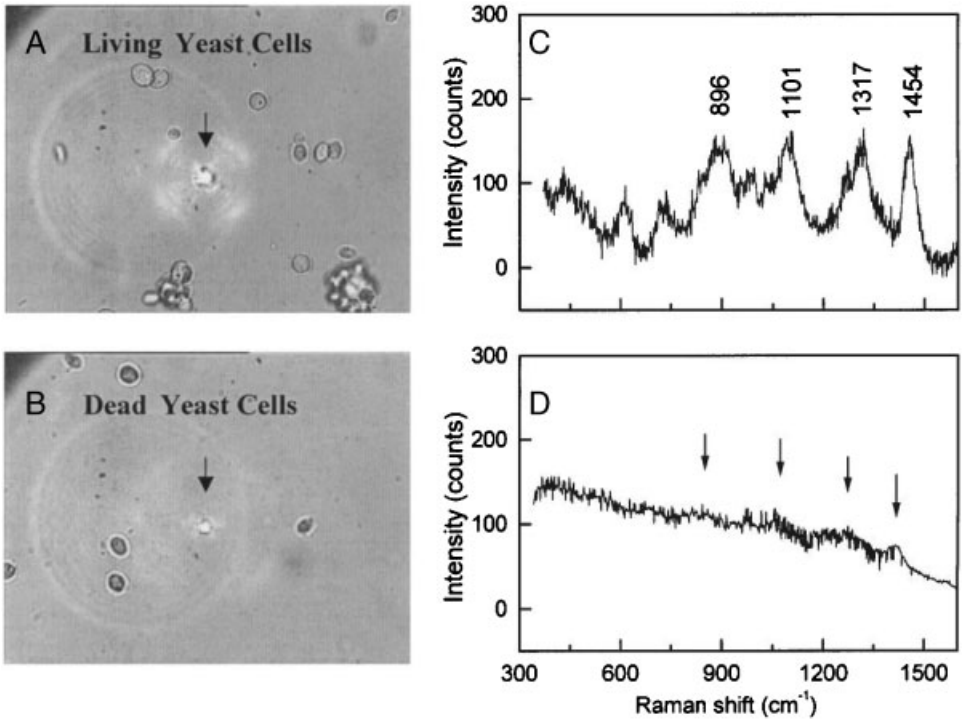

Figure 24. Images and NIR Raman spectra of a single living yeast cell (A and C) and a dead yeast cell (B and D) trapped in solution. Comparison of living and dead cell Raman spectra ((C) and (D), respectively) reveals significant differences. Reprinted with permission from [417]. Copyright (2002), Optical Society of America.

extent, spatially resolved Raman spectroscopy of the trapped cells was also possible with the arrangement of Jess *et al.* [70].

One of the drawbacks of the spontaneous Raman spectroscopy is its low scattering cross section. Therefore, obtaining Raman spectra of cells with sufficient signal-to-noise ratio typically requires tens of seconds at every location, which puts limits on the practical applicability of the Raman imaging of cells, precluding the study of fast dynamics events. However, it is possible to improve significantly this situation by using the phenomenon of the surface enhancement of Raman scattering in the proximity of metallic nanoobjects (surface-enhanced Raman scattering (SERS) [437]; see also Section 4.7). In order to use SERS for Raman imaging of eucaryotic cells, Zhang *et al.* incubated Chinese hamster ovary cells with colloidal gold nanoparticles 50 nm in diameter prior to the RT experiments [438]. Subsequently, they were able to recorded spatially resolved Raman maps of the cells. Use of SERS, however, brings along its own challenges. Comparison of normal Raman and SERS spectra reveals not only an enhancement of the normal Raman spectral features but also the appearance of spectral features absent in the normal Raman spectrum and shifts of the spectral peaks caused by various effects (chemisorption or chemical bonding, polarizability variations, change in the transition selection rules due to the molecule–substrate coupling, *etc.*) [439].

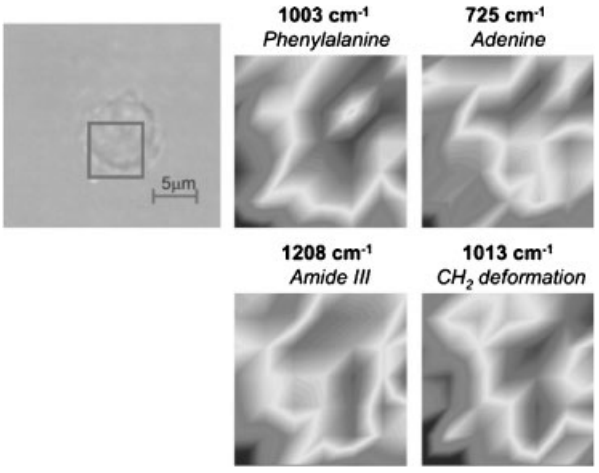

Figure 25. Visual image (left) and Raman spectral images (right) of a single optically trapped floating Jurkat cell with different Raman lines imaged. Reprinted with permission from [409]. Copyright (2007), Institute of Physics.

5 Emerging applications of combined optical micro-manipulation methods

Except the well-established techniques and methods listed in the previous section, a number of new experimental arrangements are emerging. These novel techniques are usually interdisciplinary with accent on applications in chemistry and biology.

5.1 Concurrent single-molecule optical manipulation and fluorescence

Owing to their ability to exert well-defined loads on individual molecules and follow the molecular response to the applied force, OT equipped with a sensitive position detection system have become a workhorse in the fields of single-molecule biophysics and biochemistry (see Section 4.1 for references). Another fundamental technique of the single-molecule research is wide-field or confocal single-molecule fluorescence spectroscopy; its numerous variations (fluorescence correlation spectroscopy, fluorescence polarization microscopy, Förster resonance energy transfer, *etc.*) have enabled studying subtle changes in the molecular structure, conformation, orientation, and functional state [440–443]. Marriage of the two above-mentioned techniques then provides a powerful tool for unraveling the quantitative correlation between the molecular conformation, orientation, or chemical state and the external force applied to the molecules (*e.g.* DNA–protein complexes [444–446], cytoskeleton crosslinkers [447], or DNA molecules [448–450]). In combined optical trapping-fluorescence experiments, independent light sources are used to accomplish both tasks as this allows optimizing their parameters (*e.g.* wavelength and total power) for their respective purposes.

Major challenges of combining the single-molecule optical trapping and fluorescence in a single experiment lie in detecting the weak signal of an individual fluorescent molecule within the background of enormous photon flux of the trapping laser (typically more than 10 orders of magnitude higher) [451] and decrease in the fluorophore lifetime due to photobleaching induced by multi-photon absorption of the trapping beam [452]. A possible solution to these problems is the separation of trapping and fluorescence measurements in time (sequential measurement [453]) and/or space (use of long linkers between the studied molecule and trapping handle [444, 450]). However, this precludes temporal correlation of the mechanical and fluorescence signals and imposes restrictions on the available experimental configurations. Lang *et al.* addressed the above issue by using spectrally separated fluorescence excitation beams (wavelengths 488–532 nm) and trapping/position detection beams (1064 and 975 nm, respectively) which allowed highly efficient filtering of the trapping light in the fluorescence detection path [454]. Moreover, they minimized the exposure of the sample to light during an experiment *via* computer automation; this further increased the lifetime of the studied fluorophores. In a later modification, they introduced an interlaced optical trapping-fluorescence scheme: by high-frequency out-of-phase modulation of the trapping and fluorescence excitation beam intensity (*i.e.* either the trapping or the fluorescence beam is on), they increased the Cy3 fluorophore lifetime by a factor of 20

[448]. With the modified set-up, they performed DNA unzipping experiments using the Cy3 fluorescence intensity as a marker for unzipping event. Capitanio *et al.* replaced fluorescent dye molecules with quantum dots in order to increase the maximal observation time and achieve higher signal-to-noise ratio for a more precise spatial localization of the fluorescent marker [455]. They demonstrated the spatial and temporal resolution of their set-up by imaging a single quantum dot attached to an actin filament that was suspended between two optically trapped beads.

The use of concurrent optical trapping and fluorescence for detecting the position of an optically trapped fluorescently labeled probe represents a somewhat simpler task as the problems with the probe brightness and lifetime are greatly reduced due to a large number of available fluorophors. Florin *et al.* used the two-photon fluorescence excited in the trapped particle by the continuous-wave trapping beam (wavelength 1064 nm) in order to monitor the axial and lateral displacements of the particle in the trap [298]. Agate *et al.* employed an fs-pulsed beam at 800 nm for simultaneous optical trapping and two-photon fluorescence observation; they could switch the fluorescence on and off by switching the laser source between the fs and continuous wave regimes [456].

5.2 Optically manipulated chemical micro-reactors

Recent development of analytical techniques has witnessed a still-increasing introduction of miniaturized lab-on-a-chip systems capable of performing simultaneously tens or hundreds of analyses using sub-picoliter volumes of the analyte. Thus, it reaches the level of throughput and reduction in the material consumption necessary in the genomics and proteomics era [457]. Optical micro-manipulation techniques have become an integral part of such miniaturized analytical systems. These techniques can serve for confinement, transport, and sorting of liposomes and dispersed micro-droplets – fluid particles exploitable as picoliter-sized reaction containers. With such micro-reactors, chemical reaction can be triggered in a controlled manner by bringing the liposomes or microdroplets of various chemical contents into contact by OT and inducing their fusion [458, 459]. Especially attractive is then the combination of optical micro-manipulation and spectroscopy that enables to monitor the kinetics of the chemical reaction in question [410–413, 427, 460].

Optically manipulated liposomes containing reconstituted membrane protein (γ-glutamyltransferase) were used for incorporating this protein into the plasma membrane of a selected target cell; this was achieved *via* the fusion of the vesicle and cell lipid membranes induced by the electric field applied locally through microfabricated electrodes [461]. Sun and Chiu used optically manipulated synthetic nanocapsules loaded with cellular effector to induce signaling cascade in Chinese hamster ovary cells expressing membrane receptors for the used effector; the effector molecules were released from the capsules using a single UV laser pulse [462].

5.3 Optically driven micro-pumps

Any translational or rotational motion of an optically trapped particle immersed in a liquid causes movement of the liquid in the immediate vicinity of the particle as the consequence of no-slip boundary conditions at the particle–-fluid interface. This phenomenon can be exploited for inducing controlled flow in the fluid and it has indeed been used – in combination with microfluidic systems – for fluid propulsion. Terray *et al.* demonstrated micro-pumps based on circular motion of two pairs of particles rotating in opposite directions or peristaltic motion of an array of particles trapped in time-sharing traps [463]. Similarly, Ladavac and Grier employed the synchronized orbiting motion of many particles confined in high-intensity rings of several vortex beams generated by holographic tweezers [464]. They arranged the vortex beams along two lines in which the particles orbited in opposed directions; consequently the fluid in between the two lines of traps moved, which was visualized by following the trajectory of a non-trapped tracer particle (see Fig. 26). Leach *et al.* used two spherical birefringent particles (vaterite crystallites) trapped in two beams of opposite circular polarization [465]. The rotation of vaterite particles again caused fluid movement in the gap between them.

Micro-pumps driven directly by optical forces and torques are quite versatile; however, they can provide fluid flow rates only up to tens of micrometers *per* second with very low dynamic strength. Optically induced rotation of specially tailored asymmetric micro-gears and turbines could provide another step toward achieving higher fluid flow rates [207, 223, 466]. However, it seems that fluid flow velocities and especially volume flows of the fluid will not be able to compete with fluid flow induced by electro-osmosis further enhanced by optical control [467].

5.4 Spatially resolved pH measurement

Klauke *et al.* used polystyrene spheres of 3 and 6 μm in diameter functionalized with pH-sensitive SNARF-1 fluorescent dye. The intensity of SNARF-1 emission at 580 nm decreases with increasing pH, whereas the intensity at 640 nm behaves in an opposite manner. Such an optically trapped probe then enabled examination of pH distribution in the vicinity of a pair of planar gold microelectrodes located within a microfluidic system [468]. Maruyama *et al.* used a pH-sensing gel-microbead functionalized with bromothymol blue and manipulated with OT to adhere it to a desired point in the microchip [469].

5.5 Micro-manipulation of aerosols

From the description presented so far it might appear that the optical trapping and manipulation are associated exclusively with particles immersed in liquids. However,

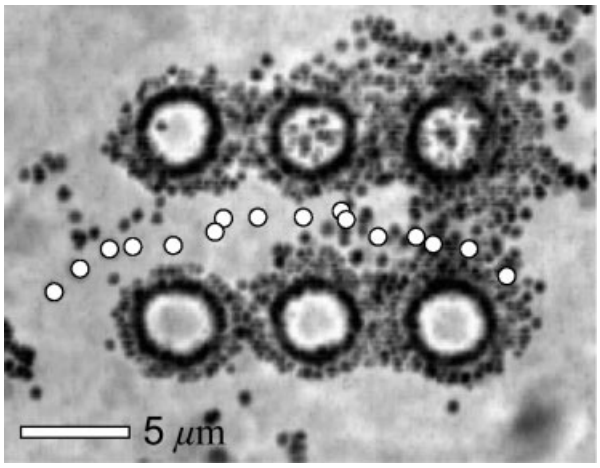

Figure 26. Time-lapse composite of 16 images in half-second intervals of colloidal spheres flowing through the holographic pump at $P = 2.4$ W. White circles identify the trajectory of a single sphere as it moves 25 μm to the left in 7 s with a peak speed of 5 μm/s. Reprinted with permission from [464]. Copyright (2004), Optical Society of America.

already the pioneering levitation experiments of Ashkin were performed in air and vacuum [6]. Twenty-five years later, Omori *et al.* also presented the single-beam gradient force optical trapping of micron-sized glass spheres in air [470]. In order to overcome the surface adhesion forces that kept the particles attached to the supporting glass slide, they used a vibrating piezoelectric transducer that lifted the microspheres off of the substrate. In general, the process of transfer of the target particle into the trap is more challenging in air than in a fluid. One reason is the above-mentioned adhesion effects (for solid particles) and, furthermore, much faster dynamics of dispersed particles whose motion in the surrounding medium is not damped by the viscous drag.

Recently, optical trapping in air has gained increased attention, mainly because of the importance of aerosols in a wide range of scientific disciplines ranging from atmospheric chemistry and physics, through the study of combustion processes, to drug delivery and spreading of airborne pathogenes and contaminant particles. Aerosol particles cover the size range of a few nanometers to tens of micrometers and can be multiphase or multi-component, with the composition at the droplet surface varying significantly from the bulk. Optical trapping techniques coupled to the methods of optical spectroscopy (*e.g.* Raman – see Section 4.8) are especially attractive for studying the properties of aerosols as they enable to isolate an individual aerosol particle and study its composition and dynamics [58, 408, 412, 413, 471]. To this end, single-beam, dual-beam, and HOT have been used to manipulate with aerosols, perform controlled coagulation of selected aerosol particles [472], or enhance their Raman scattering signal and study the evolution of the droplet size by employing size- and refractive-index-dependent structural Mie resonances in the droplets [410, 411, 473].

OT have also been used to study phase transitions in small chemical (triethylamine), polymer (poly(*N*-isopropylacrylamide)) and protein (elastin) systems at the level of single droplets [474].

6 Conclusions

For more than 30 years, mechanical effects of light have been employed to guide, levitate, spatially confine, and manipulate microobjects, nanoobjects, and atoms. Within this period, the optical trapping has been gradually developed to permit simultaneously many-particle manipulation and combined with other experimental techniques for probing the composition and structure of the illuminated objects and changing actively their properties. The combinations of optical micromanipulation with the potential offered by microfluidics, Raman microspectroscopy, precise detection of the manipulated particle's position, dynamic light wavefront shaping by the SLM, and real-time computer control of the experimental systems have lead to a number of fascinating applications. The most prominent ones include optical sorting of heterogeneous colloidal suspensions solely by illumination with light of specifically tailored spatial intensity distribution, active selection and isolation of target microobjects (such as living cells) on the basis of their material composition, optically driven micro-motors propelling fluid in microchannels, OC, optical stretcher and micro-rheometers for determining visco-elastic properties of living cells and complex fluids, detection of tiny interaction forces between single biological molecules, and other micro-opto-fluidic analytical and preparative tools. At present, intense research is carried out on both theoretical and experimental aspects of the advanced optical micro-manipulation in order to understand the physical principles and phenomena governing the functioning of the micro-manipulation systems and design new, more efficient configurations for handling specific experimental tasks.

Current trends in the field of the combined optical micro-manipulation techniques largely focus on their applications in the routine chemical, biological, and medical analyses and preparations. An obvious advantage of these techniques lies in the ease and inexpensiveness of the experimental system re-configuration for a specimen with different physical and chemical properties, the ability to handle minute volumes of the analyte/specimen with large efficiency, and the possibility of the massive parallelization of the analysis channels. On the other hand, the throughput of a single analysis channel is relatively low in comparison with conventional techniques (*e.g.* flow cytometry or FACS). Consequently, the novel micro-manipulation techniques based on the use of the optical forces complement the well-established ones in the scope of applications and provide the research community with a much wider choice of experimental analytical and

preparative tools for facing the challenges of the genomic and proteomic era.

The authors acknowledge the support from the MEYS CR (LC06007, OC08034), ISI IRP (AV0Z20650511).

The authors have declared no conflict of interest.

7 References

[1] Chu, S., *Rev. Mod. Phys.* 1998, *70*, 685–706.

[2] Phillips, W. D., *Rev. Mod. Phys.* 1998, *70*, 721–741.

[3] Cohen-Tannoudji, C. N., *Rev. Mod. Phys.* 1998, *70*, 707–719.

[4] Ketterle, W., *Rev. Mod. Phys.* 2002, *74*, 1131–1151.

[5] Ashkin, A., *Phys. Rev. Lett.* 1970, *24*, 156–159.

[6] Ashkin, A., Dziedzic, J. M., *Appl. Phys. Lett.* 1971, *19*, 283–285.

[7] Ashkin, A., *Proc. Natl. Acad. Sci. USA* 1997, *94*, 4853–4860.

[8] Ashkin, A., *IEEE J. Sel. Top. Quant. Electron.* 2000, *6*, 841–856.

[9] Ashkin, A., *Optical Trapping and Manipulation of Neutral Particles using Lasers*, World Scientific, London 2006.

[10] Ashkin, A., Dziedzic, J. M., Bjorkholm, J. E., Chu, S., *Opt. Lett.* 1986, *11*, 288–290.

[11] Mehta, A. D., Rief, M., Spudich, J. A., Smith, D. A. *et al.*, *Science* 1999, *283*, 1689–1695.

[12] Bustamante, C., Bryant, Z., Smith, S. B., *Nature* 2003, *421*, 423–427.

[13] Deniz, A. A., Mukhopadhyay, S., Lemke, E. A., *J. R. Soc. Interface* 2008, *5*, 15–45.

[14] Noy, A., *Handbook of Molecular Force Spectroscopy* Springer, Berlin, 2007.

[15] Greulich, K.-O., *Micromanipulation by Light in Biology and Medicine*, Birkhauser Verlag, Basel-Boston-Berlin 1999.

[16] Sheetz, M. P., Wilson, L., Matsudaira, P. (Eds.), Methods in cell biology, in: *Laser Tweezers in Cell Biology*, vol. 55, Academic Press, San Diego 1998.

[17] Berns, M. W., Greulich, K. O. (Eds.), Methods in cell biology, in: *Laser Manipulation of Cells and Tissues*, vol. 82, Academic Press, San Diego 2007.

[18] Andrews, D. (Ed.), *Structured Light and its Applications*, Elsevier Academic Press, Burlington, USA San Diego, USA, London, UK 2008.

[19] Lang, M. J., Block, S. M., *Am. J. Phys.* 2003, *71*, 201–215.

[20] Sato, S., Harada, Y., Waseda, Y., *Opt. Lett.* 1994, *19*, 1807–1809.

[21] Furukawa, H., Yamaguchi, I., *Opt. Lett.* 1998, *23*, 216–218.

[22] Ke, P., Gu, M., *Appl. Opt.* 1999, *38*, 160–167.

[23] Sasaki, K., Koshioka, M., Misawa, H., Kitamura, N. *et al.*, *Appl. Phys. Lett.* 1992, *60*, 807–809.

[24] Chaumet, P., Nieto-Vesperinas, M., *Opt. Lett.* 2000, *25*, 1065–1067.

[25] Draine, B., *Astrophys. J.* 1988, *333*, 848–872.

[26] Ashkin, A., Gordon, J. P., *Opt. Lett.* 1983, *10*, 511–513.

[27] Novotny, L., Hecht, B., *Principles of Nano-Optics*, Cambridge University Press, Cambridge 2006.

[28] Harada, Y., Asakura, T., *Opt. Commun.* 1996, *124*, 529–541.

[29] Zemánek, P., Karásek, V., Sasso, A., *Opt. Commun.* 2004, *240*, 401–415.

[30] Jackson, J. D., *Classical Electrodynamics*, Wiley, New York 1999.

[31] Barton, J. P., Alexander, D. R., Schaub, S. A., *J. Appl. Phys.* 1989, *66*, 4594–4602.

[32] Ren, K. F., Gréhan, G., Gouesbet, G., *Appl. Opt.* 1996, *35*, 2702–2710.

[33] Mazolli, A., Neto, P. A. M., Nussenzveig, H. M., Theory of trapping forces in optical tweezers, in: *Proceedings of the Royal Society of London A* 2003, vol. 459, p. 3021–3041.

[34] Rohrbach, A., *Phys. Rev. Lett.* 2005, *95*, 168102.

[35] Neves, A. A. R., Fontes, A., Cesar, C. L., Camposeo, A. *et al.*, *Phys. Rev. E* 2007, *76*, 061917.

[36] Viana, N. B., Rocha, M. S., Mesquita, O. N., Mazolli, A. *et al.*, *Phys. Rev. E* 2007, *75*, 021914.

[37] Xu, Y.-L., *Appl. Opt.* 1995, *34*, 4573–4588.

[38] Ng, J., Lin, Z. F., Chan, C. T., Sheng, P., *Phys. Rev. B* 2005, *72*, 085130.

[39] Nieminen, T. A., Knöner, G., Heckenberg, N. R., Rubinsztein-Dunlop, H., *Methods Cell Biol.* 2007, *82*, 207–236.

[40] Xu, F., Ren, K., Gouesbet, G., Cai, X. *et al.*, *Phys. Rev. E* 2007, *75*, 026613.

[41] Grzegorczyk, T. M., Kemp, B. A., Kong, J. A., *J. Opt. Soc. Am. A* 2006, *23*, 2324–2330.

[42] Chaumet, P. C., Billaudeau, C. J., *Appl. Phys.* 2007, *1011*, 023106.

[43] Hoekstra, A. G., Frijlink, M., Waters, L. B. F. M., Sloot, P. M. A., *J. Opt. Soc. Am. A* 2001, *18*, 1944–1953.

[44] White, D. A., *Comp. Phys. Commun.* 2000, *128*, 558–564.

[45] Collet, W. L., Ventrice, C. A., Mahajan, S. M., *Appl. Phys. Lett.* 2003, *82*, 2730–2732.

[46] Gauthier, R. C., *Opt. Express* 2005, *13*, 3707–3718.

[47] Zakharian, A. R., Mansuripur, M., Moloney, J. V., *Opt. Express* 2005, *13*, 2321–2336.

[48] Benito, D. C., Simpson, S. H., Hanna, S., *Opt. Express* 2008, *16*, 2942–2957.

[49] Nieminen, T. A., Loke, V. L. Y., Stilgoe, A. B., Knöner, G. *et al.*, *J. Opt. A: Pure Appl. Opt.* 2007, *9*, S196–S203.

[50] Ashkin, A., *Biophys. J.* 1992, *61*, 569–582.

[51] Gussgard, R., Lindmo, T., Brevik, I., *J. Opt. Soc. Am. B* 1992, *9*, 1922–1929.

[52] Gu, M., Ke, P., Gan, X., *Rev. Sci. Instrum.* 1997, *68*, 3666–3668.

[53] Ashkin, A., Dziedzic, J., *Appl. Phys. Lett.* 1976, *28*, 333–335.

[54] Ashkin, A., Dziedzic, J., *Phys. Rev. Lett.* 1977, *38*, 1351–1354.

[55] Molloy, J. E., Padgett, M. J., *Contemp. Phys.* 2002, *43*, 241–258.

[56] Grier, D. G., *Nature* 2003, *424*, 810–816.

[57] Neuman, K. C., Block, S. M., *Rev. Sci. Instrum.* 2004, *75*, 2787–2809.

[58] McGloin, D., *Philos. Trans. R. Soc. Lond. A* 2006, *364*, 3521–3537.

[59] Appleyard, D. C., Vandermeulen, K. Y., Lee, H., Lang, M. J., *Am. J. Phys.* 2007, *75*, 5–14.

[60] Dholakia, K., Reece, P., *Nanotoday* 2006, *1*, 18–27.

[61] Lee, W. M., Reece, P. J., Marchington, R. F., Metzger, N. K. *et al.*, *Nat. Protoc.* 2007, *2*, 3226–3238.

[62] Dholakia, K., Reece, P., Gu, M., *Chem. Soc. Rev.* 2008, *35*, 42–55.

[63] Zhang, H., Liu, K.-K., *J. R. Soc. Interface* 2008, *5*, 671–690.

[64] Constable, A., Kim, J., *Opt. Lett.* 1993, *18*, 1867–1869.

[65] Collins, S. D., Baskin, R. J., Howitt, D. G., *Appl. Opt.* 1999, *38*, 6068–6074.

[66] Guck, J., Ananthakrishnan, R., Moon, T. J., Cunningham, C. C. *et al.*, *Phys. Rev. Lett.* 2000, *84*, 5451–5154.

[67] Guck, J., Ananthakrishnan, R., Mahmood, H., Moon, T. *et al.*, *Biophys. J.* 2001, *81*, 767–784.

[68] Guck, J., Schinkinger, S., Lincoln, B., Wottawah, F. *et al.*, *Biophys. J.* 2005, *88*, 3689–3698.

[69] Cran-McGreehin, S. J., Krauss, T. F., Dholakia, K., *Lab Chip* 2006, *6*, 1122–1124.

[70] Jess, P., Garcés-Chávez, V., Smith, D., Mazilu, M. *et al.*, *Opt. Express* 2006, *14*, 5779–5791.

[71] Vossen, D., van der Horst, A., Dogterom, M., van Blaaderen, A., *Rev. Sci. Instrum.* 2004, *75*, 2960–2970.

[72] Rodrigo, P., Daria, V., Glückstad, J., *Appl. Phys. Lett.* 2005, *86*, 074103.

[73] Rodrigo, P., Gammelgaard, L., Boggild, P., Perch-Nielsen, I. *et al.*, *Opt. Express* 2005, *13*, 6899–6904.

[74] Svoboda, K., Block, S. M., *Annu. Rev. Biophys. Biomol. Struct.* 1994, *23*, 247–285.

[75] Zemánek, P., Jonáš, A., Jákl, P., Šerỳ, M. *et al.*, *Opt. Commun.* 2003, *220*, 401–412.

[76] Rohrbach, A., Stelzer, E. H. K., *Appl. Opt.* 2002, *41*, 2494–2507.

[77] Neuman, K., Abbondanzieri, E., Block, S., *Opt. Lett.* 2005, *30*, 1318–1320.

[78] Pesce, G., Sasso, A., Fusco, S., *Rev. Sci. Instrum.* 2005, *76*, 115105.

[79] Reihani, S. N. S., Oddershede, L. B., *Opt. Lett.* 2007, *32*, 1998–2000.

[80] Rohrbach, A., Tischer, C., Neumayer, D., Florin, E.-L. *et al.*, *Rev. Sci. Instrum.* 2004, *75*, 2197–2210.

[81] Mellor, C. D., Bain, C. D., *Chemphyschem* 2006, *7*, 329–332.

[82] Garcés-Chávez, V., Dholakia, K., Spalding, G. C., *Appl. Phys. Lett.* 2005, *86*, 031106:1–031106:3.

[83] Reece, P. J., Garcés-Chávez, V., Dholakia, K., *Appl. Phys. Lett.* 2006, *88*, 221116.

[84] Reece, P. J., Wright, E. M., Dholakia, K., *Phys. Rev. Lett.* 2007, *98*, 203902.

[85] Čižmár, T., Garcés-Chávez, V., Dholakia, K., Zemánek, P., *Appl. Phys. Lett.* 2005, *86*, 174101:1–174101:3.

[86] Zhao, Y., Zhan, Q., Zhang, Y., Li, Y.-P., *Opt. Lett.* 2005, *7*, 848–850.

[87] Šiler, M., Čižmár, T., Šerý, M., Zemánek, P., *Appl. Phys. B* 2006, *84*, 157–165.

[88] Bingelyte, V., Leach, J., Courtial, J., Padgett, M., *Appl. Phys. Lett.* 2003, *82*, 829–831.

[89] Knöner, G., Parkin, S., Heckenberg, N., Rubinsztein-Dunlop, H., *Phys. Rev. E* 2005, *72*, 031507.

[90] Di Leonardo, R., Leach, J., Mushfique, H., Cooper, J. *et al.*, *Phys. Rev. Lett.* 2006, *96*, 134502.

[91] Sasaki, K., Koshioka, M., Misawa, H., Kitamura, N. *et al.*, *Opt. Lett.* 1991, *16*, 1463–1465.

[92] Mio, C., Marr, D. W. M., *Langmuir* 1999, *15*, 8565–8568.

[93] Arai, F., Yoshikawa, K., Sakami, T., Fukuda, T., *Appl. Phys. Lett.* 2004, *85*, 4301–4303.

[94] Mio, C., Gong, T., Terray, A., Marr, D. W. M., *Rev. Sci. Instrum.* 2000, *71*, 2196–2200.

[95] Visscher, K., Gross, S. P., Block, S. M., *IEEE J. Sel. Top. Quant. Electron.* 1996, *2*, 1066–1076.

[96] Valentine, M. T., Guydosh, N. R., Gutierrez-Medina, B., Fehr, A. N. *et al.*, *Opt. Lett.* 2008, *33*, 599–601.

[97] Ozcan, M., Onal, C., Akatay, A., *J. Mod. Opt.* 2006, *53*, 357–364.

[98] Fällman, E., Axner, O., *Appl. Opt.* 1997, *36*, 2107–2113.

[99] Dufresne, E. R., Grier, D. G., *Rev. Sci. Instrum.* 1998, *69*, 1974–1977.

[100] Reicherter, M., Haist, T., Wagemann, E. U., Tiziani, H. J., *Opt. Lett.* 1999, *24*, 608–610.

[101] Curtis, J. E., Koss, B. A., Grier, D. G., *Opt. Commun.* 2002, *207*, 169–175.

[102] Jesacher, A., Maurer, C., Schwaighofer, A., Bernet, S. *et al.*, *Opt. Express* 2008, *16*, 4479–4486.

[103] Grier, D., Roichman, Y., *Appl. Opt.* 2006, *45*, 880–887.

[104] Eriksen, R. L., Mogensen, P. C., Glückstad, J., *Opt. Lett.* 2002, *27*, 267–269.

[105] Ferrari, E., Emiliani, V., Cojoc, D., Garbin, V. *et al.*, *Microelectron. Eng.* 2005, *78–79*, 575–581.

[106] Whyte, G., Gibson, G., Leach, J., Padgett, M. *et al.*, *Opt. Express* 2006, *14*, 12497–12502.

[107] Pleguezuelos, E., Carnicer, A., Andilla, J., Martin-Badosa, E. *et al.*, *Comput. Phys. Commun.* 2007, *176*, 701–709.

[108] Ogura, Y., Kagawa, K., Tanida, J., *Appl. Opt.* 2001, *40*, 5430–5435.

[109] Tam, J. M., Biran, I., Walt, D. R., *Appl. Phys. Lett.* 2006, *89*, 194101.

[110] Sun, Y. Y., Ong, L. S., Yuan, X.-C., *Appl. Phys. Lett.* 2006, *89*, 141108:1–141108:3.

[111] Sun, Y. Y., Yuan, X.-C., Ong, L. S., Bu, J. *et al.*, *Appl. Phys. Lett.* 2007, *90*, 031107:1–031107:3.

[112] Merenda, F., Rohner, J., Fournier, J.-M., Salathé, R.-P., *Opt. Express* 2007, *15*, 6075–6086.

[113] Burns, M. M., Fournier, J.-M., Golovchenko, J. A., *Science* 1990, *249*, 749–754.

[114] Chiou, A. E., Wang, W., Sonek, G. J., Hong, J. *et al.*, *Opt. Commun.* 1997, *133*, 7–10.

[115] MacDonald, M. P., Paterson, L., Sibbett, W., Dholakia, K., *Opt. Lett.* 2001, *26*, 863–865.

[116] Rubinov, A. N., Katarkevich, V. M., Afanas, A. A., Efendiev, T. S., *Opt. Commun.* 2003, *224*, 97–106.

[117] Casaburi, A., Pesce, G., Zemánek, P., Sasso, A., *Opt. Commun.* 2005, *251*, 393–404.

[118] Schonbrun, E., Pistun, R., Jordan, P., Cooper, J. *et al.*, *Opt. Express* 2005, *13*, 3777–3786.

[119] Čižmár, T., Kollárová, V., Bouchal, Z., Zemánek, P., *New J. Phys.* 2006, *8*, 43.

[120] Zemánek, P., Jonáš, A., Šrámek, L., Liška, M., *Opt. Commun.* 1998, *151*, 273–285.

[121] Zemánek, P., Jonáš, A., Šrámek, L., Liška, M., *Opt. Lett.* 1999, *24*, 1448–1450.

[122] Čižmár, T., Šiler, M., Zemánek, P., *Appl. Phys. B* 2006, *84*, 197–203.

[123] Šiler, M., Zemánek, P., *Opt. Commun.* 2007, *275*, 409–420.

[124] Grzegorczyk, T. M., Kong, J. A., *Opt. Express* 2007, *15*, 8010–8020.

[125] MacDonald, M. P., Spalding, G. C., Dholakia, K., *Nature* 2003, *426*, 421–424.

[126] Gahagan, K., Swartzlander, G., *Opt. Lett.* 1996, *21*, 827–829.

[127] Gahagan, K., Swartzlander, G., *J. Opt. Soc. Am. B* 1998, *15*, 524–534.

[128] Gahagan, K. T., Swartzlander, G. A., *J. Opt. Soc. Am. B* 1999, *16*, 533–537.

[129] Ye, J., Chang, G., Norris, T., Tse, C. *et al.*, *Opt. Lett.* 2004, *29*, 2136–2138.

[130] Zemánek, P., Foot, C. J., *Opt. Commun.* 1998, *146*, 119–123.

[131] Arlt, J., Padgett, M. J., *Opt. Lett.* 2000, *25*, 191–193.

[132] Freegarde, T., Dholakia, K., *Phys. Rev. A* 2002, *66*, 013413.

[133] McGloin, D., Spalding, G., Melville, H., Sibbett, W. *et al.*, *Opt. Commun.* 2003, *225*, 215–222.

[134] Ahluwalia, B., Yuan, X., Tao, S., *Opt. Commun.* 2004, *238*, 177–184.

[135] Ahluwalia, B. P. S., Yuan, X. C., Tao, S. H., Cheong, W. C. *et al.*, *J. Appl. Phys.* 2006, *99*, 113104.

[136] Rodrigo, P., Daria, V., Glückstad, J., *Opt. Express* 2004, *12*, 1417–1425.

[137] Prentice, P., MacDonald, M., Frank, T., Cuschieri, A. *et al.*, *Opt. Express* 2004, *12*, 593–600.

[138] Mohanty, K. S., Liberale, C., Mohanty, S. K., Degiorgio, V., *Appl. Phys. Lett.* 2008, *92*, 151113.

[139] Jones, P. H., Marago, O. M., Stride, E. P. J., *J. Opt. A: Pure Appl. Opt.* 2007, *9*, S278–S283.

[140] Mohanty, S. K., Verma, R. S., Gupta, P. K., *Appl. Phys. B* 2007, *87*, 211–215.

[141] Girard, C. *Rep. Prog. Phys.* 2005, *68*, 1883–1933.

[142] Wazawa, T., Ueda, M., *Microsc. Tech.* 2005, *95*, 77–106.

[143] Hecht, B., Sick, B., Wild, U., Deckert, V. *et al.*, *J. Chem. Phys.* 2000, *112*, 7761–7774.

[144] Greffet, J., Carminati, R., *Prog. Surf. Sci.* 1997, *56*, 133–237.

[145] Novotny, L., Stranick, S., *Annu. Rev. Phys. Chem.* 2006, *57*, 303–331.

[146] Kawata, S., Sugiura, T., *Opt. Lett.* 1992, *17*, 772–774.

[147] Kawata, S., Tani, T., *Opt. Lett.* 1996, *21*, 1768–1770.

[148] Oetama, R. J., Walz, J. Y., *Colloid Surf. A* 2002, *211*, 179–195.

[149] Wada, K., Sasaki, K., Masuhara, H., *App. Phys. Lett.* 2000, *76*, 2815–2817.

[150] Wada, K., Sasaki, K., Masuhara, H., *Appl. Phys. Lett.* 2002, *81*, 1768–1770.

[151] Ruiz-Cortés, V., Vite-Frías, J. P., *Opt. Express* 2008, *16*, 6600–6608.

[152] Nieto-Vesperinas, N., Chaumet, P. C., Rahmani, R., *Philos. Trans. R. Soc. Lond. A* 2004, *362*, 719–737.

[153] Renn, M. J., Montgomery, D., Vdonin, O. V., Anderson, D. Z. *et al.*, *Phys. Rev. Lett.* 1995, *75*, 3253–3256.

[154] Brambilla, G., Murugan, G. S., Wilkinson, J. S., Richardson, D. J., *Opt. Lett.* 2007, *32*, 3041–3043.

[155] Tanaka, T., Yamamoto, S., *Appl. Phys. Lett.* 2000, *77*, 3131–3133.

[156] Grujic, K., Hellesø, O., Wilkinson, J., Hole, J., *Opt. Commun.* 2004, *239*, 227–235.

[157] Grujic, K., Hellesø, O. G., Hole, J. P., Wilkinson, J. S., *Opt. Express* 2005, *13*, 1–7.

[158] Hole, J., Wilkinson, J., Grujic, K., Hellesø, O., *Opt. Express* 2005, *13*, 3896–3901.

[159] Gaugiran, S., Gétin, S., Fedeli, J. M., Colas, G. *et al.*, *Opt. Express* 2005, *13*, 6956–6963.

[160] Schmidt, B. S., Yang, A. H. J., Erickson, D., Lipson, M., *Opt. Express* 2007, *15*, 14322–14334.

[161] Gaugiran, S., Getin, S., Fedeli, J. M., Derouard, J., *Opt. Express* 2007, *15*, 8146–8156.

[162] Ng, L. N., Zervas, M. N., Wilkinson, J. S., Luff, B. J., *Appl. Phys. Lett.* 2000, *76*, 1993–1995.

[163] Ng, L. N., Luff, B. J., Zervas, M. N., Wilkinson, J. S., *Opt. Commun.* 2002, *208*, 117–124.

[164] Schmidt, H., Hawkins, A., *Microfluid. Nanofluid.* 2008, *4*, 3–16.

[165] Grujic, K., Hellesø, O. G., *Opt. Express* 2007, *15*, 6470–6477.

[166] Čižmár, T., Šiler, M., Šerý, M., Zemánek, P. *et al.*, *Phys. Rev. B* 2006, *74*, 035105.

[167] Mellor, C. D., Fennerty, T. A., Bain, C. D., *Opt. Express* 2006, *14*, 10079–10088.

[168] Jaising, H. Y., Hellesø, O. G., *Opt. Commun.* 2005, *246*, 373–383.

[169] Kaiser, R., Lévy, Y., Vansteenkiste, N., Aspect, A. *et al.*, *Opt. Commun.* 1994, *104*, 234–240.

[170] Labeyrie, G., Landragin, A., von Zanthier, J., Kaiser, R. *et al.*, *Quantum Semiclassical Opt.* 1996, *8*, 603–627.

[171] Okamoto, K., Kawata, S., *Phys. Rev. Lett.* 1999, *83*, 4534–4537.

[172] Novotny, L., Bian, R. X., Xie, X. S., *Phys. Rev. Lett.* 1997, *79*, 645–648.

[173] Chaumet, P., Rahmani, A., Nieto-Vesperinas, M., *Phys. Rev. Lett.* 2002, *88*, 123601-1–123601-4.

[174] Gu, M., Haumonte, J.-B., Micheau, Y., Chon, J. W. M. *et al.*, *Appl. Phys. Lett.* 2004, *84*, 4236–4238.

[175] Gu, M., Kuriakose, S., Gan, X., *Opt. Express* 2007, *15*, 1369–1375.

[176] Volpe, G., Quidant, R., Badenes, G., Petrov, D., *Phys. Rev. Lett.* 2006, *96*, 238101.

[177] Garcés-Chávez, V., Quidant, R., Reece, P. J., Badenes, G. *et al.*, *Phys. Rev. B* 2006, *73*, 085417.

[178] Song, Y., Han, B., Chang, S., *Opt. Commun.* 2001, *198*, 7–19.

[179] Tan, Y. Y., Yuan, X.-C., Ong, B. H., Bu, J. *et al.*, *Appl. Phys. Lett.* 2007, *91*, 141108.

[180] Arias-González, J., Nieto-Vesperinas, M., *Opt. Lett.* 2002, *27*, 2149–2151.

[181] Arias-González, J., Nieto-Vesperinas, M., Lester, M., *Phys. Rev. B* 2002, *65*, 115402.

[182] Arias-González, J., Nieto-Vesperinas, M., *J. Opt. Soc. Am. A* 2003, *20*, 1201–1209.

[183] Quidant, R., Zelenina, S., Nieto-Vesperinas, M., *Appl. Phys. A* 2007, *89*, 233–239.

[184] Zelenina, A. S., Quidant, R., Nieto-Vesperinas, M., *Opt. Lett.* 2007, *32*, 1156–1158.

[185] Quidant, R., Petrov, D., Badenes, G., *Opt. Lett.* 2005, *30*, 1009–1011.

[186] Quidant, R., Badenes, G., Cheylan, S., Alcubilla, R. *et al.*, *Opt. Express* 2004, *12*, 282–287.

[187] Righini, M., Zelenina, A. S., Girard, C., Quidant, R., *Nature Phys.* 2007, *3*, 477–480.

[188] Baev, A., Furlani, E. P., Prasad, P. N., Grigorenko, A. N. *et al.*, *J. Appl. Phys.* 2008, *103*, 084316.

[189] Righini, M., Volpe, G., Girard, C., Petrov, D. *et al.*, *Phys. Rev. Lett.* 2008, *100*, 186804.

[190] Miao, X., Lin, L. Y., *IEEE J. Sel. Top. Quant. Electron.* 2007, *13*, 1655–1662.

[191] Quidant, R., Girard, C., *Laser Photon. Rev.* 2008, *2*, 47–57.

[192] Righini, M., Girard, C., Quidant, R. J., *Opt. A: Pure Appl. Opt.* 2008, *10*, 093001.

[193] Vasnetsov, M., Staliunas, K. (Eds.), *Optical Vortices*, Nova Science Publishers, New York 1999.

[194] Parkin, S., Knöner, G., Singer, W., Nieminen, T. A. *et al.*, *Methods Cell Boil.* 2007, *82*, 525–561.

[195] Paterson, L., MacDonald, M. P., Arlt, J., Sibbett, W. *et al.*, *Science* 2001, *292*, 912–914.

[196] MacDonald, M., Volke-Sepúlveda, K., Paterson, L., Arlt, J. *et al.*, *Opt. Commun.* 2002, *201*, 21–28.

[197] O'Neil, A., Padgett, M., *Opt. Lett.* 2002, *27*, 743–745.

[198] Santamato, E., Sasso, A., Piccirillo, B., Vella, A., *Opt. Express* 2002, *10*, 871–878.

[199] Parkin, S., Nieminen, T., Heckenberg, N., Rubinsztein-Dunlop, H., *Phys. Rev. A* 2004, *70*, 023816.

[200] Beth, R., *Phys. Rev.* 1936, *50*, 115–125.

[201] Moothoo, D., Arlt, J., Conroy, R., Akerboom, F. *et al.*, *Am. J. Phys.* 2001, *69*, 271–276.

[202] Friese, M., Nieminen, T., Heckenberg, N., Rubinsztein-Dunlop, H., *Nature* 1998, *394*, 348–350.

[203] La Porta, A., Wang, M., *Phys. Rev. Lett.* 2004, *92*, 190801.

[204] Bishop, A., Nieminen, T., Heckenberg, N., Rubinsztein-Dunlop, H., *Phys. Rev. Lett.* 2004, *92*, 198104.

[205] Singer, W., Nieminen, T., Gibson, U., Heckenberg, N. *et al.*, *Phys.Rev. E* 2006, *73*, 021911.

[206] Galajda, P., Ormos, P., *Opt. Express* 2003, *11*, 446–451.

[207] Neale, S. L., MacDonald, M. P., Dholakia, K., Krauss, T. F., *Nat. Mater.* 2005, *4*, 530–533.

[208] Cheng, Z., Chaikin, P., Mason, T., *Phys. Rev. Lett.* 2002, *89*, 108303.

[209] Bayoudh, S., Nieminen, T., Heckenberg, N., Rubinsztein-Dunlop, H. J., *Mod. Opt.* 2003, *50*, 1581–1590.

[210] Oroszi, L., Galajda, P., Kirei, H., Bottka, S. *et al.*, *Phys. Rev. Lett.* 2006, *97*, 058301.

[211] Gosse, C., Croquette, V., *Biophys. J.* 2002, *82*, 3314–3329.

[212] Romano, G., Sacconi, L., Capitanio, M., Pavone, F., *Opt. Commun.* 2003, *215*, 323–331.

[213] Fisher, J., Cummings, J., Desai, K., Vicci, L. *et al.*, *Rev. Sci. Instrum.* 2005, *76*, 053711.

[214] Fisher, J., Cribb, J., Desai, K., Vicci, L. *et al.*, *Rev. Sci. Instrum.* 2006, *77*, 023702.

[215] Ritort, F., *J. Phys Condens. Matter* 2006, *18*, R531–R583.

[216] Greenleaf, W. J., Woodside, M. T., Block, S. M., *Annu. Rev. Biophys. Biomol. Struct.* 2007, *36*, 171–190.

[217] Neuman, K. C., Lionnet, T., Allemand, J.-F., *Annu. Rev. Mater. Res.* 2007, *37*, 33–67.

[218] Neuman, K. C., Nagy, A., *Nat. Methods* 2008, *5*, 491–505.

[219] Higurashi, E., Ukita, H., Tanaka, H., Ohguchi, O., *Appl. Phys. Lett.* 1994, *64*, 2209–2210.

[220] Higurashi, E., Sawada, R., Ito, T., *Appl. Phys. Lett.* 1998, *72*, 2951–2953.

[221] Galajda, P., Ormos, P., *Appl. Phys. Lett.* 2002, *80*, 4653–4655.

[222] Galajda, P., Ormos, P., *J. Opt. B Quantum Semiclassical Opt.* 2002, *4*, S78–S81.

[223] Kelemen, L., Valkai, S., Ormos, P., *Appl. Opt.* 2006, *45*, 2777–2779.

[224] Galajda, P., Ormos, P., *Appl. Phys. Lett.* 2001, *78*, 249–251.

[225] Khan, M., Sood, A., Deepak, F., Rao, C., *Nanotechnology* 2006, *17*, S287–S290.

[226] Merkt, F. S., Erbe, A., Leiderer, P., *New J. Phys.* 2006, *8*, 216.

[227] Allen, L., Beijersbergen, M., Spreeuw, R., Woerdman, J., *Phys. Rev. A* 1992, *45*, 8185–8189.

[228] Allen, L., Padgett, M., Babiker, M., *Prog. Opt.* 1999, *39*, 291–372.

[229] Padgett, M., Allen, L., *Contemp. Phys.* 2000, *41*, 275–285.

[230] Bouchal, Z., *Czech. J. Phys.* 2003, *53*, 537–578.

[231] Padgett, M., Courtial, J., Allen, L., *Phys. Today* 2004, *57*, 35–40.

[232] Soifer, V., Kotlyar, V., Khonina, S., *Phys. Part. Nuclei* 2004, *35*, 733–766.

[233] Knöner, G., Parkin, S., Nieminen, T. A., Loke, V. L. Y. *et al.*, *Opt. Express* 2007, *15*, 5521–5530.

[234] He, H., Friese, M., Heckenberg, N., Rubinsztein-Dunlop, H., *Phys. Rev. Lett.* 1995, *75*, 826–829.

[235] Friese, M., Enger, J., RubinszteinDunlop, H., Heckenberg, N., *Phys. Rev. A* 1996, *54*, 1593–1596.

[236] Simpson, N. B., Dholakia, K., Allen, L., Padgett, M. J., *Opt. Lett.* 1997, *22*, 52–54.

[237] Rubinsztein-Dunlop, H., Nieminen, T., Friese, M., Heckenberg, N., *Adv. Quantum Chem.* 1998, *30*, 469–492.

[238] Volke-Sepúlveda, K., Garcés-Chávez, V., Chávez-Cerda, S., Arlt, J. *et al.*, *J. Opt. B Quantum Semiclassical Opt.* 2002, *4*, S82–S89.

[239] Garcés-Chávez, V., Volke-Sepúlveda, K., Chávez-Cerda, S., Sibbett, W. *et al.*, *Phys. Rev. A* 2002, *66*, 063402.

[240] Garcés-Chávez, V., McGloin, D., Padgett, M. J., Dultz, W. *et al.*, *Phys. Rev. Lett.* 2003, *91*, 093602-1–093602-4.

[241] Gascoyne, P., Vykoukal, J., *Electrophoresis* 2002, *23*, 1973–1983.

[242] Hughes, M., *Electrophoresis* 2002, *23*, 2569–2582.

[243] Gonzalez, C., Remcho, V., *J. Chromatogr. A* 2005, *1079*, 59–68.

[244] Lapizco-Encinas, B. H., Rito-Palomares, M., *Electrophoresis* 2007, *28*, 4521–4538.

[245] Chiou, P., Otha, A., Wu, M. C., *Nature* 2005, *436*, 370–372.

[246] Waigh, T., *Rep. Prog. Phys.* 2005, *68*, 685–742.

[247] Pullarkat, P. A., Fernandez, P. A., Ott, A., *Phys. Rep.* 2007, *449*, 29–53.

[248] Simonnet, C., Groisman, A., *Appl. Phys. Lett.* 2005, *87*, 114104.

[249] Sundararajan, N., Pio, M., Lee, L., Berlin, A., *J. Micromech. Syst.* 2004, *13*, 559–567.

[250] Zhao, B. S., Koo, Y.-M., Chung, D. S., *Anal. Chim. Acta* 2006, *556*, 97–103.

[251] Lewittes, M., Arnold, S., Oster, G., *Appl. Phys. Lett.* 1982, *40*, 455–457.

[252] Braun, D., Libchaber, A., *Phys. Rev. Lett.* 2002, *89*, 188103.

[253] Zhang, J., Kim, T., Jeoung, S., Yao, F. *et al.*, *Opt. Commun.* 2006, *267*, 260–263.

[254] Kotz, K., Noble, K., Faris, G., *Appl. Phys. Lett.* 2004, *85*, 2658–2660.

[255] Farahi, R., Passian, A., Ferrell, T., Thundat, T., *Opt. Lett.* 2005, *30*, 616–618.

[256] Farahi, R. H., Passian, A., Zahrai, S., Lereu, A. L. *et al.*, *Ultramicroscopy* 2006, *106*, 815–821.

[257] Passian, A., Zahrai, S., Lereu, A. L., Farahi, R. H. *et al.*, *Phys. Rev. E* 2006, *73*, 066311.

[258] Ohta, A. T., Jamshidi, A., Valley, J. K., Hsu, H.-Y. *et al.*, *Appl. Phys. Lett.* 2007, *91*, 074103.

[259] Louchev, O. A., Juodkazis, S., Murazawa, N., Wada, S. *et al.*, *Opt. Express* 2008, *16*, 5673–5680.

[260] Bustamante, C., Macosko, J., Wuite, G., *Nat. Rev. Mol. Cell Biol.* 2000, *1*, 130–136.

[261] Vogel, A., Venugopalan, V., *Chem. Rev.* 2003, *103*, 577–644.

[262] Tschachotin, S., *Biol. Zentralbl.* 1912, *32*, 623–630.

[263] Bessis, M., Gires, F., Mayer, G., Nomarski, G., *C. R. Acad. Sci.* 1962, *255*, 1010–1012.

[264] McNeill, P., Berns, M. J., *Cell Biol.* 1981, *88*, 543–553.

[265] Liang, H., Wright, H. W., Cheng, S., He, W. *et al.*, *Exp. Cell Res.* 1993, *204*, 110–120.

[266] König, K., Riemann, I., Fritzsche, W., *Opt. Lett.* 2001, *26*, 819–821.

[267] Khodjakov, A., Cole, R., Oakley, B., Rieder, C., *Curr. Biol.* 2000, *10*, 59–67.

[268] Berns, M., Gamelaja, N., Olson, R., Duffy, C. *et al.*, *J. Cell. Physiol.* 1970, *76*, 207–213.

[269] Khodjakov, A., Rieder, C., Manella, C., Kinnally, K., *Mitochondrion* 2004, *3*, 217–227.

[270] Grill, S., Gonczy, P., Stelzer, E., Hyman, A., *Nature* 2001, *409*, 630–633.

[271] Colombelli, J., Reynaud, E., Rietdorf, J., Pepperkok, R. *et al.*, *Traffic* 2005, *6*, 1093–1102.

[272] Russo, R., Mao, X., Liu, H., Gonzalez, J. *et al.*, *Talanta* 2002, *57*, 425–451.

[273] Yang, G. W., *Prog. Mater. Sci.* 2007, *52*, 648–698.

[274] Tenne, R., *Angew. Chem. Int. Ed.* 2003, *42*, 5124–5132.

[275] Becker, H., Gaertner, C., *Anal. Bioanal. Chem.* 2008, *390*, 89–111.

[276] Chen, Y., Naessens, K., Baets, R., Liao, Y. *et al.*, *Opt. Rev.* 2005, *12*, 427–441.

[277] Gattass, R. R., Mazur, E., *Nat. Phot.* 2008, *2*, 219–225.

[278] Holmes, A., *RIKEN Rev.* 2002, *43*, 63–69.

[279] Dittrich, P., Tachikawa, K., Manz, A., *Anal. Chem.* 2006, *78*, 3887–3907.

[280] Haeberle, S., Zengerle, R., *Lab Chip* 2007, *7*, 1094–1110.

[281] González Crevillén, A., Hervas, M., Angel López, M., Cristina González, M. *et al.*, *Talanta* 2007, *74*, 342–357.

[282] Foret, F., Kusỳ, P., *Electrophoresis* 2006, *27*, 4877–4887.

[283] Vogel, A., Lorenz, K., Horneffer, V., Huettmann, G. *et al.*, *Biophys. J.* 2007, *93*, 4481–4500.

[284] Schütze, K., Lahr, G., *Nat. Biotechnol.* 1998, *16*, 737–742.

[285] Walz, J. Y., Prieve, D. C., *Langmuir* 1992, *8*, 3073–3082.

[286] Clapp, A. R., Dickinson, R. B., *Langmuir* 2001, *17*, 2182–2191.

[287] Svoboda, K., Schmidt, C. F., Schnapp, B. J., Block, S. M., *Nature* 1993, *365*, 721–727.

[288] Allersma, M. W., Gittes, F., deCastro, M. J., Stewart, R. J. *et al.*, *Biophys. J.* 1998, *74*, 1074–1085.

[289] Gelles, J., Schnapp, B., Sheetz, M., *Nature* 1988, *331*, 450–453.

[290] Crocker, J. C., Grier, D. G., *J. Colloid Interface Sci.* 1996, *179*, 298–310.

[291] Speidel, M., Jonáš, A., Florin, E.-L., *Opt. Lett.* 2003, *28*, 69–71.

[292] Gittes, F., Schmidt, C. F., *Opt. Lett.* 1998, *23*, 7–9.

[293] Pralle, A., Prummer, M., Florin, E.-L., Stelzer, E. H. K. *et al.*, *Microsc. Res. Tech.* 1999, *44*, 378–386.

[294] Tischer, C., Altmann, S., Fisinger, S., Hörber, J. *et al.*, *Appl. Phys. Lett.* 2001, *79*, 3878–3880.

[295] Volpe, G., Kozyreff, G., Petrov, D. J., *Appl. Phys.* 2007, *102*, 084701.

[296] Denk, W., Webb, W. W., *Appl. Opt.* 1990, *29*, 2382–2391.

[297] Ghislain, L. P., Switz, N. A., Webb, W. W., *Rev. Sci. Instrum.* 1994, *65*, 2762–2768.

[298] Florin, E.-L., Hörber, J. K. H., Stelzer, E. H. K., *Appl. Phys. Lett.* 1996, *69*, 446–448.

[299] Florin, E.-L., Pralle, A., Hörber, J. K. H., Stelzer, E. H. K., *J. Struct. Biol.* 1997, *119*, 202–211.

[300] Wang, M., Yin, H., Landick, R., Gelles, J. *et al.*, *Biophys. J.* 1997, *72*, 1335–1346.

[301] Wuite, G. J. L., Smith, S. B., Young, M., Keller, D. *et al.*, *Nature* 2000, *404*, 103–106.

[302] Visscher, K., Schnitzer, M., Block, S., *Nature* 1999, *400*, 184–189.

[303] Block, S., Asbury, C., Shaevitz, J., Lang, M., *Proc. Natl. Acad. Sci. USA* 2003, *100*, 2351–2356.

[304] Greenleaf, W. J., Woodside, M. T., Abbondanzieri, E. A., Block, S. M., *Phys. Rev. Lett.* 2005, *95*, 208102.

[305] Tolić-Nørrelykke, I. M., Berg-Sørensen, K., Flyvbjerg, H., *Comput. Phys. Commun.* 2004, *159*, 225–240.

[306] Hansen, P., Tolić-Nørrelykke, I., Flyvbjerg, H., Berg-Sørensen, K., *Comput. Phys. Commun.* 2006, *174*, 518–520.

[307] Hansen, P. M., Tolić-Nørrelykke, I. M., Flyvbjerg, H., Berg-Sørensen, K., *Comput. Phys. Commun.* 2006, *175*, 572–573.

[308] Florin, E.-L., Pralle, A., Stelzer, E. H. K., Hörber, J. K. H., *Appl. Phys. A* 1998, *66*, 75–78.

[309] Pralle, A., Florin, E.-L., Stelzer, E. H. K., Hörber, J. K. H., *Appl. Phys. A* 1998, *66*, 71–73.

[310] Wottawah, F., Schinkinger, S., Lincoln, B., Ebert, S. *et al.*, *Acta Biomater.* 2005, *1*, 263–271.

[311] Lincoln, B., Schinkinger, S., Travis, K., Wottawah, F. *et al.*, *Biomed. Microdevices* 2007, *9*, 703–710.

[312] Lincoln, B., Erickson, H., Schinkinger, S., Wottawah, F. *et al.*, *Cytometry A* 2004, *59A*, 203–209.

[313] Furst, E., *Curr. Opin. Colloid Interface Sci.* 2005, *10*, 79–86.

[314] Buosciolo, A., Pesce, G., Sasso, A., *Opt. Commun.* 2004, *230*, 357–368.

[315] Lugowski, R., Kolodziejczyk, B., Kawata, Y., *Opt. Commun.* 2002, *202*, 1–8.

[316] Parkin, S. J., Knöner, G., Nieminen, T. A., Heckenberg, N. R. *et al.*, *Phys. Rev. E* 2007, *76*, 041507.

[317] Addas, K., Schmidt, C., Tang, J., *Phys. Rev. E* 2004, *70*, 021503.

[318] Starrs, L., Bartlett, P., *Faraday Discuss.* 2003, *123*, 323–334.

[319] Chen, D., Weeks, E., Crocker, J., Islam, M. *et al.*, *Phys. Rev. Lett.* 2003, *90*, 108301.

[320] Atakhorrami, M., Addas, K. M., Schmidt, C. F., *Rev. Sci. Instrum.* 2008, *79*, 043103.

[321] Caspi, A., Granek, R., Elbaum, M., *Phys. Rev. E* 2002, *66*, 011916.

[322] Tolić-Nørrelykke, I., Munteanu, E., Thon, G., Oddershede, L. *et al.*, *Phys. Rev. Lett.* 2004, *93*, 078102.

[323] Janmey, P., Weitz, D., *Trends Biochem. Sci.* 2004, *29*, 364–370.

[324] De Luca, A. C., Volpe, G., Drets, A. M., Geli, M. I. *et al.*, *Opt. Express* 2007, *15*, 7922–7932.

[325] Wirtz, D., Tseng, Y., Wirtz, D., *Intermediate Filament Cytoskeleton* 2004, *78*, 45–64.

[326] Bayraktar, T., Pidugu, S., *Int. J. Heat Mass Transfer* 2006, *49*, 815–824.

[327] Schimpf, M., Caldwell, K., Giddings, J. C., *Field-Flow Fractionation Handbook: A*, Wiley, New York 2000.

[328] Imasaka, T., Kawabata, Y., Kaneta, T., Ishidzu, Y., *Anal. Chem.* 1995, *67*, 1763–1765.

[329] Kaneta, T., Ishidzu, Y., Mishima, N., Imasaka, T., *Anal. Chem.* 1997, *69*, 2701–2710.

[330] Makihara, J., Kaneta, T., Imasaka, T., *Talanta* 1999, *48*, 551–557.

[331] Siegman, A. E., *Lasers*, University Science Books, Sausalito, CA 1986.

[332] Hatano, T., Kaneta, T., Imasaka, T., *Anal. Chem.* 1997, *69*, 2711–2715.

[333] Miki, S., Kaneta, T., Imasaka, T., *Anal. Chim. Acta* 2000, *404*, 1–6.

[334] Hart, S. J., Terray, A. V., *Appl. Phys. Lett.* 2003, *83*, 5316–5318.

[335] Terray, A., Arnold, J., Hart, S. J., *Opt. Express* 2005, *13*, 10406–10415.

[336] Hart, S. J., Terray, A. V., Arnold, J., Leski, T. A., *Opt. Express* 2007, *15*, 2724–2731.

[337] Kim, S. B., Kim, J. H., Kim, S. S., *Appl. Opt.* 2006, *45*, 6919–6924.

[338] Giddings, J. C., *Science* 2000, *260*, 1456–1465.

[339] Janča, J., *Anal. Chim. Acta* 2005, *540*, 187–196.

[340] Janča, J., *Int. J. Polym. Anal. Charact.* 2006, *11*, 57–70.

[341] Korda, P. T., Taylor, M. B., Grier, D. G., *Phys. Rev. Lett.* 2002, *89*, 128301.

[342] Dholakia, K., MacDonald, M. P., Zemánek, P., Čižmár, T., *Methods Cell Biol.* 2007, *82*, 467–495.

[343] Dholakia, K., Lee, W. M., Paterson, L., MacDonald, M. P. *et al.*, *IEEE J. Sel. Top. Quant. Electron.* 2007, *13*, 1646–1654.

[344] Herzenberz, L. A., Parks, D., Sahaf, B., Perez, O. *et al.*, *Clin. Chem.* 2002, *48*, 1819–1827.

[345] Wang, M. M., Tu, E., Raymond, D. E., Yang, J. M. *et al.*, *Nat. Biotechnol.* 2005, *23*, 83–87.

[346] Buican, T. N., Smyth, M. J., Crissman, H. A., Salzman, G. C. *et al.*, *Appl. Opt.* 1987, *26*, 5311–5316.

[347] Cran-McGreehin, S. J., Dholakia, K., Krauss, T. F., *Opt. Express* 2006, *14*, 7723–7729.

[348] Applegate, R. W., Jr., Squier, J., Vestad, T. Oakey, J. *et al.*, *Opt. Express* 2004, *12*, 4390–4398.

[349] Applegate, R. W., Jr., Squier, J., Vestad, T. Oakey, J. *et al.*, *Lab Chip* 2006, *6*, 422–426.

[350] Applegate, R. W., Jr., Squier, J., Vestad, T. Oakey, J. *et al.*, *Appl. Phys. Lett.* 2008, *92*, 013904.

[351] Roichman, Y., Wong, V., Grier, D. G., *Phys. Rev. E* 2007, *75*, 011407.

[352] Chapin, S. C., Germain, V., Dufresne, E. R., *Opt. Express* 2006, *14*, 13095–13100.

[353] Rodrigo, P. J., Eriksen, R. L., Daria, V. R., Glückstad, J., *Opt. Express* 2002, *10*, 1550–1556.

[354] Zemánek, P., Jonáš, A., Liška, M., *J. Opt. Soc. Am. A* 2002, *19*, 1025–1034.

[355] Lekner, J., *J. Opt. A: Pure Appl. Opt.* 2005, *7*, 238–248.

[356] Ricárdez-Vargas, I., Rodríguez-Montero, P., Ramos-García, R., Volke-Sepúlveda, K., *Appl. Phys. Lett.* 2006, *88*, 121116.

[357] Pelton, M., Ladavac, K., Grier, D. G., *Phys. Rev. E* 2004, *70*, 031108.

[358] Ladavac, K., Kasza, K., Grier, D. G., *Phys. Rev. E* 2004, *70*, 010901.

[359] Reichhardt, C., Reichhardt, C. J. O., *Phys. Rev. E* 2004, *69*, 041405.

[360] Reichhardt, C., Reichhardt, C. J. O., Hastings, M. B., *Phys. Rev. E* 2004, *69*, 056115.

[361] Lacasta, A. M., Sancho, J. M., Romero, A. H., Lindenberg, K., *Phys. Rev. Lett.* 2005, *94*, 160601.

[362] Libál, A., Reichhardt, C., Jankó, B., Reichhardt, C. J. O., *Phys. Rev. Lett.* 2006, *96*, 188301.

[363] Gleeson, J. P., Sancho, J. M., Lacasta, A. M., Lindenberg, K., *Phys. Rev. E* 2006, *73*, 041102.

[364] Milne, G., Rhodes, D., MacDonald, M., Dholakia, K., *Opt. Lett.* 2007, *32*, 1144–1146.

[365] Marchington, R. F., Mazilu, M., Kuriakose, S., Garcés-Chávez, V. *et al.*, *Opt. Express* 2008, *16*, 3712–3726.

[366] Zhang, H., Tu, E., Hagen, N., Schnabel, C. *et al.*, *Biomed. Microdevices* 2004, *6*, 11–21.

[367] Forster, A., Wang, M., Butler, W., Chachisvilis, M. *et al.*, *Anal. Biochem.* 2004, *327*, 14–22.

[368] Gherardi, D. M., Carruthers, A. E., Čižmár, T., Wright, E. M. *et al.*, *Appl. Phys. Lett.* 2008, *93*, 041110.

[369] Paterson, L., Papagiakoumou, E., Milne, G., Garcés-Chávez, V. *et al.*, *Appl. Phys. Lett.* 2005, *87*, 123901.

[370] Tatarkova, S. A., Sibbett, W., Dholakia, K., *Phys. Rev. Lett.* 2003, *91*, 038101.

[371] Hayashi, Y., Ashihara, S., Shimura, T., Kuroda, K., *Opt. Commun.* 2008, *281*, 3792–3798.

[372] Jákl, P., Čižmár, T., Šerỳ, M., Zemánek, P., *Appl. Phys. Lett.* 2008, *92*, 161110.

[373] Koss, B. A., Grier, D. G., *Appl. Phys. Lett.* 2003, *82*, 3985–3987.

[374] Lee, S.-H., Grier, D. G., *J. Phys. Condens. Matter* 2005, *17*, S3685–S3695.

[375] Smith, R. L., Spalding, G. C., Dholakia, K., MacDonald, M. P., *J. Opt. A: Pure Appl. Opt.* 2007, *9*, S134–S138.

[376] Svoboda, K., Block, S. M., *Opt. Lett.* 1994, *19*, 930–932.

[377] Hofkens, J., Hotta, J., Sasaki, K., Masuhara, H. *et al.*, *Langmuir* 1997, *13*, 414–419.

[378] Borowicz, P., Hotta, J., Sasaki, K., Masuhara, H., *J. Phys. Chem. B* 1998, *102*, 1896–1901.

[379] Tanaka, Y., Yoshikawa, H., Masuhara, H., *J. Phys. Chem. C* 2007, *111*, 18457–18460.

[380] Smith, T., Hotta, J., Sasaki, K., Masuhara, H. *et al.*, *J. Phys. Chem. B* 1999, *103*, 1660–1663.

[381] Ito, S., Yoshikawa, H., Masuhara, H., *Appl. Phys. Lett.* 2001, *78*, 4046.

[382] Yoshikawa, H., Matsui, T., Masuhara, H., *Phys. Rev. E* 2004, *70*, 061406.

[383] Hosokawa, C., Yoshikawa, H., Masuhara, H., *Phys. Rev. E* 2004, *70*, 061410.

[384] Hansen, P. M., Bhatia, V. K., Harrit, N., Oddershede, L., *Nano Lett.* 2005, *5*, 1937–1942.

[385] Sugiura, T., Okada, T., Inouye, Y., Nakamura, O. *et al.*, *Opt. Lett.* 1997, *22*, 1663–1665.

[386] Prikulis, J., Svedberg, F., Kall, M., Enger, J. *et al.*, *Nano Lett.* 2004, *4*, 115–118.

[387] Svedberg, F., Li, Z., Xu, H., Kall, M., *Nano Lett.* 2006, *6*, 2639–2641.

[388] Yoshikawa, H., Adachi, T., Sazaki, G., Mastui, T. *et al.*, *J. Opt. A: Pure Appl. Opt.* 2007, *9*, S164–S171.

[389] Bosanac, L., Aabo, T., Bendix, P. M., Oddershede, L. B., *Nano Lett.* 2008, *8*, 1486–1491.

[390] Pelton, M., Liu, M., Kim, H., Smith, G. *et al.*, *Opt. Lett.* 2006, *31*, 2075–2077.

[391] Dienerowitz, M., Mazilu, M., Reece, P. J., Krauss, T. F. *et al.*, *Opt. Express* 2008, *16*, 4991–4999.

[392] Toussaint, K. C., Jr., Liu, M., Pelton, M., Pesic, J. *et al.*, *Opt. Express* 2007, *15*, 12017–12029.

[393] Juodkazis, S., Mizeikis, V., Matsuo, S., Ueno, K. *et al.*, *Bull. Chem. Soc. Jpn.* 2008, *81*, 411–448.

[394] Numata, T., Takayanagi, A., Otani, Y., Umeda, N., *Jpn. J. Appl. Phys. Part 1* 2006, *45*, 359–363.

[395] Pauzauskie, P., Radenovic, A., Trepagnier, E., Shroff, H. *et al.*, *Nat. Mater.* 2006, *5*, 97–101.

[396] Pan, L., Ishikawa, A., Tamai, N., *Phys. Rev. B* 2007, *75*, 161305.

[397] Plewa, J., Tanner, E., Mueth, D., Grier, D., *Opt. Express* 2004, *12*, 1978–1981.

[398] Shi, C., Zhang, Y., Gu, C., Seballos, L. *et al.*, *Nanotechnology* 2008, *19*, 215304.

[399] Kerssemakers, J., Janson, M., van der Horst, A., Dogterom, M., *Appl. Phys. Lett.* 2003, *83*, 4441–4443.

[400] Zhang, J., Kim, H., Oh, C., Sun, X. *et al.*, *Appl. Phys. Lett.* 2006, *88*, 053123.

[401] Nicholson, J. W., Windeler, R. S., DiGiovanni, D. J., *Opt. Express* 2007, *15*, 9176–9183.

[402] Kashiwagi, K., Yamashita, S., Set, S. Y., *Jpn. J. Appl. Phys. Part 2* 2007, *46*, L988–L990.

[403] Kumar, S., Kumar, R., Jindal, V. K., Bharadwaj, L. M., *Mater. Lett.* 2008, *62*, 731–734.

[404] Marago, O. M., Gucciardi, P. G., Bonaccorso, F., Calogero, G. *et al.*, *Physica E* 2008, *40*, 2347–2351.

[405] Navratil, M., Mabbott, G., Arriaga, E., *Anal. Chem.* 2006, *78*, 4005–4019.

[406] Urlaub, E., Popp, J., Roman, V., Kiefer, W. *et al.*, *Chem. Phys. Lett.* 1998, *298*, 177–182.

[407] Rusciano, G., De Luca, A. C., Sasso, A., Pesce, G., *Anal. Chem.* 2007, *79*, 3708–3715.

[408] Thurn, R., Kiefer, W., *Appl. Spectrosc.* 1984, *38*, 78–83.

[409] Petrov, D. V., *J. Opt. A: Pure Appl. Opt.* 2007, *9*, S139–S156.

[410] Urlaub, E., Lankers, M., Hartmann, I., Popp, J. *et al.*, *Fresenius J. Anal. Chem.* 1996, *355*, 329–331.

[411] Esen, C., Kaiser, T., Schweiger, G., *Appl. Spectrosc.* 1996, *50*, 823–828.

[412] Mund, C., Zellner, R., *Chemphyschem* 2003, *4*, 638–645.

[413] King, M. D., Thompson, K. C., Ward, A. D., Pfrang, C. *et al.*, *Faraday Discuss.* 2008, *137*, 173–192.

[414] Ajito, K., Morita, M., Torimitsu, K., *Anal. Chem.* 2000, *72*, 4721–4725.

[415] Houlne, M., Sjostrom, C., Uibel, R., Kleimeyer, J. *et al.*, *Anal. Chem.* 2002, *74*, 4311–4319.

[416] Ajito, K., Torimitsu, K., *Lab Chip* 2002, *2*, 11–14.

[417] Xie, C., Dinno, M., Li, Y., *Opt. Lett.* 2002, *27*, 249–251.

[418] Xie, C., Li, Y., Tang, W., Newton, R. J., *Appl. Phys.* 2003, *94*, 6138–6142.

[419] Singh, G., Creely, C., Volpe, G., Grotsch, H. *et al.*, *Anal. Chem.* 2005, *77*, 2564–2568.

[420] Deng, J., Wei, Q., Zhang, M., Wang, Y. *et al.*, *J. Raman Spectrosc.* 2005, *36*, 257–261.

[421] De Luca, A. C., Rusciano, G., Ciancia, R., Martinelli, V. *et al.*, *Opt. Express* 2008, *16*, 7943–7957.

[422] Chan, J., Esposito, A., Talley, C., Hollars, C. *et al.*, *Anal. Chem.* 2004, *76*, 599–603.

[423] Xie, C., Mace, J., Dinno, M., Li, Y. *et al.*, *Anal. Chem.* 2005, *77*, 4390–4397.

[424] Chen, D., Huang, S.-S., Li, Y.-Q., *Anal. Chem.* 2006, *78*, 6936–6941.

[425] Baumgart, T., Hammond, A. T., Sengupta, P., Hess, S. T. *et al.*, *Proc. Natl. Acad. Sci. USA* 2007, *104*, 3165–3170.

[426] Barry, B., *Eur. J. Pharm. Sci.* 2001, *14*, 101–114.

[427] Cherney, D., Conboy, J., Harris, J., *Anal. Chem.* 2003, *75*, 6621–6628.

[428] Fox, C. B., Myers, G. A., Harris, J. M., *Appl. Spectrosc.* 2007, *61*, 465–469.

[429] Fox, C. B., Uibel, R. H., Harris, J. M., *J. Phys. Chem. B* 2007, *111*, 11428–11436.

[430] Fox, C. B., Horton, R. A., Harris, J. M., *Anal. Chem.* 2006, *78*, 4918–4924.

[431] Lau, A., Lee, L. P., Chan, J. W., *Lab Chip* 2008, *8*, 1116–1120.

[432] Hunt, H. C., Wilkinson, J. S., *Microfluid. Nanofluid.* 2008, *4*, 53–79.

[433] Ramser, K., Enger, J., Goksör, M., Hanstorp, D. *et al.*, *Lab Chip* 2005, *5*, 431–436.

[434] Eriksson, E., Scrimgeour, J., Graneli, A., Ramser, K. *et al.*, *J. Opt. A: Pure Appl. Opt.* 2007, *9*, S113–S121.

[435] Creely, C., Volpe, G., Singh, G., Soler, M. *et al.*, *Opt. Express* 2005, *13*, 6105–6110.

[436] Creely, C., Mercadal, S., Volpe, G., Soler, M. *et al.*, *Proc. SPIE* 2006, *6326*, 63260U-1–63260U-8.

[437] Kneipp, K., Kneipp, H., Itzkan, I., Dasari, R. P. *et al.*, *J. Phys.: Condens. Matter* 2002, *14*, R597–R624.

[438] Zhang, X., Yin, H., Cooper, J. M., Haswell, S. J., *Anal. Bioanal. Chem.* 2008, *390*, 833–840.

[439] Pieczonka, N., Aroca, R., *Chemphyschem* 2005, *6*, 2473–2484.

[440] Xie, X., Trautman, J., *Annu. Rev. Phys. Chem.* 1998, *49*, 441–480.

[441] Weiss, S., *Science* 1999, *283*, 1676–1683.

[442] Moerner, W., *J. Phys. Chem. B* 2002, *106*, 910–927.

[443] Gell, C., Brockwell, D., Smith, A., *Handbook of Single Molecule Fluorescence Spectroscopy*, Oxford University Press, New York 2006.

[444] Harada, Y., Funatsu, T., Murakami, K., Nonoyama, Y. *et al.*, *Biophys. J.* 1999, *76*, 709–715.

[445] Ishijima, A., Yanagida, T., *Trends Biochem. Sci.* 2001, *26*, 438–444.

[446] van Mameren, J., Modesti, M., Kanaar, R., Wyman, C. *et al.*, *Biophys. J.* 2006, *91*, L78–L80.

[447] Wang, Y., Botvinick, E., Zhao, Y., Berns, M. *et al.*, *Nature* 2005, *434*, 1040–1045.

[448] Brau, R. R., Tarsa, P. B., Ferrer, J. M., Lee, P. *et al.*, *Biophys. J.* 2006, *91*, 1069–1077.

[449] Tarsa, P. B., Brau, R. R., Barch, M., Ferrer, J. M. *et al.*, *Angew. Chem. Int. Ed.* 2007, *46*, 1999–2001.

[450] Hohng, S., Zhou, R., Nahas, M. K., Yu, J. *et al.*, *Science* 2007, *318*, 279–283.

[451] Lang, M. J., Fordyce, P. M., Block, S. M., *J. Biol.* 2003, *2*, 2–6.

[452] van Dijk, M., Kapitein, L., van Mameren, J., Schmidt, C. *et al.*, *J. Phys. Chem. B* 2004, *108*, 6479–6484.

[453] Funatsu, T., Harada, Y., Higuchi, H., Tokunaga, M. *et al.*, *Biophys. Chem.* 1997, *68*, 63–72.

[454] Lang, M., Fordyce, P., Engh, A., Neuman, K. *et al.*, *Nat. Methods* 2004, *2*, 6.1–6.4.

[455] Capitanio, M., Maggi, D., Vanzi, F., Pavone, F. S., *J. Opt. A: Pure Appl. Opt.* 2007, *9*, S157–S163.

[456] Agate, B., Brown, C., Sibbett, W., Dholakia, K., *Opt. Express* 2004, *12*, 3011–3017.

[457] Griffiths, A. D., Tawfik, D. S., *Trends Biotechnol.* 2006, *24*, 395–402.

[458] Kulin, S., Kishore, R., Helmerson, K., Locascio, L., *Langmuir* 2003, *19*, 8206–8210.

[459] Lorenz, R. M., Edgar, J. S., Jeffries, G. D. M., Zhao, Y. *et al.*, *Anal. Chem.* 2007, *79*, 224–228.

[460] Cherney, D. P., Myers, G. A., Horton, R. A., Harris, J. M., *Anal. Chem.* 2006, *78*, 6928–6935.

[461] Stromberg, A., Ryttsen, F., Chiu, D., Davidson, M. *et al.*, *Proc. Natl. Acad. Sci. USA* 2000, *97*, 7–11.

[462] Sun, B., Chiu, D., *Langmuir* 2004, *20*, 4614–4620.

[463] Terray, A. V., Oakey, J., Marr, D. W. M., *Science* 2002, *296*, 1841–1844.

[464] Ladavac, K., Grier, D., *Opt. Express* 2004, *12*, 1144–1149.

[465] Leach, J., Mushfique, H., di Leonardo, R., Padgett, M. *et al.*, *Lab Chip* 2006, *6*, 735–739.

[466] Maruo, S., Inoue, H., *Appl. Phys. Lett.* 2006, *89*, 144101.

[467] Oroszi, L., Dér, A., Kirei, H., Ormos, P., *Appl. Phys. Lett.* 2006, *89*, 263508.

[468] Klauke, N., Monaghan, P., Sinclair, G., Padgett, M. *et al.*, *Lab Chip* 2006, *6*, 788–793.

[469] Maruyama, H., Arai, F., Fukuda, T., *Lab Chip* 2008, *8*, 346–351.

[470] Omori, R., Kobayashi, T., Suzuki, A., *Opt. Lett.* 1997, *22*, 816–818.

[471] Mitchem, L., Hopkins, R. J., Buajarern, J., Ward, A. D. *et al.*, *Chem. Phys. Lett.* 2006, *432*, 362–366.

[472] McGloin, D., Burnham, D. R., Summers, M. D., Rudd, D. *et al.*, *Faraday Discuss.* 2008, *137*, 335–350.

[473] Mitchem, L., Reid, J. P., *Chem. Soc. Rev.* 2008, *37*, 756–769.

[474] Luchette, P., Abiy, N., Mao, H., *Sens. Actuators B Chem.* 2007, *128*, 154–160.

